In The Name of Allah, Most Gracious, Most Merciful.

UNIVERSITY OF SOUTHAMPTON

INSTITUTE OF CRYOGENICS

THE EFFECTS OF MOISTURE ON THE THERMAL PROPERTIES OF CONCRETE BETWEEN -80°C AND 0°C

by

Kamarudin bin Mohd Yusof

The thesis is submitted for the degree of

Doctor of Philosophy

September 1984

UNIVERSITY OF SOUTHAMPTON

ABSTRACT

FACULTY OF ENGINEERING AND APPLIED SCIENCE

INSTITUTE OF CRYOGENICS

Doctor of Philosophy

THE EFFECTS OF MOISTURE ON THE THERMAL PROPERTIES OF CONCRETE BETWEEN -80°C AND 0°C

by Kamarudin bin Mohd Yusof

Samples of saturated moist-cured micro-concrete and paste with w/c ratios between 0.30 and 0.70 have been investigated and compared with samples of dry and rewetted paste between -80°C and 0°C. The freezable water in these pastes has been measured from the enthalpy difference between moist-cured and dry samples, and is significantly less than evaporable water content. The NMR spectra of these pastes have been studied at temperatures down to -80°C and suggest that the evaporable water is adsorbed and not free.

Thermal strains of samples with different degrees of saturation between 0°C and -80°C have been measured and the effect of rewetted water also investigated. It is concluded that the physically adsorbed water which causes a large thermal strain in concrete paste comprises 75% of the total evaporable water. The permanent expansion of concrete paste during a thermal cycle only occurred in a rewetted, resoaked, fully moist-cured concrete paste.

LIST OF CONTENTS

LIST OF CONTENTS

Chapter Three

Nuclear magnetic resonance studies of water

Chapter Four

The studies of moisture in concrete paste

LIST OF CONTENTS

Chapter Five

Experiments and results

LIST OF CONTENTS

Chapter Six

Discussions

LIST OF CONTENTS

GLOSSARY OF WORDS

ABSORBED WATER - Water that goes into the paste during resoaking or rewetting. Some at least is adsorbed(see Fig.6.1)

ADSORBED WATER - Water which is being held by the surface forces in the internal structure of the paste.

CAPILLARY PORE - Part of the cement paste which has not been filled by the products of the cement hydration or the residual voids after the paste matured.

CAPILLARY WATER - Water occupying the capillary pores.

COEFFICIENT OF DILATION - The change of dilation per degree celcius.

DEGREE OF SATURATION - A ratio of the weight of freezable water to the weight of water and air that occupying the pores of the saturated paste.

DILATION FACTOR - The deviation of the thermal strain curve from the contraction line of concrete paste between 20^{0}C and 0^{0}C.

GEL - The product of cement hydration is a hardened paste consisting of hydrates of calcium silicate hydrate and small quantities of other substances. These solid compounds are collectively described as the gel.

GEL PORE - The interstitial spaces between the gel

particles.

GEL WATER - Water occupying the gel pores.

HYDRATION - The reaction process between cement compound and water.

LNG - Liquid Natural Gas.

MOISTURE - Water and water solution.

MOIST-CURED CONCRETE - Concrete which has been kept in water at 20°C to 24°C for at least 28 days.

NMR - Nuclear Magnetic Resonance.

PASTE - Comprises all the solid parts such as cement gel and all types of water present.

RESOAKING - Water that goes into moist-cured paste which has been dried in a dry chamber.

REWETTING - Water that goes into a paste which has been dried to constant weight at 100°C.

SATURATED PASTE - Paste which cannot absorb any more water and which has been kept in water.

CHAPTER ONE

INTRODUCTION

1.1 GENERAL

Concrete is well known as a constructional material. It possesses a wide range of properties which can be varied to meet a wide range of applications.

In the fifties and sixties, research on concrete at low temperatures was centred on the effect of frost action and the durability of the frozen paste under temperature cycling in cold climatic regions. Powers(1), who has contributed a great deal of work in this field, reported that under some circumstances, concrete does not suffer from frost damage. In particular, specimens with entrained air show more reliable resistance to frost damage.

Present day concrete technology is not only extended to structures influenced by cold weather but it is being used in the cryogenic industry, e.g. in LNG tanks. In many cryogenic tanks, prestressed concrete is used as a secondary wall. The main reason is that

concrete has a high compressive strength at low temperature which may be 200-300% greater than the strength at normal temperatures(2). This increase in strength may be even greater when the concrete paste is made with a higher water-cement ratio.

After the disaster at Cleveland, Ohio in 1944, due to a failure of a steel LNG tank, people began to think of the safety requirements for the storage of LNG. Looking at the promising performance shown by concrete, this material has now been used as a structure for the secondary containment of cold liquids.

Since safety comes first,designers of concrete cryogenic tanks need to consider and study the problems governing the properties of concrete at low temperatures. The properties such as vapour and liquid tightness, permeability and strains after several thermal cycles should be understood clearly.

Designs should not be based solely on the limited data reported by researchers in the last decades because the present usage of concrete includes exposure to severe thermal cycles with large temperature gradients. For instance , during the sixties, Hansen(3) had reported that only 13% of his specimens which had been exposed to cold weather and frost for 20 years, had

damaged. Meanwhile, Jackson(4), who exposed his specimens to frost action in the laboratory under fast cooling conditions found them all damaged after only several cycles.

Although increasing the water content, will increase the compressive strength and reduce porosity of concrete paste, the water content in the paste produces disadvantageous effects on other properties. Therefore it is wise to study the role of the water in great detail,as many people have reported(5,6,7) that the main controlling parameter in the concrete paste seems to be the water in all its various forms in the cement structure.

The range of temperature covered in this study is 0^0 to $-80\ ^0C$ which is the range in which ice nucleation is taking place. Particular properties which have been studied include dilation, enthalpy-temperature variation, and nuclear magnetic resonance studies on concrete of different water contents and aggregate.

1.2 PAST EXPERIENCES ON FROST ACTION

Previous publications(1,3,4,8,9,10) have

shown that water in concrete paste plays a significant role in damaging the paste at low temperatures. The freezing of water or moisture in the paste and the growth of ice bodies as the temperature is lowered, are the possible cause of the internal damage. Neville(11) has given two factors which cause dilation of the paste with reducing temperature.

The first is the freezing of water in capillary pores which forces the excess volume of water to be expelled from the frozen parts. The resistance to such flow of water generates an internal pressure. Powers(10) reported that the internal stress produced by the hydraulic pressure appears at the same instant as the freezing begins.

The second factor is the diffusion of gel water into the capillary pores. Powers(10) said that as the gel water diffuses out, the paste tends to shrink, but the growth of ice crystals in the capillaries make the overall result a volume increase. Therefore, he said the dilation may not be apparent at the beginning of freezing; it also does not stop when the cooling ceases.

Powers(10) in discussing the mechanism of dilation also mentioned a third factor which caused dilation. The freezing of water in capillaries disturbs

the thermodynamic equilibrium of the solutions in the gel pores and the capillaries. The more concentrated solution tends to diffuse to the less concentrated. As the movement of water is opposed, an osmotic pressure is produced which can also contribute to the dilation.

Dilation in aggregates or rocks is different from that of concrete because of the differences in their internal structure. The pores in rocks are few and large(10) compared to concrete paste in which they are small and well distributed in the whole paste. Rocks consist of crystals; so the pores which are accesible to water are limited to the spaces between the crystals. This water will freeze immediately once the freezing starts. In rare occasions(12), water in rocks can cause crystal growth after the initial freezing. The water may be taken from outside sources. In the case of aggregates in concrete paste, water can be obtained from the surrounding cement paste.

Powers(10) reported that under long cold spells, ice bodies in aggregate pores could grow, as unfrozen water from the concrete paste diffused into them. If the paste can obtain water from outside sources, then dilation might be produced; in practice the required combination of circumstances is rare.

Therefore, aggregate is very unlikely to be damaged by the hydraulic pressure mechanism.

Apart from the above, the size of the specimen and the degree of saturation of the concrete paste also effect the dilation(10). If a body is finite, the excessive water volume produced by freezing may cause water to escape from the body and there will be less dilation. However, this mechanism depends on the continuity of the capillaries. It has been reported (13) that for a particular type of cement, there is a maximum water-cement ratio, 0.7, above which complete hydration does not produce enough gel to block all the capillary pores. For cement, with a specific surface area 1800 square cm/gm or greater, the limiting water-cement ratio was about 0.7. A finer cement had a limiting value higher than 0.7.

In less saturated specimens, large pores tend to be empty and the smaller pores may be only half full of water. When freezing takes place, the empty pores can accomodate the excess volume of water flowing away from the frozen parts. So, the paste experiences less hydraulic pressure. With this idea, the role of empty pores can be utilized in reducing the effect caused by the hydraulic pressure mechanism, as has been

discussed by Power(14). In normal concrete specimens, the empty pores are not well distributed throughout the whole paste and with prolonged contact with water source, they can eventually become filled. With an air entraining agent, discrete artificial pores(11) which are empty and very difficult to fill with water(14) can be distributed evenly throughout the paste. These empty cavities can provide spaces to contain ice and displaced solution during freezing. It has been reported(14) that, paste with entrained air shows no development of osmotic pressure and hydraulic pressure because the frozen water from the gel diffused into the unfilled cavities unopposed. On cooling down a normal concrete specimen and a specimen with entrained air to -25 ^{0}C, the latter specimen showed less dilation.

On the chemistry side, it has been reported(14) that at a given concentration of alkali, the melting point of ice varies from one point to another according to the size of the pores in which the moisture is being held. As the temperature goes down, the melting point of ice in the presence of alkali also becomes correspondingly reduced. This is because as the water freezes, the remaining solution become more concentrated, thus depressing the freezing point of ice.

However, Helmuth(15) has another way of looking at the depression of the freezing point of ice in the concrete paste. He reported that the spaces between the cement gel are too small to accomodate the ice crystals. This restriction on the propagation of ice, made the solution remain unfrozen at its melting point. Table 1.1 shows the calculated relationship between the size of ice crystal at particular melting points and the size of capillary pore at which it is able to contain the crystal.

Table 1.1: After Helmuth (15)

The Melting points		crystal size	capillary size
°C	°F	Å	Å
-2	28.4	180	208
-6	21.2	58	83
-10	14.0	36	59
-15	5.0	24	44
-20	-4.0	18	35

This water will only freeze when the temperature drops to a very low one at which spontaneous freezing will

take place. However, in the smallest pores, like gel pores, freezing is unlikely to take place because the space is too small for the formation of ice nuclei. It has been reported that(11), even at -78 ^{0}C, the water in gel pores does not freeze. Thus the water must diffuse to larger pores to freeze.

As we have seen above, dilation of the concrete paste depends on the state of water and how it flows and on the distribution of pores in the paste. In understanding the behaviour of water in the paste, it is incomplete if the state of water is not classified because water in a porous medium such as concrete paste may be present in several physical states.

1.3 CLASSIFICATION OF WATER IN CONCRETE PASTE

Verbeck et al(16) has arbitrarily classified the water in concrete paste into (1) evaporable and (2) non-evaporable water. Water which cannot be removed under a standard drying condition, i.e. at the boiling point of water, is classified as non-evaporable while the weight loss of the specimen on heating to constant weight at standard condition corresponds to the evaporable water.

Powers and Brownyard(17), classified the water in concrete paste as gel water and capillary water. The classification is based upon the concept that cement gel has a certain minimum porosity, in which the gel water is arbitrarily defined as the water contents of a saturated, well hydrated, low water-cement ratio pastes. In other words a low w/c ratio of a saturated and well hydrated cement paste should contain only gel water. In such paste, it has been reported that(18) the cement hydration virtually ceases before all the cement is hydrated and it has been assumed that the paste contains only gel water. Capillary water is then defined as the difference between the total evaporable water and its gel water content.

Verbeck et al also said, water in capillary pores can easily be varied while gel water cannot be varied. Copeland(19) in his paper on the specific volume of evaporable water has reported that water in capillary pores is similar to normal water or free water.

The state of water in concrete paste has been studied further by Seligmann(20) by using a NMR (nuclear magnetic resonance) technique. He reported that the adsorbed water in cement paste is similar to the interlayer water in clay or zeolitic water. Apart from

free water, he divided the physically adsorbed water into two categories. One is the adsorbed water which is easily evaporated, similar to water in many adsorbents and the other is the water which is more tightly bound as the interlayer water in clay.

Verbeck et al(16) also reported that much of the evaporable water in concrete paste seems to be part of the solid structure, a conclusion which he based upon observing the decrease of elastic moduli on drying the concrete specimens.

Thus, it seems that the water in concrete paste can be divided into several categories dependent on the energy of binding of the water. These categories are given in the following table:

a. Free water.
b. Capillary water which is very loosely bound.
c. Adsorbed water. This class of water has several degrees of binding with binding energies comparable to the latent heat of freezing, i.e. in the range 100 to 1000 KJ/Kg.
d. Chemically bound water such as water in calcium hydroxide with binding energies of 13,400 KJ/Kg.

1.4 THE USE OF CONCRETE AT LOW TEMPERATURE

Concrete technology has now entered a new era. The material has now been used for secondary walls or containment walls in many large cryogenic tanks(2) where they are exposed to large temperature gradients and to severe thermal cycles.

The concrete containment wall, is used to contain the cryogenic liquid in the event of failure of the primary steel wall. Evaporation of the liquid would then progress in a more or less controlled manner and there might be enough time to pump the liquid into other storage. Besides the internal hydraulic load, external loads such as impact loads and those induced by fire have to be considered(21).

In future, there may be the possibility of using concrete as a primary wall or as a single containment conrete tank because the necessary low permeability and liquid tightness concrete is not impossible to achieve.

1.5 MACROSCOPIC PROPERTIES OF CONCRETE

In design, traditionally compressive strength, elastic modulus and thermal contraction are taken into consideration. Browne and Bamforth(6) have made a review of these properties and also of the properties of prestressed concrete at cryogenic temperatures. The compressive strength shows an increase with reducing temperature, which is greater for test samples with higher water content. In their paper, they concluded that the most important factor is the moisture content of the concrete, and that other parameters should be considered as of secondary importance.

In other conclusions(22), it has been reported that many properties of concrete experience major changes at low temperature because of the influence of moisture content. The changes occur at a rate which is governed by the pore structure. Rostasy and Wiedemann(23) reported that the strain increased to a maximum on cooling between $-20\,^{0}C$ and $-50\,^{0}C$ in saturated samples. Between these temperatures most of water nucleation of supercooled water takes place(24). As the temperature decreases further, the strain diminishes and the specimens contract. They have also

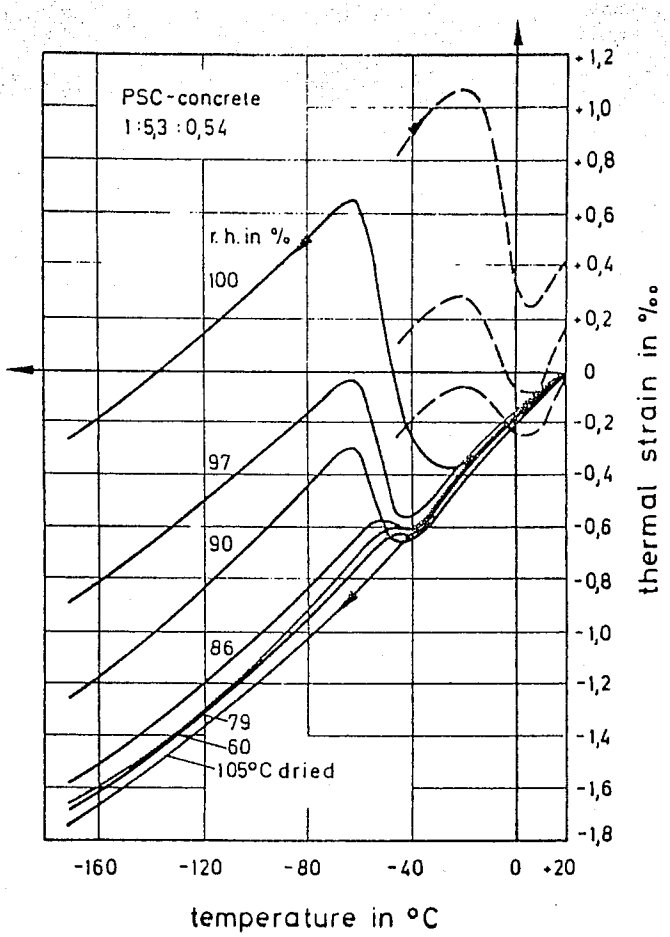

Fig. 1.1
Thermal strains of concrete with variable equilibrium moisture content as a function of temperature
(Reference 23)

reported(23) that the peak of the strain increases as the relative humidity increases while in dry specimens there was no expansion at all. On rewarming to room temperature, the specimens had been expanded permanently. This permanent expansion is larger for the paste with larger water-cement ratio, as shown in figure 1.1.

Planas et al(25) reported that for concrete paste which shows thermal strain on cooling with liquid nitrogen vapour and has shown a hysterisis on rewarming, the strain decreases almost linearly under a compressive stress. On a "prestressed" concrete sample they also found that a similar characteristic happened. The strain curves are shown in figure 1.2. However, in their experiments the strain, which was measured, was parallel to applied stress. No lateral dilation of the samples was measured. Therefore, this must does not necessarily mean that the compressed or loaded concrete paste does not experience thermal strain on cooling.

On permeability properties, Hanaor and Sullivan(26) recently have obtained a paste with a permeability coefficient as low as $5x10^{-19}$ sq.metres. They have said that by using lightweight and round shape aggregates,there maybe the possibility of achieving a

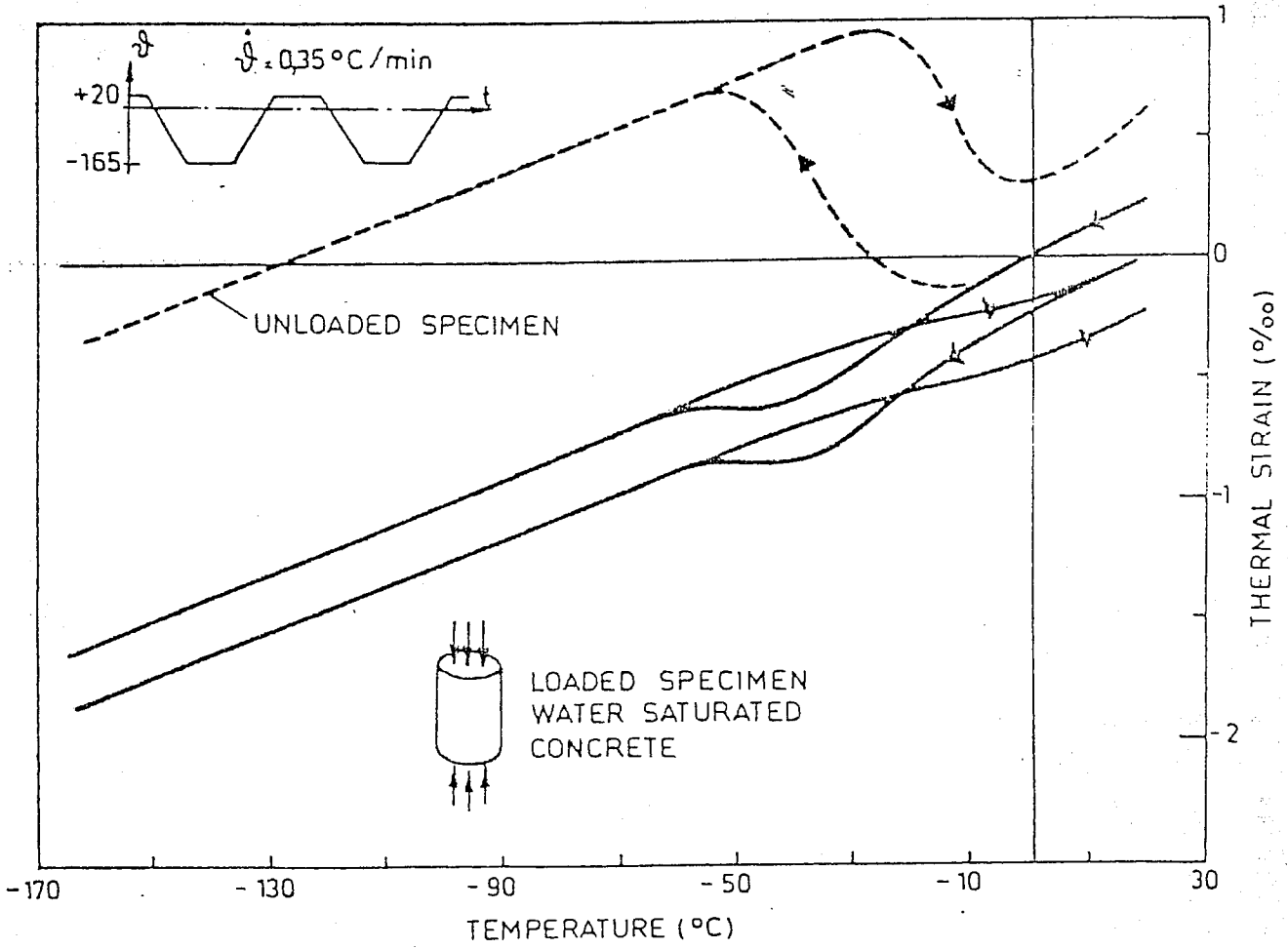

Figure 1.2: Thermal strain of a loaded concrete sample.
(Reference 25)

coefficient of permeability at around 10^{-20} sq.metres which is suitable for use in cryogenic storages. They also published micro photographs of concrete paste with irregularly shaped aggregates; on cooling, this paste had suffered microcracks around the aggregate particles. Thus cracks might be expected to increase the permeability of the paste.

It has been reported(28) that to achieve a concrete structure which is impermeable to LNG, a concrete of one metre thickness with coefficient of permeability at around $3x10^{-20}$ sq.metres should be used. Based on their calculations, this structure can prevent completely a 25 metres head of LNG from penetrating into the concrete paste over a period of 30 years. They claimed that a permeability which was **less** than $3x10^{-20}$ sq.metres had been achieved by using an air entrained lightweight aggregate concrete paste.

Lastly, on the state of water in concrete paste, it has been reported(27) that only some of the physically adsorbed water freezes over the whole range between $0^{0}C$ and $-60\ ^{0}C$.They also mentioned that in concrete paste there is a rewetting water most of which freezes over a narrow temperature range just below 0 degree celcius.

CHAPTER TWO

THE FREEZING OF WATER

2.1 GENERAL

We have discussed how the effects of moisture on the properties of concrete paste at low temperatures is associated with the freezing of water. Let us now look at some of the important physical properties of water in relation to the freezing of water.

Bulk water in its purest state freezes at 0 ^{0}C at one atmosphere pressure. However, in small quantities it may freeze between 0^{0}C and -80^{0}C and form ice crystals which are called hexagonal ice. Cubic ice crystals are only formed when water freezes on a substrate at temperatures between -80 ^{0}C and -130^{0}C, whilst lower than -130^{0}C water freezes into vitreous ice. Thus, in the scope of this study only hexagonal ice crystals are produced. Another eight forms of ice crystal(29) can also be produced at very high pressure, which is unlikely to happen in the concrete paste.

When water freezes, its density decreases

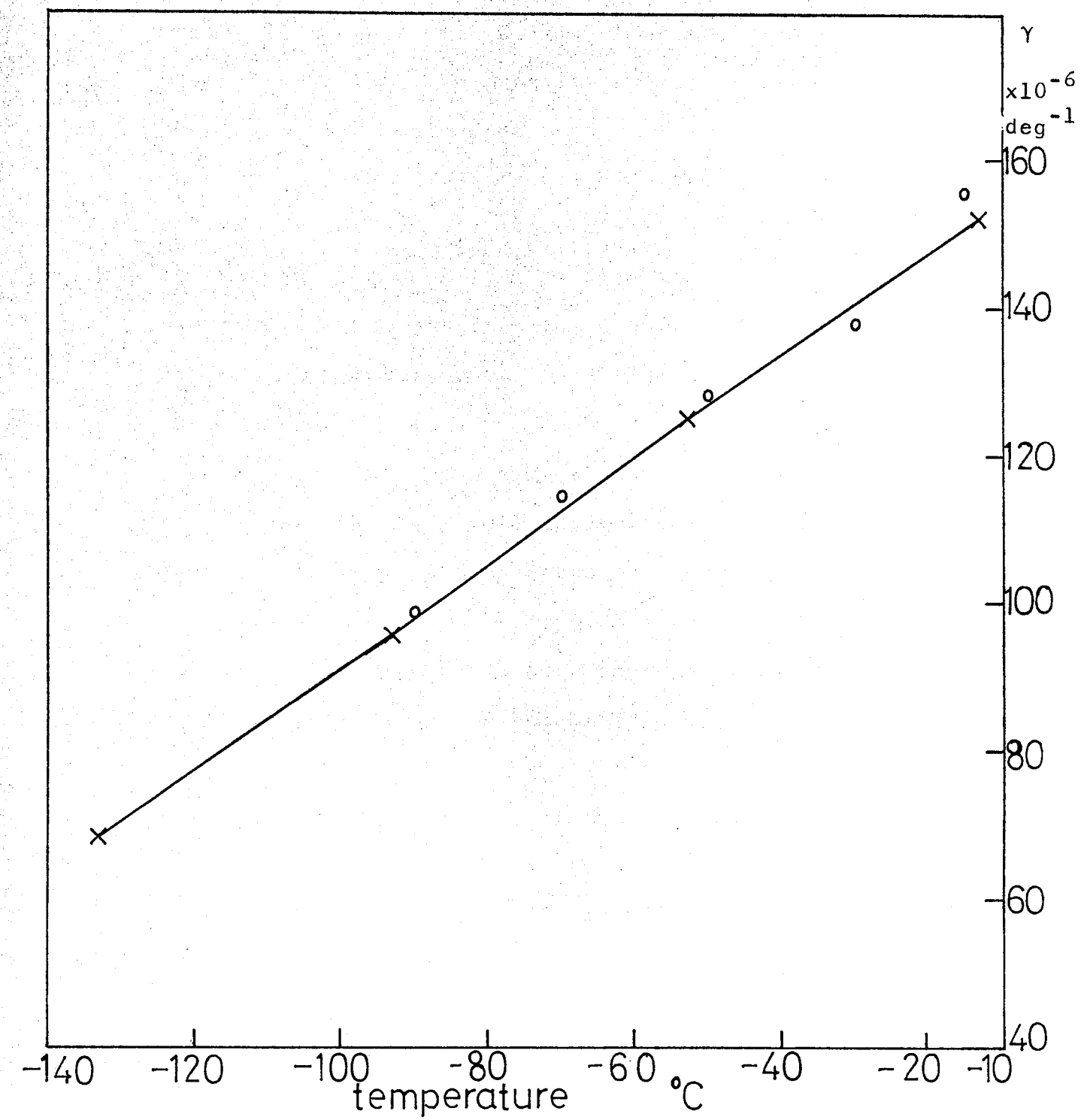

Figure 2.1 : Coefficient of Cubical expansions of ice γ against the temperature:o data from Eisenberg and Kauzmann; x from Powell and Dantl

from 0.9998 gm/c.c. to 0.917 gm/c.c. and there is a volume increase of 8.3%. However, it has been reported(45) that the density of ice increases to 0.927 gm/c.c. when it is cooled down to $-90\,^{0}C$.

The coefficient of linear expansion and of cubical expansion of ice decrease when the temperature is lowered. Figure 2.1 shows the coefficient of cubical expansion of ice between $-10\,^{0}C$ and $-140\,^{0}C$. The data was taken from Powell(30), Dantl(31) and Eisenberg and Kauzmann(32).

The compressibility of ice, which is defined as the fractional change in its volume per unit change in applied hydrostatic pressure, either at constant temperature (isothermal compressibility) or adiabatically, decreases as temperature decreases. From Hobbs(29), data for the adiabatic compressibility (κ_a) decreases by 8.6% when the temperature is lowered from $-13\,^{0}C$ to $-93\,^{0}C$. Dantl has deduced an expression for the adiabatic compressibility according to the following equation and is shown in figure 2.2.

$$\kappa_a = 11.94(1+1.653\times10^{-3}t_c+3.12\times10^{-6}t_c^2)\pm15\% \qquad (2.1)$$

where the unit is in 10^{-6} bar^{-1} and t_c is the temperature.

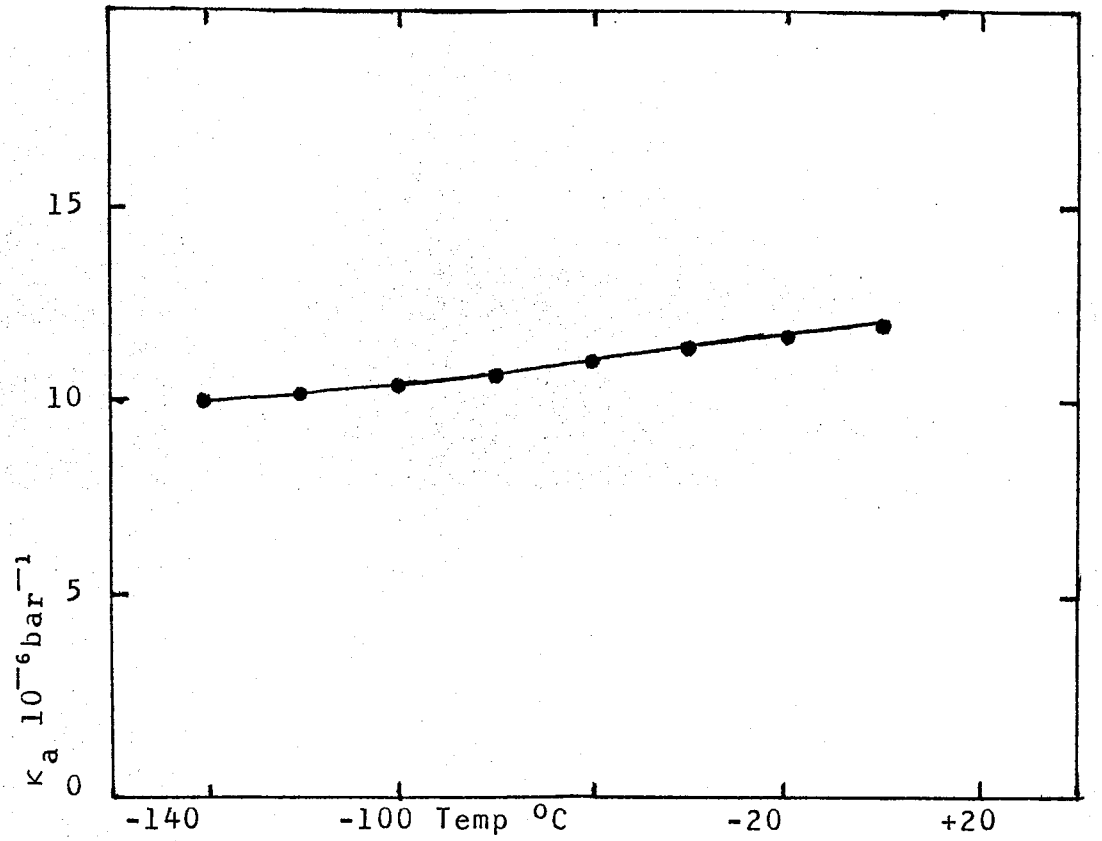

Figure 2.2: The adiabatic compressibility of ice

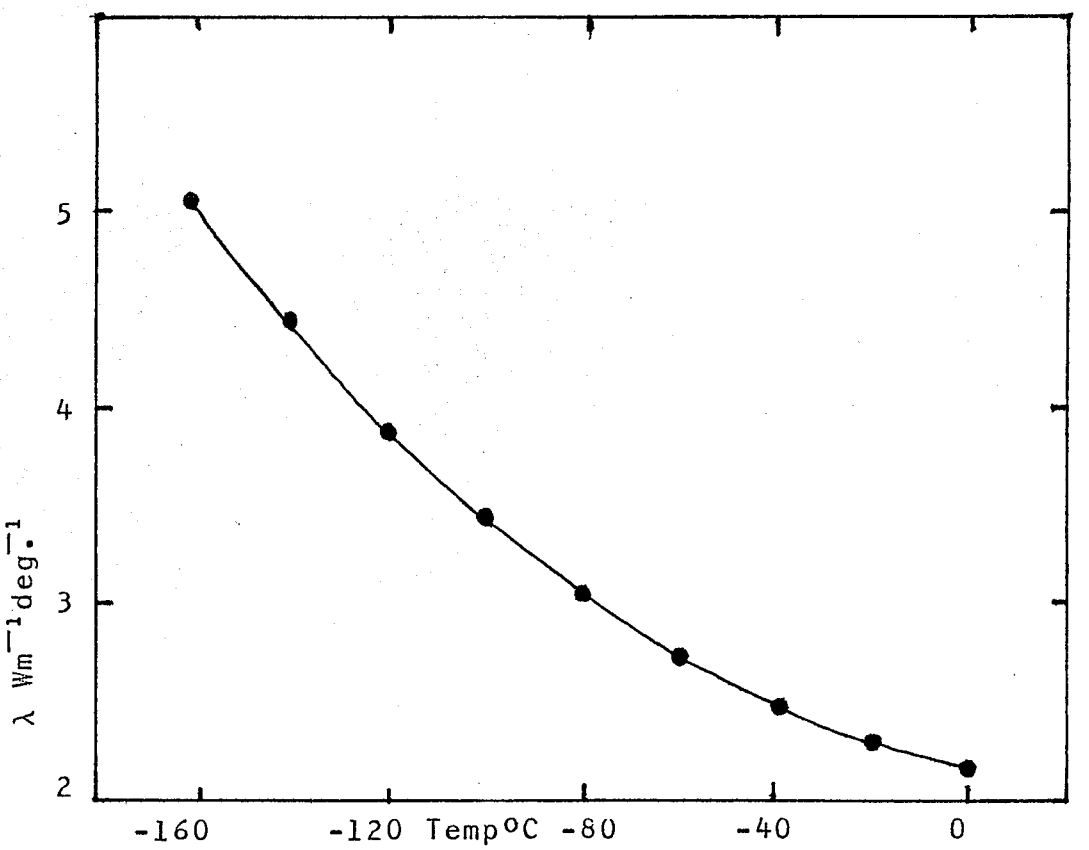

Figure 2.3: The thermal conductivity of ice

With reference to the thermal conductivity of ice, it has been reported(34) that on decreasing the temperature from -20^0C to -60^0C, the coefficient of thermal conductivity increases by 1 $Wm^{-1}deg^{-1}$. The variation of the coefficient of thermal conductivity with temperature was represented empirically later by Hobbs(29) as in the following equation,

$$\lambda = 2.1725 - 3.403\times10^{-3}t_c + 9.085\times10^{-5}t_c^2 \qquad (2.2)$$

where the unit of λ is in $Wm^{-1}deg^{-1}$ and t_c is the temperature in degree celcius. This formula only applies to the value of within the temperature range between 0^0C and $-165\ ^0$C. The plot of the formula is shown in figure 2.3.

Water, when changing phase into ice gives out a latent heat which is defined as the change of enthalpy when unit mass of ice is converted isothermally and reversibly into liquid water. The best value of the latent heat has been measured by Rossini et al(35), and is equal to 333.5 kJ per Kg of ice at 0^0C Hobbs(29) states that the latent heat of fusion of ice decreases by 29.6% when the temperature is lowered down to -22^0C.

Lastly, we look at the specific heat

capacities of ice, i.e. c_v and c_p which is the specific heat at constant volume and constant pressure respectively. These specific heat capacities are related to each other by the thermodynamic relation below.

$$c_p - c_v = (\gamma^2 VT)/\kappa_T \qquad (2.3)$$

where V is the specific volume of the solid ice, κ_T and γ are the isothermal compressibility and the coefficient of cubical expansion of ice respectively, and T is the absolute temperature. The derivation of equation 2.3 is in appendix D.

Measurements of the heat capacity of hexagonal ice at constant pressure over the temperature range 15 ^{0}K to 273 ^{0}K have been made by Giauque and Stout(71) and are shown in figure 2.4. At the melting point of ice the specific heat is about 37.5J $mol^{-1} deg.^{-1}$ and decreases with decreasing temperature.

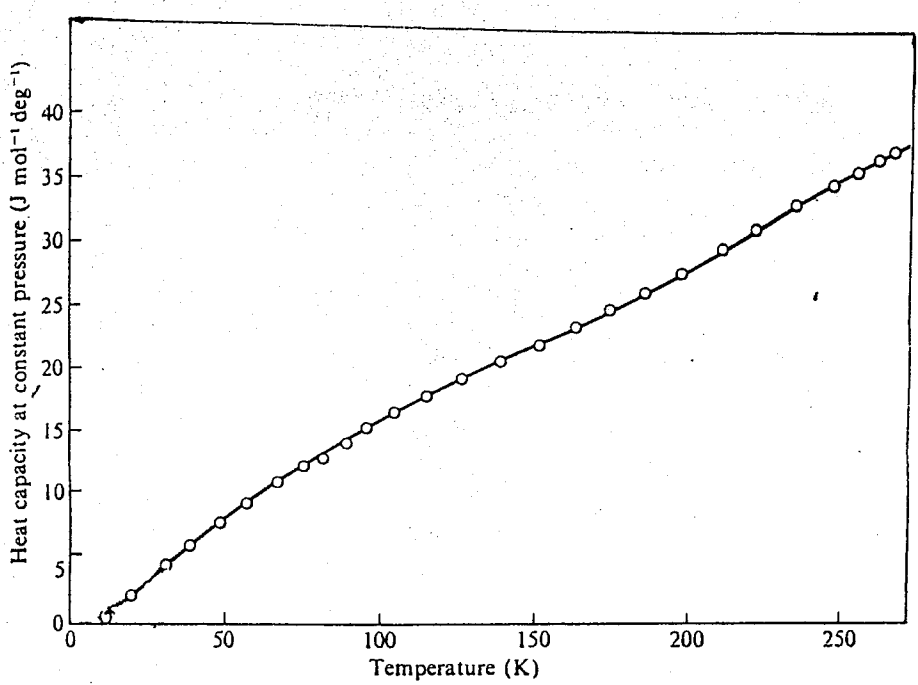

Figure 2.4: Heat capacity of ice at constant pressure (C_p) as a function of temperature. (Ref.71)

2.2 THE NUCLEATION OF ICE

2.2.1 HOMOGENOUS NUCLEATION

Homogenous nucleation of ice is the nucleation without foreign influence on the formation of ice crystals. Therefore, the nucleation is only possible in deeply supercooled pure water.

One of the earliest observations of the nucleation was made by Rumpf and Geigl(36) on water droplets of radius 2 to 3 μmetre, which solidified at -35 ^{0}C. Later, Cwilong(37)and Mossop(38), working with better equipment, observed that the nucleation of ice occurred at -40^{0}C for a droplet size of one μmetre. Then Pound et al(39), based on their own observations, reported that supercooled pure water droplets may freeze between -36^{0}C and -42 ^{0}C. We therefore conclude that homogenous nucleation of ice may happen between -35^{0}C and -42^{0}C.

The theory of homogenous nucleation by Fletcher(24) was based on a model of "flickering clusters"(40) assuming that the cluster consists of two groups of molecules, those belonging to hydrogen bonded molecules and those which are unbonded. Nemethy et al(40) calculated the number of the molecules and found

that 30% are bonded and 24% are unbonded, while the rest are in a mixed state. However, they said the number of these molecules is fluctuating because in supercooled water, the process of formation and disintegration of the bonded molecules occurs continously. This group of molecules is the initial group or the embryo of ice nucleation. Nucleation may only take place when the size of the embryo increases beyond a certain critical radius.

From Turnbull and Fisher(41) the nucleation rate J_{LS} of ice embryos which can grow spontaneously into ice crystals, per unit volume of supercooled water in a unit time, is given in equation (2.4).

$$J_{LS}=(n_L kT)/h \exp(-\Delta g/kT) \exp(-\Delta G_B/kT) \qquad (2.4)$$

The derivation of the equation is in appendix A. From appendix A, the total free energy ΔG_{LS} of the system can be written as the equation 2.5.

$$\Delta G_{LS}=Ai^{2/3} -Bi \qquad (2.5)$$

where i is the number of molecules, A and B are quantities which are dependent on the surface free

energy of the ice-water interface and the bulk free energy difference between supercooled water and ice respectively. Figure 2.5 shows the variation of the total free energy of supercooled water with the number of molecules i in an ice embryo. The total free energy ΔG_{LS} required to form ice embryos increases sharply as i increases but after ΔG_{LS} reaches a critical value when the embryos contain i_B molecules, the energy decreases indefinitely. Therefore, for the value of i smaller than i_B , the bonded molecules in the clusters are unstable and tend to disappear. But when the number of molecules in the clusters are enough to give the total free energy equal to ΔG_B, the clusters quickly develop and form ice crystals.

Theoretical calculations of the nucleation temperature from the above theory have been made by many people(24,29). By assuming the cluster shape as spherical they found the nucleation temperature for droplets of a few μmetre in radius must fall within the range -20^0C and -50^0C.

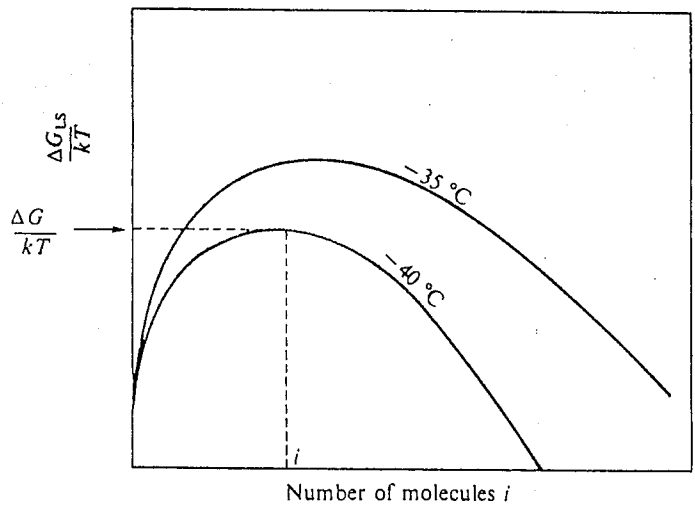

Figure 2.5: Change in the free energy ΔG_{LS} of supercooled liquid water due to the formation of an ice embryo containing i molecules.(ref.29)

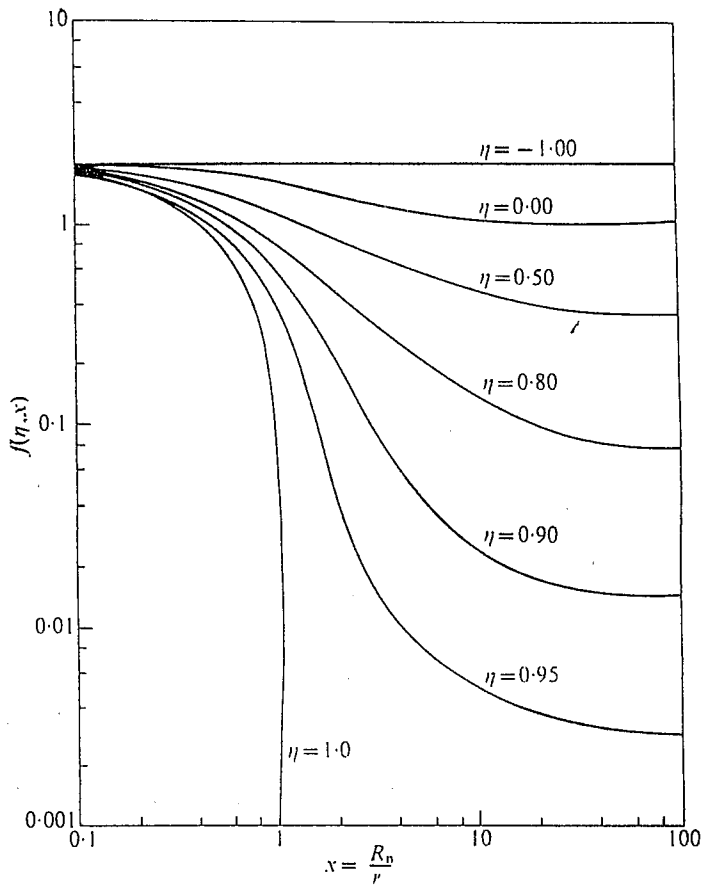

Figure 2.6: The geometrical factor f(η,x) in terms of the ratio $x = R_n/r$ (reference 29)

2.2.2 HETEROGENOUS NUCLEATION

The theory of heterogenous nucleation on foreign nuclei, such as dust particles, can be developed in a similar way to that of homogenous nucleation except that the free energy barrier $\Delta G_B'$ in heterogenous nucleation takes the form as in equation 2.6.

$$\Delta G_B' = \Delta G_B f(\eta, x) \tag{2.6}$$

where ΔG_B is the total free energy of the homogenous nucleation. $f(\eta, x)$ is a function which depends on the details of the geometry of the ice cluster and the foreign particles suspended in the supercooled water. x is the dimension of the particle and η is a ratio of surface free energies as given by equation 2.7.

$$\eta = \frac{\sigma_{particle/water} - \sigma_{particle/ice}}{\sigma_{ice/water}} \tag{2.7}$$

Figure 2.6 shows the variation of the function $f(\eta, x)$ with and the geometry factor. The factor $f(\eta, x)$ is given algebraically by Fletcher(55) in equation 2.8.

$$f(\eta,x) = 1 + \left(\frac{1-\eta x}{g}\right)^3 + x^3\left(2 - \frac{3(x-\eta)}{g} + \left(\frac{x-\eta}{g}\right)^3\right) + 3\eta x^2\left(\frac{x-\eta}{g} - 1\right) \tag{2.8}$$

where $g = (1+x^2-2\eta x^2)^{\frac{1}{2}}$

x is the ratio of the particle radius (assumed to be a sphere) to the critical size of the ice embryo at which the total free energy is equal to ΔG_B.

The value of equation 2.8 is always less than unity and may approach zero. Therefore, the total energy barrier $\Delta G'_B$ is less than ΔG_B; thus, heterogenous nucleation is much more likely to happen than homogenous nucleation, in the presence of nucleating particles.

2.2.3 EFFECT OF COOLING RATE

Figure 2.7 which is from Vali and Stansbury (42),shows the distribution of frozen droplets of distilled water plotted against temperature for two different rates of cooling, i.e. at 0.5 degree celcius per minute and 2.0 degree celcius per minute. The slopes of both graphs are closely the same which indicates that the distribution of freezing temperature has no effect on the rate of cooling.

However, when taking the mean temperature

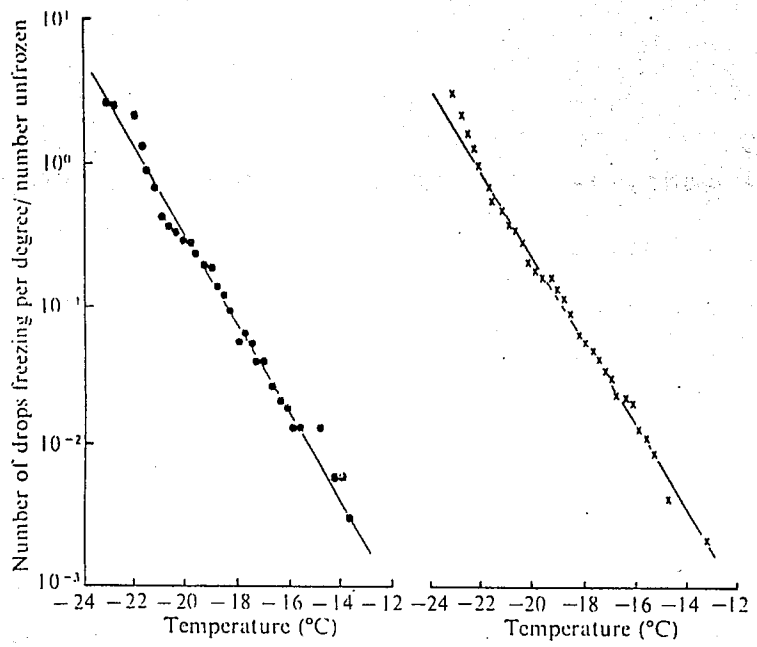

Figure 2.7: The probability of freezing as a function of temperature for distilled water drop cooled at a steady rate.● -cooling rate=0.5°C/min. X-at 2.0°C/min. (reference 42).

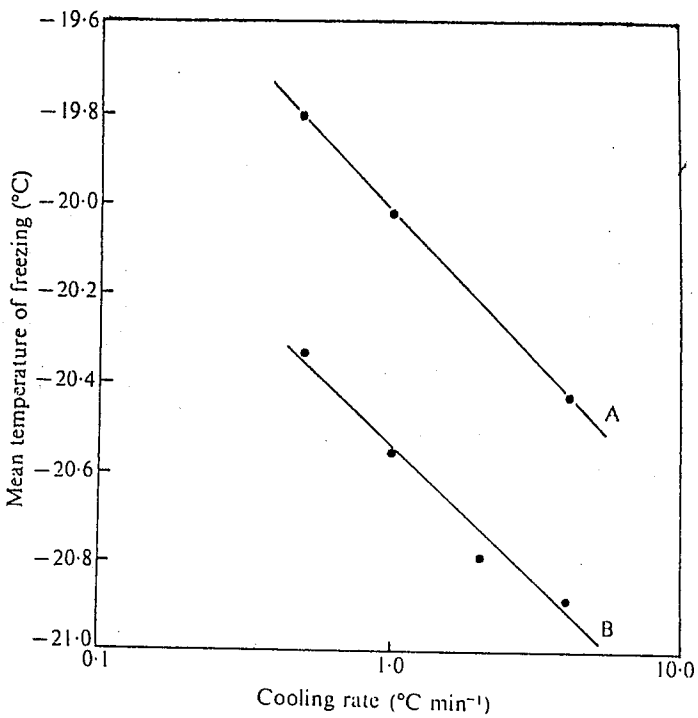

Figure 2.8: The variation of the mean temperature of freezing with the rate of cooling. Lines A and B are for two sets of experiments.(ref.29)

of freezing of groups of the droplets,they found that an increase in the rate of cooling by tenfold will depress the freezing point of the supercooled water by 0.65^{0}C.

Figure 2.8, line A

and line B

show that the cooling rate has some effect on the freezing temperature of the system.

Carte(43) also reported that when the rate of cooling was increased from 2^{0}C per minute to 20^{0}C per minute, the freezing points of 3 different sizes of droplets were depressed by 0.5^{0}C.

Thus,while the cooling rate has some effect on the freezing point of water, the depression of the temperature is very small and negligible, at the cooling rates applicable to the concrete samples.

2.2.4 EFFECT OF DROPLET SIZE

Figure 2.9 and 2.10 show the freezing temperature of droplets against the droplet diameters for homogenous and heterogenous nucleation of ice respectively. Droplets with smaller diameter freeze at lower temperatures in both types of the nucleation.

Looking at figure 2.10, data from Biggs

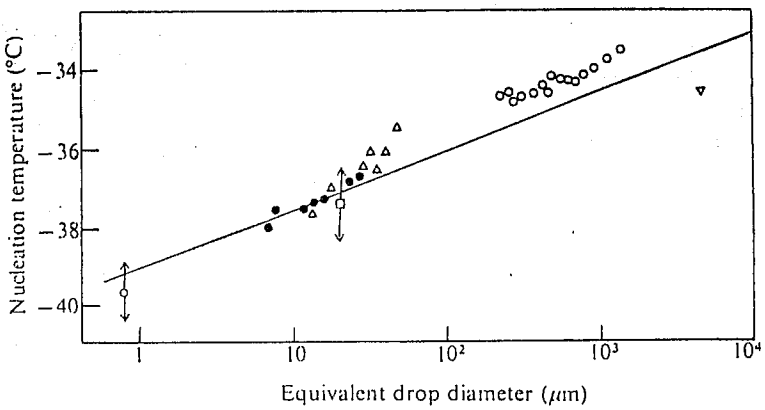

Figure 2.9: Temperature for 95% probability of nucleation at a cooling rate of 0.5°C/min. plotted against the diameter of sphere having same volume as sample. ● Carte(1956), ○ Mossop(1955), △ Bigg(1953), □ Schaefer(1952), ▽ Bayardelle(1955). (ref.43).

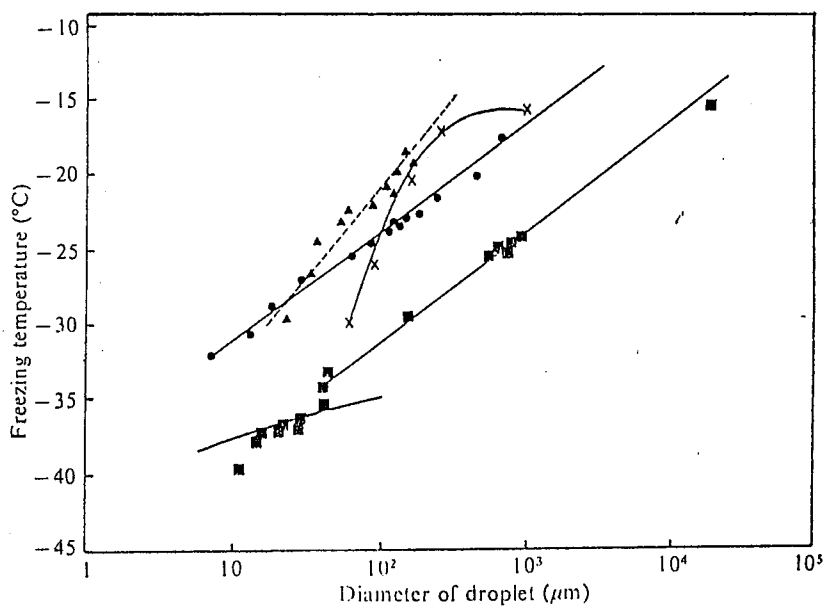

Figure 2.10: Freezing temperature of water drops as a function of their diameters. ▲ Hosler(1953), × Haverly(1949), ● Dorsch and Hacker(1950) ■ Bigg(1953). (reference 29).

shows nucleation temperatures of the droplets are much lower than the others. This is because in Biggs experiments, the droplets were protected from airborne contaminants, leading to either heterogenous nucleation at the higher temperatures, or homogenous nucleation at the lower temperatures. Hobbs(29), has reported that these data agreed with the relation shown in equation 2.9.

$$\ln(1/V) = aT_s + b \qquad (2.9)$$

where V is the volume of the droplet, T_s is the supercooling required for 50% freezing and a is equal to $1/\tau_o$ where τ_o can be found in equations 10.18, 10.20 and 10.24 which characterizes the nucleating ability of the ice nuclei. b is a constant related to the constant term of equations 10.20 or 10.24 in appendix B.

It has been reported that(29) in Biggs' data (figure 2.10) for droplet diameters smaller than 30 μm, the nucleation temperature which he had measured was in fact that for homogenous nucleation. The nucleation temperature for these size of diameters was between -35^0C and -40^0C. Therefore, for droplet diameters of less than 30 μm, and under suitable freezing

conditions, it appears that the nucleation of ice can only happen through homogenous nucleation when the temperature will lie between -35^0C and -40^0C.

It would appear that water in droplet form will always freeze above -40^0C. Whether this conclusion can be applied to water in concrete is not clear; if no, it would contradict the predictions of Helmuth(15).

2.2.5 EFFECT OF THE NATURE OF THE SURFACE

Carte(43) has reported observations on hundreds of water droplets on six different surfaces which froze at different temperatures. He thereby showed that the freezing temperature of supercooled water is dependent on the nature of the surface.

He also found that water droplets on metal surfaces freeze at a higher temperature than on a non-metal surface. In addition, water droplets on a polished surface freeze at a lower temperature than on an unpolished one. Thus, the roughness of the surface also contributes to the distribution of the freezing temperature. However, the lowest freezing temperature attained by some of the droplets was independent of the nature of the surface. In Carte's experiment, the

lowest temperature of freezing attainable by the droplets was -38 ^{0}C and it is believed that it was caused by the homogenous nucleation.

The ability of ice to nucleate on some mineral dust has been investigated by Mason and Maybank(46). From 28 substances of naturally-occuring mineral dusts, they have found that 19 substances, which are mainly silicates of the clay and mica groups, are effective ice nuclei at -18 ^{0}C. They also found that some of the silicate substances, once having been involved in ice-crystal formation, become more efficient as ice nuclei. i.e. they can be pre-activated. Particles of montmorillonite, an important constituent of clays,are initially inactive even at -25^{0}C, but once they have become ice nuclei,they can become ice nuclei at the considerably high temperature of about -10^{0}C.

The ability of copper sulphate particles to form ice nuclei is very low. Hobbs(29) reported that ice can only be produced when the temperature of the droplets was lowered to at least -20^{0}C.

Generally the substances which are effective ice nuclei have similar characteristics to the crystal structure of ice. Fukuta(47), based on his own experimental results, concluded that there is no water

soluble salts which form effective ice nuclei at temperatures above -11^0C except the crystals with close similarities to ice such as silver iodide.

2.2.6 HEAT BALANCE IN THE FREEZING OF WATER DROP

When a supercooled water drop which is in equilibrium with its environment, is nucleated, a fraction dm of the mass of the drop freezes and a latent heat L_f is released. The heat raises the temperature of the whole drop by ΔT. If the original supercooled temperature is T_s and c_w is the specific heat of the liquid, then,

$$\frac{dm}{m} = \frac{\Delta T c_w}{L_f} = \frac{(T-T_s)c_w}{L_f} \qquad (2.10)$$

In the first stage of freezing, the drop freezes at the surface. The latent heat evolved is taken up by the unfrozen part of the water and raises its temperature to the freezing temperature. The unfrozen part of the water drop cannot freeze further until the energy is released to the environment.

During this second stage of the freezing, the frozen part which enclosed the unfrozen water, moves

inwards. As the freezing continues, a form like a shell thickens and a pressure builds up in the drop causing the shell to change shape, crack and eject unfrozen water.

The speed and the manner, in which the ice shell moves inwards are determined by the rate at which heat exchange takes place with the environment. The heat released by the frozen water is taken up by the environment by two processes, (1): the thermal transfer process which includes conduction, convection and radiation and (2): the sublimation process.

The sublimation process is defined as a reversible change of ice into water vapour at constant temperature, and releases a latent heat of sublimation L_s. The heat loss through the drop in temperature of the water compared with the heat loss by these two processes is negligible(29). Therefore, we can write the heat balance of the freezing as in the following:

$$L_f \frac{dm_i}{dt} = q_h + q_m \qquad (2.11)$$

where q_h is the rate of heat loss by the thermal process and q_m is the rate of heat loss through the sublimation process or mass transfer. For a spherical drop the

values of q_h and q_m are given in equations 2.12 and 2.13 respectively.

$$q_h = 2\pi r \lambda_e (T_d - T_e) Nu \qquad (2.12)$$

$$q_m = 2\pi r L_s \frac{P}{P-e} D(\rho_d - \rho_e) Sh \qquad (2.13)$$

where,

λ_e= the thermal conductivity of the environment.

T_d= the surface temperature of the drop.

T_e= the environment temperature.

Nu= the Nusselt number.

P = the total pressure.

e = the partial pressure of the water vapour.

D = the diffusion coefficient of water vapour in the environment.

ρ_d= the density of water vapour at the surface.

ρ_e= the density of water vapour in the environment.

Sh= the Sherwood number (analoques to Nu for the mass transfer).

r = the radius of the drop.

The freezing of water on a substrate was

briefly discussed by Brownscombe and Hallet(59). In the initial stage of freezing, the drop deforms into the shape of a spherical cap of height h and base radius a. The temperature of the ice particles remains at T_e, the environment temperature, until the temperature of all parts of the drop has fallen to the freezing temperature. Then in the second stage, the temperature of the drop remains at the freezing temperature until the drop is completely frozen. Thus the heat transfer Q can be written as in equation 2.14.

$$Q = \pi\lambda a(T_d - T_e) \qquad (2.14)$$

where λ is the thermal conductivity of ice and T_d is the temperature of the drop.

Hobbs(29) has reported that the heat loss in the freezing of a drop by the thermal process is very little compared with the heat loss through the ice substrate. Consequently, a drop of water on a substrate will freezes in a direction outwards from the substrate. The following table 2.1 shows the values of heat transfer q_h and mass transfer q_m for a drop 1 mm in diameter freezing in natural convection of air at -10^0 C and -20^0 C and also the value of Q for a drop of the same diameter.

(In unit $10^{-3} Js^{-1}$)

Environment at temperature	q_h (thermal)	q_m (sublim.)	$q_h + q_m$ (total)	Q (substra.)
-10^0C	1.81	1.30	3.11	37.70
-20^0C	3.62	1.33	4.95	81.68

Table 2.1: Heat losses by thermal transfer compared with heat losses through substrate.

CHAPTER THREE

NUCLEAR MAGNETIC RESONANCE STUDIES OF WATER

3.1 INTRODUCTION

The determination of water in substances by nuclear magnetic resonance is not a new technique. It has been utilized in the studies of foods, soils and also in studying the structure of inorganic and organic compounds.

The characteristic of an NMR spectrometer is its unique ability to single out hydrogen nuclei in a substance and to give some information or the state of binding of the nuclei in the substance. Figure 3.1 shows an example of the NMR spectrum of ethyl alcohol which has 3 peaks corresponding to the three states of binding of hydrogen in the alcohol.

In a similar way, NMR is also suitable for the determination of the state of water in the concrete paste.

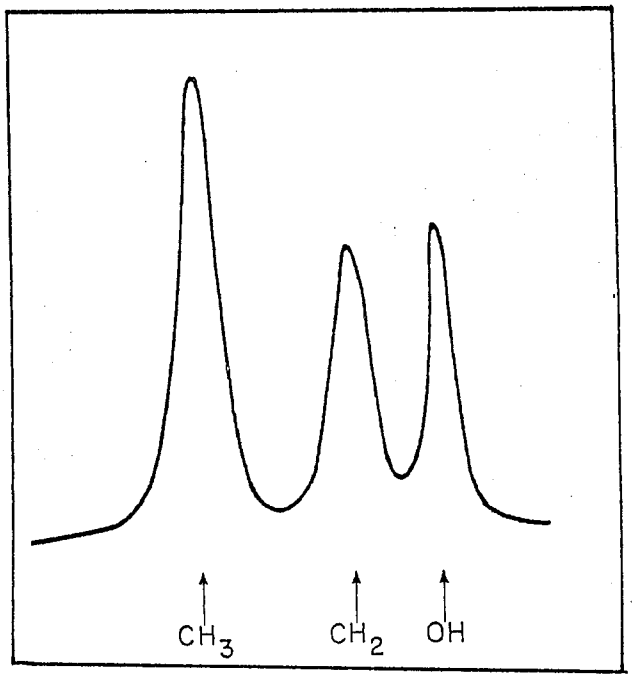

Figure 3.1: The nuclear magnetic resonance absorption spectrum of Ethanol. Showing the three peaks corresponding to three types of chemical binding of hydrogen atoms. (Ref. 54)

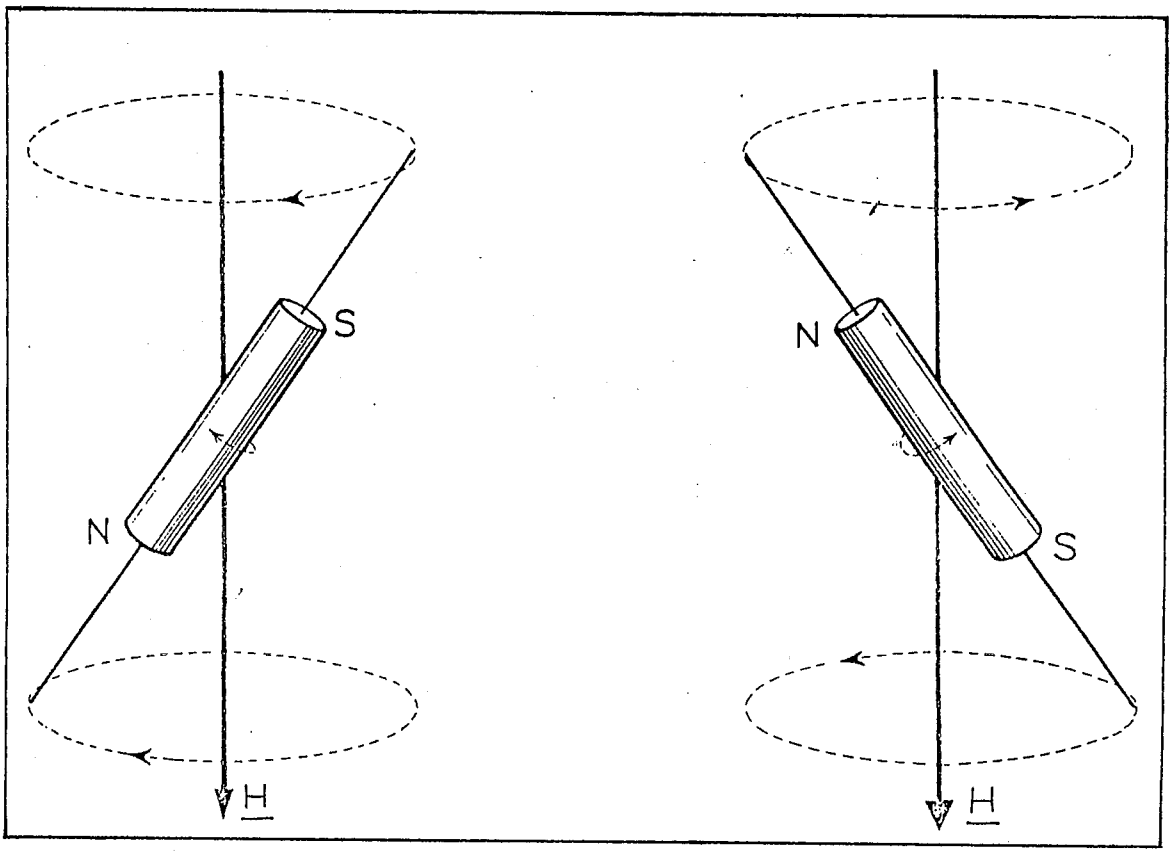

Figure 3.2: The two orientations of a spinning proton in a magnetic field. The orientation on the left represents the normal state and the one the right, the excited state. (Ref.54)

3.2 PRINCIPLES OF NMR MEASUREMENTS

All odd mass number nuclei possess angular momentum or spin of total magnitude $hI(I+1)^{\frac{1}{2}}$, where h is the reduced Plank constant, and I is the nuclear spin quantum number which may have integral or half integral values. For the hydrogen nucleus or proton, I=1/2 and for isotopes with no spin, I=0.

Quantum theory demands that the allowable nuclear spin states are quantised and the angular momentum quantum number M_I, takes the values I,I-1,I-2,...,-I, so that there are 2I+1 spin states of the nucleus. For the proton with I=1/2, M_I may only take the values of 1/2 or -1/2.

A nucleus with spin I also has an associated magnetic moment μ, arising from the effect of the spinning nuclear charge. This associated magnetic moment also has 2I+1 components with magnitudes given in equation 3.1.

$$\mu = \mu_o(I(I+1))^{\frac{1}{2}} \qquad (3.1)$$

where,

μ_o= the nuclear magneton = $(eh/4\pi m_n c)$.

e = the charge of the nucleus.

m_n= the mass of the nucleus.

c = the velocity of light.

In the absence of an external magnetic field, all of the spin states possess the same potential energy; but take different energy values when an external magnetic field is applied. The difference in the energy between these states in a magnetic field is used by the NMR technique.

Water molecules contain only protons and oxygen nuclei, where the oxygen nuclei have I=0 while the spin for the proton is equal to 1/2. With only 2 possible spin states. In the presence of an external magnetic field H_o, these protons will orientate themselves in these two possible ways as shown diagramatically in figure 3.2. The spin state 1/2 is parallel to the applied field and the spin state -1/2 is anti-parallel to the field. The energy difference between the two states is given in equation 3.2(48).

$$\Delta E = \mu H_o(\cos\theta_1 - \cos\theta_2) \qquad (3.2)$$

where θ_1 and θ_2 are the angles between the applied

magnetic field and the magnetic moment of the proton in the two states.

From the Bohr relation for spectral phenomena, we have equation 3.3.

$$h\nu = \Delta E \qquad (3.3)$$

Therefore,

$$\nu = \frac{\mu H_o}{h}(\cos\theta_1 - \cos\theta_2) \qquad (3.4)$$

From equations 3.1 and 3.4, we observe that the frequency of radiation emitted or absorbed during the transitions between the two states depends on the external magnetic field H_o and the mass of the proton. Since the emission or absorption of the energy is discrete for a particular proton, the transition can only take place at the correct frequency.

In order to detect the nuclear resonance frequency, a sinusoidally oscillating magnetic field H is applied to perturb the atomic system. The protons, which have a higher population in the lower energy state, are promoted to the higher energy states or excited states with a net absorption of energy. If the magnitude of the applied field is swept across the range

of the nuclear resonance, then a sharp absorption signal or spectrum is observed.

However, the shape of the spectrum is affected by the interactions of magnetic fields from neighbouring nuclei, electrons and also adjacents molecules.The interaction of magnetic fields from neigbouring nuclei and electrons, which is known as spin-spin interaction, makes the local magnetic field at the spinning nucleus vary from one point to another. As a result, the resonance frequency varies and instead of a sharp line, the absorption spectrum becomes broadened over a small range of frequency.

The effect of material structure and the state of binding of the protons on the range of resonance frequency or the "line-width" of the observed spectrum, can be explained as follows.

Atoms in solid are strongly bound and closely arranged, so that the influence from the magnetic field of adjacent atoms is relatively large and the absorption spectrum is shallow and broaden.

On the other hand, molecules in liquids are loosely arranged and move randomly, so that the influence from the magnetic field of other molecules averages to zero. Thus, the proton NMR absorption

spectrum of liquids is sharp and narrow.

From the above discussions, we see that the area under the absorption spectrum gives a measure of the number of protons present, while the state of binding of the protons can be deduced from the line-width of the spectrum.

3.3 INTERPRETATION OF NMR SIGNALS

The line-width of the observed absorption spectra can be measured directly to give some measure of the degree of freedom of protons and their neigbouring atoms in a system. A narrow line- width corresponds to a higher degree of freedom such as the spectrum for free water which we shall discuss in the next section.

When an external magnetic field is applied ,the protons occupy a thermal distribution between the 2 magnetic states according to the Boltzmann distribution. On removal of the external magnetic field, the system will return to its original equilibrium condition. However, it takes a finite time to readjust or relax back to that original condition. The characteristic time taken is called the spin-lattice relaxation time T_1. This relaxation time is related to the environment of each particular proton. In a liquid, the molecules are moving rapidly and randomly, so that the effect of the magnetic field from other molecules averages to zero in the first order pertubation. The second order pertubation does not average to zero and provides a weak coupling between nuclei and the liquid lattice so that the relaxation time T_1 is large in a liquid.

The nuclei are also coupled together via the magnetic fields of their environment. The degree of coupling is characterised by the spin-spin relaxation time T_2. In solids the nuclei are coupled together very strongly because the effect of magnetic fields from neigbouring atoms is large. In a pure liquid, however, the average effect of the random motion of the liquid molecules provides a weak coupling between nuclei and the spin-spin relaxation time is large and of the same order of magnitude as T_1.

The spread of magnetic fields seen by each nucleus causes the absorption spectrum to extend over a finite range of frequency. This spread in frequency is called the line-width and is inversely proportional to the spin-spin relaxation time T_2. For the purpose of practical interpretation, T_2 is defined in relation to the line-width at intensity at the resonance frequency of the normalised absorption spectrum curve(20). The relationship between the line-width and T_2, is approximately given in equation 3.5

$$T_2 = (6.86 \times 10^{-5})/\Delta H \qquad (3.5)$$

where ΔH is in gauss. The derivation of equation 3.5 is

given in appendix C.

Thus, the amplitude of a normalised resonance spectra can give a measure of the number of protons in a system. After a suitable calibration by using a system of a known number of protons such as the very narrow line of free water, the quantity of water contained in the unknown system can be measured, in principle.

3.4 NMR SPECTRA OF LIQUID WATER AND ICE

Isolated protons should give a single line at the resonance frequency. In liquid water the effect of adjacent nuclei and the orbital electrons become obvious since the magnetic field from the neigbouring molecules are averaged to zero due to the Brownian motion. The value of the line-width in pure water has been calculated by Seligmann(20) to have a value of 2.7×10^{-5} gauss.

Molecules in ice are closely arranged in a tetrahedral structure and the bonds between them are much stronger. Thus, the NMR absorption energy of the protons has a large variation. Rabideau et al(56) have measured the line-width of several forms of ice, the

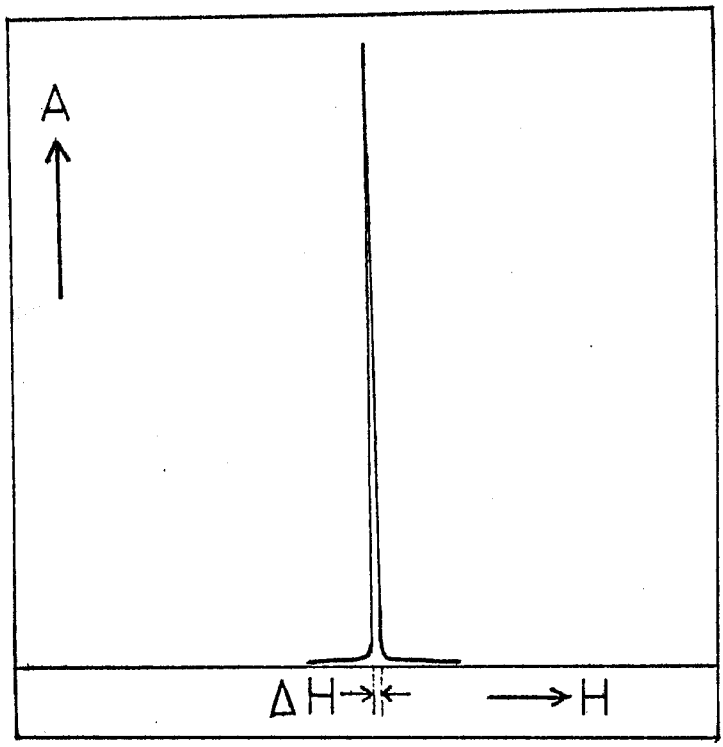

Fig 3.3 a: Spectrum of water

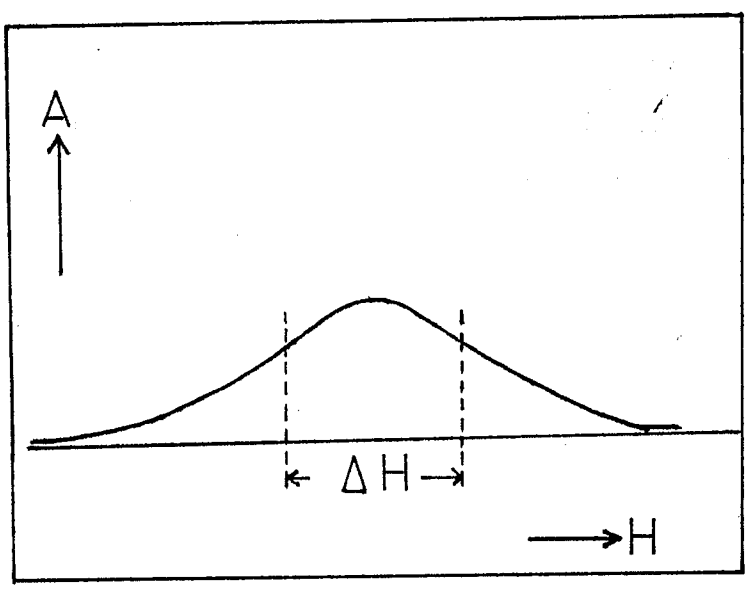

Fig 3.3 b: Spectrum of ice

smallest value they measured was for hexagonal ice, with a value of 16 gauss. Other forms of ice give greater values of line-width. Figures 3.3 (a) and (b) show the spectra of free water and ice respectively.

3.5 NMR STUDIES OF WATER IN POROUS MATERIALS

The state of water held in porous materials is the subject of study by NMR technique because of the ability of the shape of the observed spectrum to reveal the state of water.

Porous materials to be discussed here are almost similar, or at least have similarities with the characteristics of water being held in concrete paste. Blaine(50), has used the NMR technique to understand the state of water in some clay minerals, such as Kaolin, halloysites, sepiollite and illites. Others(20,51) have utilised the same technique in the study of water in silica gel and cement paste.

All the materials mentioned, are similar in that they are porous and have the ability to absorb water. The adsorbed water is subject to evaporation either by heating or as a result of in low humidity conditions at ambient temperature.

3.5.1 NMR STUDIES OF WATER IN CLAYS

Figure 3.4, 3.5 and 3.6 were taken from Blaine(50), and show the NMR spectra of kaolin, illite and pyrophyllite respectively. Spectra of kaolin samples clearly have 2 peaks. A narrow 1 gauss peak near the central resonance frequency while a broad and shallow one extends outside the central peak with a width of approximately 6 gauss. On evacuation for 3 days the sharp line peak of kaolin decreased to a certain limit. After heating for 18 hours at 100 ^{0}C the height of the central peak decreased further; the peak only diminished to a small size after the sample had been heated at 350 ^{0}C for another 18 hours. Throughout this treatment, the 6 gauss broad line did not change. What we can deduce is that the kaolin sample has strongly bound water which may be related to structural water. It also has physically bound water with varying degrees of binding energy as shown by the various stages of evaporation and heating.

In another sample of clay mineral, i.e illite, the spectrum which is shown in figure 3.5, had no obvious broad line peak as in kaolin, only a narrow 1 gauss peak. It was reported by Blaine(50) that on

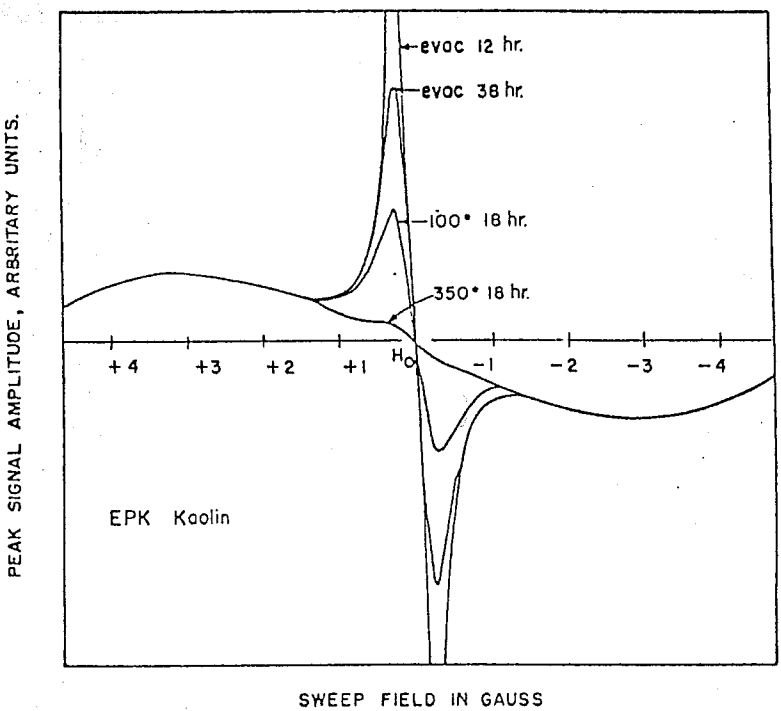

Figure 3.4: Derivative of absorption curves of kaolin sample after removal of various amounts of water. (Reference 50)

drying to 200^{0}C, the narrow peak diminished and a low peak with a line-width of 3 gauss appeared which suggests that, in illite, there is physically bound water which does not evaporate even at 200 ^{0}C. In pyrophyllite, after heating, the spectrum shows 2 peaks as shown in figure 3.6. The broad 3 gauss line corresponds to a structural water or chemical bound water and the narrow one with the line-width of 1 gauss, corresponds to strongly held physically bound water.

The line-width normally obtained with hydroxides or water of crystallization is about 8 to 11 gauss(50). Thus, in the above results, the kaolin broad line peak may be associated with chemical water while the narrow 1 gauss peak in kaolin, illite and pyrophyllite spectra arise from the strongly held physical water.

3.5.2 STUDIES OF WATER IN CALCIUM SILICATE PASTES

Heating calcium carbonate with silicon dioxide at a very high temperature will produces calcium silicate and β-calcium silicate. This is one of the basic processes in the making of cement. Therefore, it

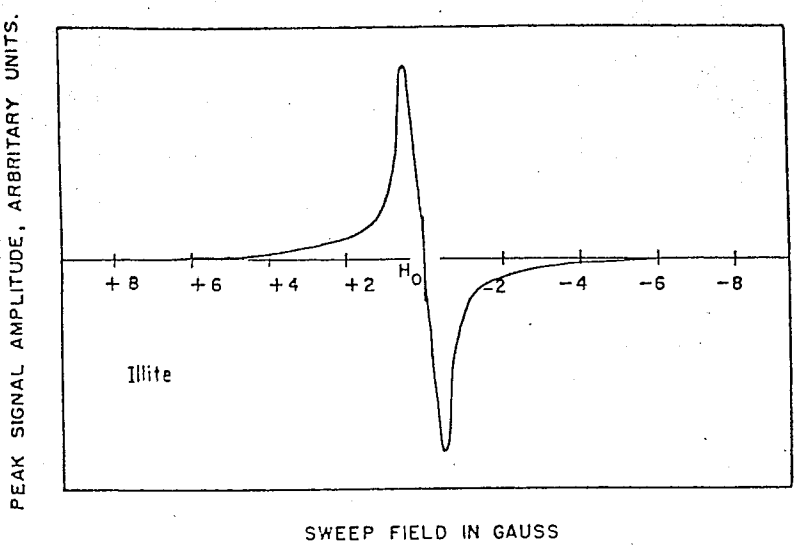

Figure 3.5: Derivative of absorption curve obtained on illite sample. (Reference 50)

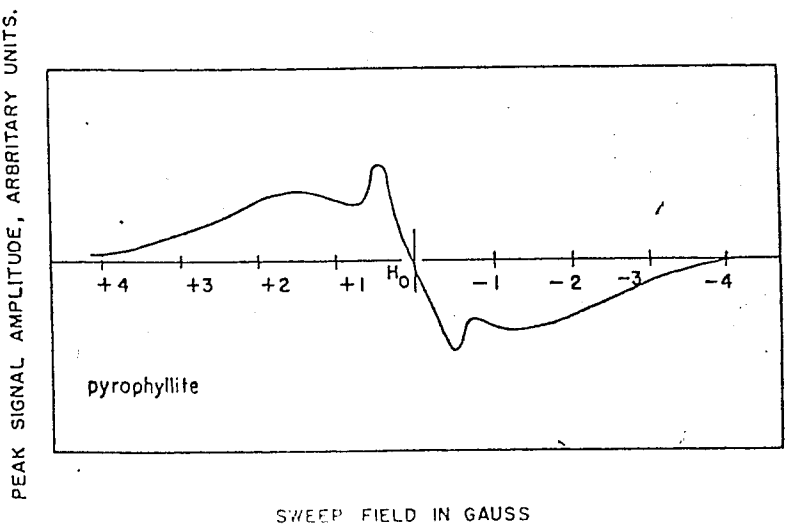

Figure 3.6: Derivative of absorption curve obtained on pyrophyllite sample. (Reference 50)

may be useful to know the characteristics of water present in the paste at low temperature because the water may have some similar properties to the one in concrete paste.

Ochiai et al(60) have reported that calcium silicate and β-calcium silicate pastes, which they made by heating a mixture of calcium carbonate and silicon dioxide several times at 1550 ^{0}C, showed 3 NMR peaks at low temperatures between -30^{0} and -80^{0}C. The plot of line-width of the spectra against temperature is shown in figure 3.7.

For control purposes, they also reported the characteristics of water in individual compounds of calcium hydroxide and silicon dioxide pastes. The similar plot for these compounds is shown in figure 3.8.

Figure 3.7 also shows the variation of line- width of the 3 peaks of calcium silicate and β-calcium silicate pastes which had been stored in water for 1 day and 20 days. All the three peaks co-exist at temperature -70 ^{0}C at the line-width of about 1, 10 and 17 gauss.

Figure 3.8 shows a similar pattern of line-width of the individual compounds. The line-width of ice at very low temperature is 16.5 gauss. Calcium

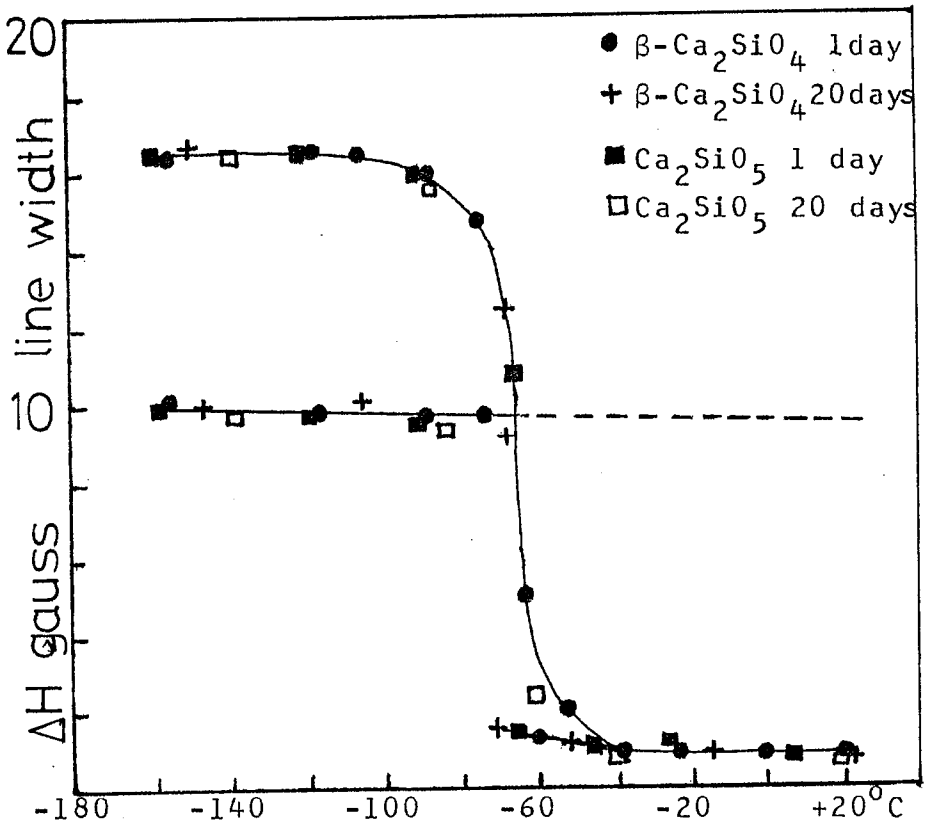

Fig 3.7: Line-width vs temperature for β-di- and tri-Calcium Silicate stored in water.

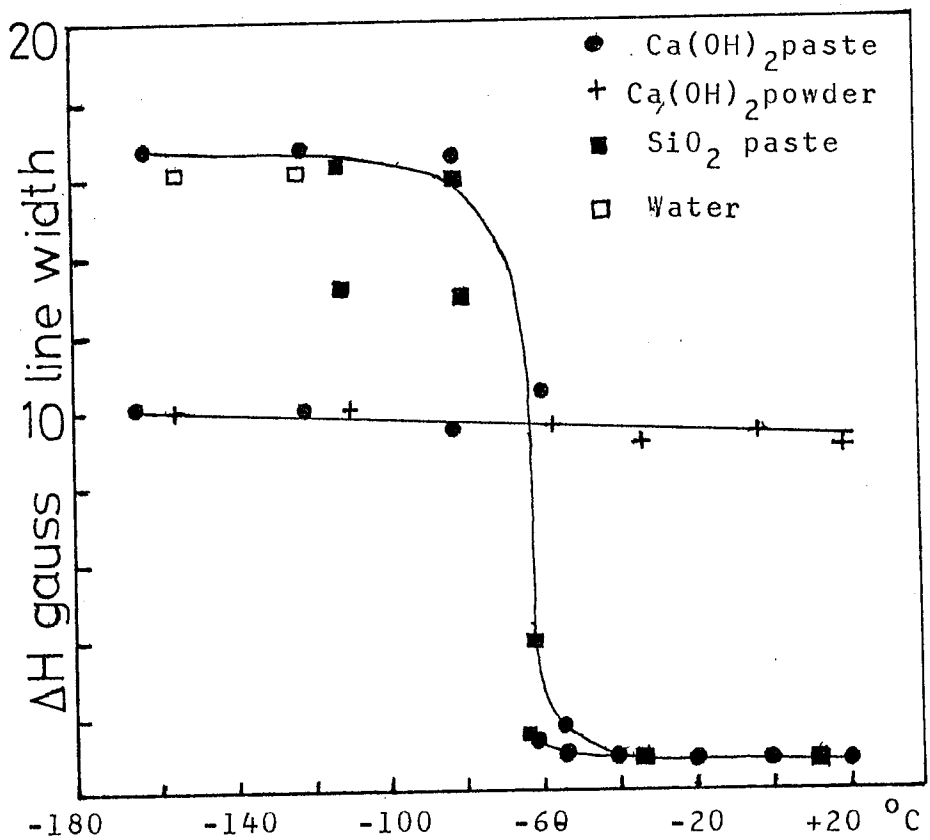

Fig 3.8:Line-width vs temperature for various reference samples.

hydroxide powder gives an absorption spectra of line-width 9.5 gauss with a little variation over the temperature range. Meanwhile, the hydrated calcium hydroxide paste has a similar line-width to calcium silicate paste at 10 gauss. Silicon dioxide paste gives a line-width at 13 and 17 which is almost similar to ice at low temperature.

Ochiai et al concluded that the 3 peaks observed were due to the 3 phases of water in the calcium silicate paste. i.e. solid ice at the line width of 17 gauss which only appeared below $-60\ ^{0}C$, hydroxyl ion at 10 gauss and adsorbed water molecules at 1 gauss.

From this conclusion, calcium silicate paste contains a chemically bound water, i.e. hydroxyl ion, adsorbed water and some free water which only freezes at very low temperature.

3.5.3 NMR STUDIES OF WATER IN CEMENT PASTE

First experimental studies on hardened cement paste by NMR technique were done by Kawachi et al(52) in attempting to understand the characteristics

of water in the hydration process of cement. These were followed by those of French and Warder(53), before the method was reviewed by Seligmann(54) for the study of water in hardened cement paste.

Seligmann(20) in investigating the state of water in cement paste utilized the spin-spin relaxation time parameter for various compounds, including some of the compounds contained in the cement paste. Table 3.1 shows the relaxation time T_2 and their corresponding line-width which were calculated from the relation in equation 3.5.

Table 3.1: Relaxation time and line-width of various substances.

State of water	T_2 relaxation time μsec.	Line-width H gauss	Ref.
1. Liquid	2.5×10^{6}	2.7×10^{-5}	20
2. Ice at 0^{0}C	7	10	20
3. Protons in chemical reagents(hydroxides)	9	8	50
4. Bauxite (water of crystallization)	6	11	50

5. Physically adsorbed water in adsorbents	1000-3000	0.03-0.1	20, 51
6. Zeolitic water	100-1000	0.1-1.0	20
7. Interlayer water in clay minerals	30-1000	0.1-3.0	50
8. Silica gel	2300	0.029	20
9. Cement paste	300-500	0.13-0.23	20
10.Broad peak in Kaolin	11	6	50

From table 3.1, the line-width and relaxation time T_2 of adsorbed water in cement paste falls within the ranges of the relaxation time of zeolitic water and the interlayer water in clay minerals.

Compared with water of crystallization in bauxite and the hydroxyl ions of chemical reagents, adsorbed water in cement paste is far less strongly bound. However, it is more strongly bound than water in adsorbents or silica gel.

Thus the physically adsorbed water in cement paste is bound with a strength somewhere between that of water of crystallization and that of adsorbed water in many adsorbents.

If we look back to the work of Ochiai et

al(60) which has been discussed in section 3.5.2, the 1 gauss line-width of the narrow peak of calcium silicate paste is similar to the one of cement paste in table 3.1 above. It is therefore possible that water in cement paste may have a similar characteristic to water in calcium silicate paste.

CHAPTER FOUR

THE STUDIES OF MOISTURE IN CONCRETE PASTE

4.1 GENERAL STRUCTURE OF CONCRETE PASTE

Apart from water, aggregate or other type of reinforcement material, concrete consists mainly of cement paste. The cement paste, which is a product of the reaction of water with cement mixture, has a firm and hardened characteristic which bonds together between the reinforcement material particles in the concrete.

Before we go into details of the role of water in the hardening process, let us look at composition of the cement, the aggregate stone and the effect of cooling and thawing upon them.

4.1.1 COMPOSITION

There are four main constituents of cement as given by Neville(11) and these are tabulated in table 4.1 below:

Name of compound	Composition
Tricalcium Silicate	$3CaO.SiO_2$
Dicalcium Silicate	$2CaO.SiO_2$
Tricalcium Aluminate	$3CaO.Al_2O_3$
Tetracalcium Aluminoferrite	$4CaO.Al_2O_3.Fe_2O_3$

Table 4.1: Composition of cement

In addition to the above compounds, there also exist, in minor percentages, the oxides of alkali metals which are corrosive to some extent and can cause damage to the internal structure of the concrete paste.

Among the four main compounds, tricalcium-silicate is the most abundant(11), although the relative quantities of the compounds depend on the type of the cement.

4.1.2 THE AGGREGATES

Aggregate may be the second most important component after water, in influencing the properties of the hardened concrete paste. It has been mentioned by Neville(11) that the interlocking of the aggregates and

the cement paste, results in a strong bonding. However, the strength of the bonding depends on the aggregate surface texture, its shape and its pore characteristics(61).

As mentioned in chapter one, section 1.5, cracks which occur around the aggregates during freeze-thaw cycles may be reduced by using aggregates of similar shapes and sizes.

One might think that the moisture contents of the aggregate might have some influence on the dilation of concrete paste at low temperatures. However, Powers(10) has stated that water in aggregate only occupies large pores and this water freezes just below 0^0 C. Rhoades and Mielenz(61) also reported that aggregates which contained an abundance of large pores cannot be damaged by freezing. Their conclusion was based upon the excellent performance shown by basalt rock at low temperatures. Powers said that this type of rock may be protected in the same way as by the use of entrained air in concrete paste.

Another aspect which has to be considered is the chemical stability of the aggregate against chemical reactions, such as those from alkaline solutions.If the surface of the aggregate is reactive to

the alkaline solutions, then the integrity of the original bond may be lost to some extent. On cooling, water from the frozen parts may escape into the space around the aggregate and cracks may then occur when this water freezes and expands.

The size of aggregates contained in the concrete paste also has an important role on the distribution of moisture in the concrete paste. Smaller aggregate particles have a larger surface area, therefore, there is more surface area to be wetted by moisture. Paste with a small size of aggregates is more compact with very small voids.

4.1.3 PROCESS OF HYDRATION

The reaction of water with cement compounds is called the process of hydration. The stiffness of the paste is a result of the reaction of water with dicalcium silicate and tricalcium silicate. The product of the hydration process of both compounds are similar, i.e. calcium silicate hydrates(62), and this has been confirmed experimentally by Ochiai et al(60). The equations of the reactions as follows;

$$3CaO.SiO_2+H_2O \rightarrow Ca(OH)_2+2CaO.SiO_2.Aq \rightarrow 3CaO.2SiO_2.Aq+Ca(OH)_2$$

$$2CaO.SiO_2+H_2O \rightarrow 2CaO.SiO_2.Aq \rightarrow 3CaO.2SiO_2.Aq+Ca(OH)_2$$

Both of the compounds use approximately the same amount of water in the hydration process, but the reaction with tricalcium silicate produces more calcium hydroxide.

Matured cement paste described by Diamond(63) consists of roughly 70% calcium silicate hydrates, 20% well crystallized calcium hydroxide and a small percentage of ettringite (calcium sulphoaluminate hydrate) and some other minor substances. The main products of the hydration i.e. calcium silicate hydrates, have a low solubility in water which is demonstrated in practice by the stability of the hardened cement paste in contact with water. Therefore the products of hydration form a cover around the unreacted cement compounds, and the rate of hydration decreases. With an increase in the amount of the insoluble products, it becomes more difficult for the water to reach the unreacted cement compounds. As a result, the rate of hydration is decreasing continously.

Therefore, in order to achieve a mature concrete paste, the paste has to be cured for a long period of time. The time required is dependent on the type of cement, i.e. the size of the cement grains and the ratio of water to cement. The curing time to achieve a paste with an appreciable strength is normally 28 days in contact with water at a temperature of about 20^{0} C.

Theoretically the total volume of the solid products of hydration is about 2.1 times(13) that of the cement compounds. Therefore the hydration products not only replace the cement but also the space occupied by water. As the process continues, the space which was initially occupied by water, decreases. This space is normally called the capillary pores. However in practice, Neville(11) has calculated the total volume of original water and cement and compared this with the total volume of matured paste and found that the final volume is less. Thus, even after the hydration is almost complete, capillary pores must be present in the paste. Whether the pores are occupied by water or not is dependent on the method of curing. If the paste was given a surplus of water during the curing process, then the pores are filled with water.

The rate of hydration is also dependent on

the curing temperature. At a higher temperature the hydrate compounds are produced faster(16).This, faster hydration process may produce a dense coating of hydration products in the zone immediately surrounding the hydrating cement grains and the subsequent hydration becomes even slower. It has been shown(66) that this effect is independent of water-cement ratio.

The physical properties of calcium silicate hydrate is said by Verbeck and Helmuth(16),as porous and similar to swelling clay. Bernal(64) had mentioned that the solid is in the form of very thin fibrous crystals. The space in between the grains of the hydrated compounds is called the gel pore.These pores are interconnected and their sizes are very small. The diameter of the pores is between 15 Å and 20 Å, and they occupy approximately 28% of the total volume of the gel or the solid products of hydration(11). Verbeck and Helmuth (16) have reported that to get a uniform distribution of gel, the gel to space ratio should be about 0.6.

The size of capillary pores can vary between 0.01 and 13 μmetre and comprises less than 14% by volume of the matured paste. However, the actual range of sizes of the pores depends upon the original

water-cement ratio and the degree of hydration of the paste.

4.1.4 PORES DISTRIBUTION

We have seen that there two type of pores in the concrete paste, the gel pores and the capillary pores.

The gel pores are the interstitial spaces between gel particles and they are interconnected together. However, the capillary pores are not neccessarily interconnected. This is because in the process of hydration, capillary pores are filled by cement gel and the pores may become disconnected and blocked and so become capillary cavities. Thus, the amount of discontinuities of the capillary pores depends on the curing period and the amount of water contained in the fresh paste. Powers et al(13) reported that paste with w/c ratio 0.4, had lost 50% of the capillary pore continuity after the paste had matured. The time required to achieve the degree of the maturity as defined in figure 4.1, for various w/c ratios for ordinary Portland cement under standard laboratory conditions are given in table 4.2 below.

Water-cement ratio	time required
0.40	3 days
0.45	7 days
0.50	14 days
0.60	6 months
0.70	1 year
Greater 0.70	impossible

Table 4.2: Curing period for various w/c ratio.

Powers et al have also estimated the fraction of cement hydrated for various water-cement ratios at which the capillary pores continuity is lost. For w/c=0.7, the cement must all be hydrated in order to block all of the capillary pores (see figure 4.1). It follows that after 28 days of curing time, only pastes with water-cement ratio smaller than 0.6 have their capillary pores blocked completely, i.e. the pastes have matured.

Let us now examine the distribution of pores in term of their volume and radii. Figures 4.2 and 4.3 are taken from Brunauer et al(65), which show the pore volume distribution of hardened Portland cement paste with w/c ratios 0.5 and 0.7 respectively. The

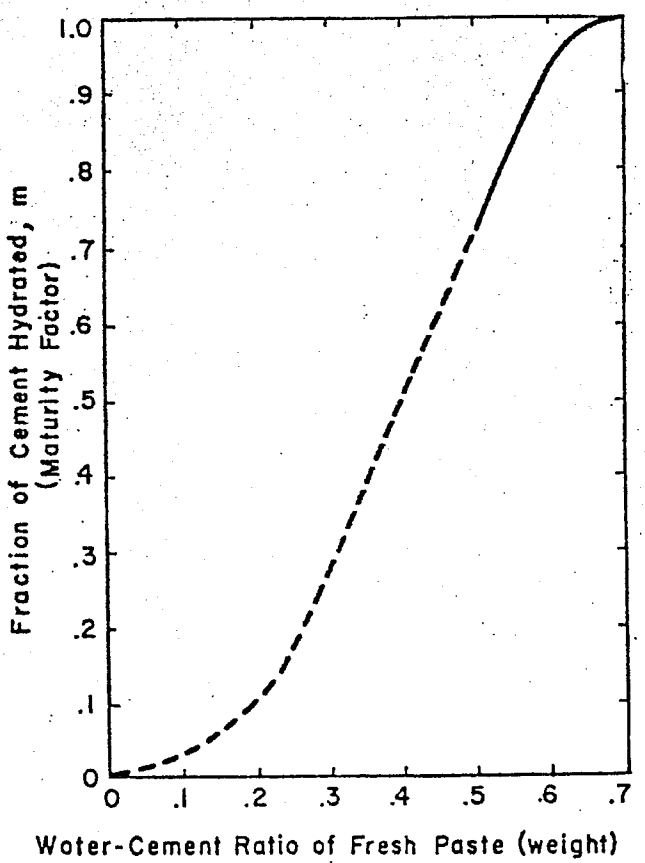

Figure 4.1: Estimated relationship between water-cement ratio of fresh paste and maturity of hardened paste at which capillary continuity is lost.(Reference 13)

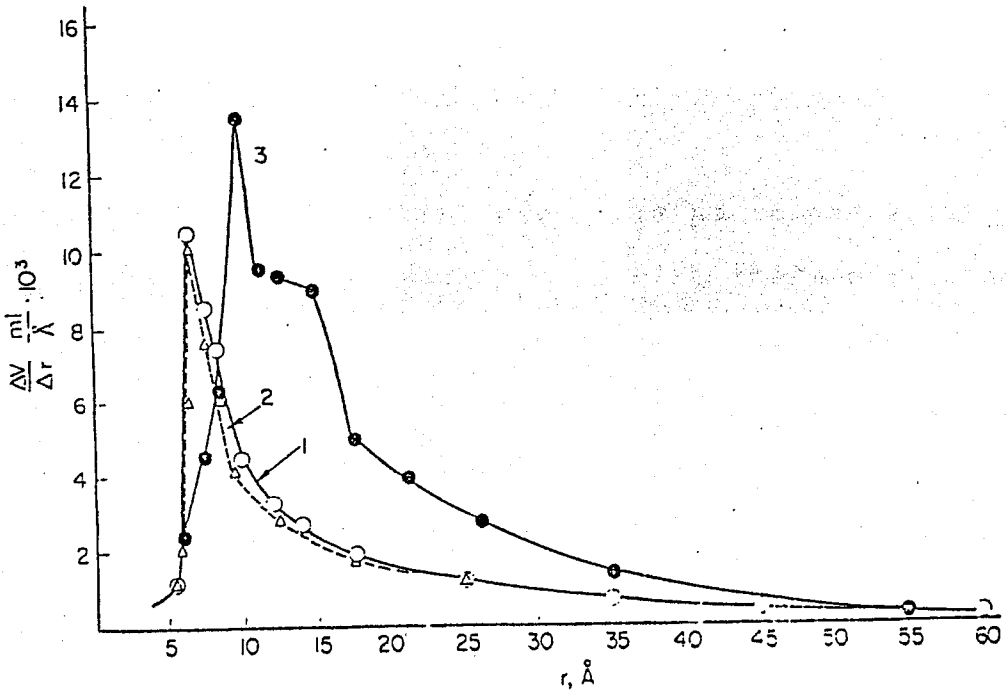

Figure 4.2: Pore volume distribution of a hardened cement paste w/c=0.5. Curve 1 - Brunaeur's method;curve 2 - Brunaeur's method with corrections; curve 3 - Method of Cranston and Inkley. (Reference 65).

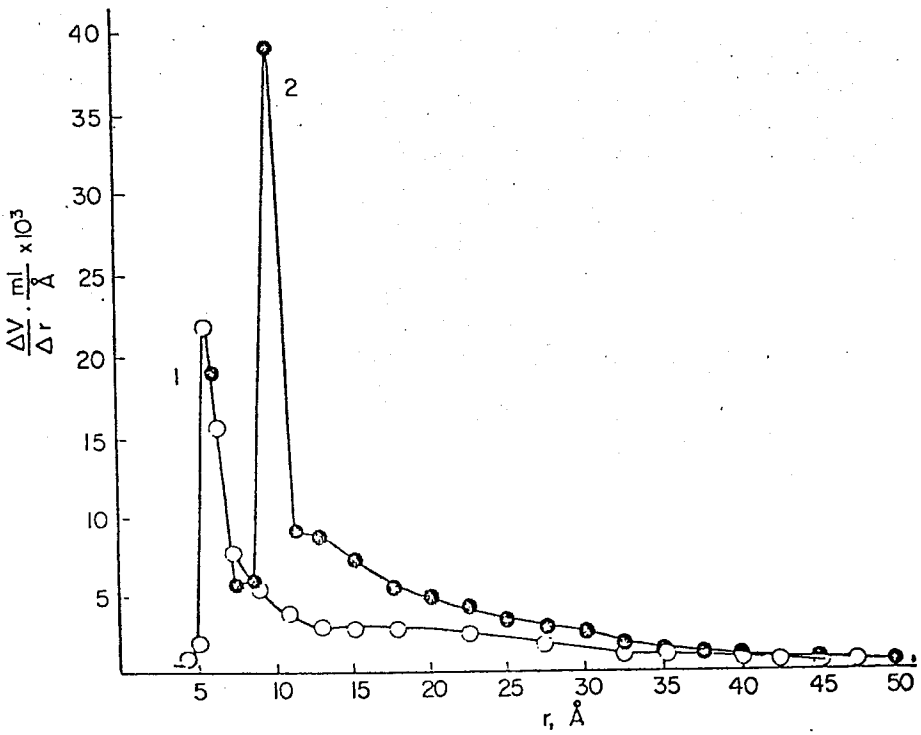

Figure 4.3: Pore volume distribution of a hardened cement paste w/c= 0.7. Curve 1 - Brunaeur's method; curve 2 - method of Cranston and Inkley (Reference 65).

data shows that the higher w/c ratio paste has a larger distribution of pore volume. Comparing the two figures, the integrated pores volume of 0.7 w/c paste has almost twice the volume of the pores in 0.5 w/c paste. Most of the pores in both pastes have diameters in the range between 10 Å to 50 Å. Because the data is limited to pores diameter less than 100 Å, the distribution only covered the range for gel pores.

Verbeck and Helmuth(16) have measured the distribution of pore sizes for a bigger size range, from 40 Å to 10,000 Å in diameter of 0.35, 0.65 and 0.80 w/c pastes. The distributions are shown in figure 4.4. They claimed that the pastes had been moist-cured for 11 years. Each curve shows two maxima. The occurence of the maxima are tabulated in table 4.3 below.

Water-cement ratio	The maxima occurred at:		
0.35	45Å	and	550Å
0.65	105Å	and	2100Å
0.80	110Å	and	3500Å

Table 4.3: Maxima of pore diameter distribution

Maxima at larger pore diameters are clearly shown to vary with water-cement ratio but the maxima at the small diameter are almost independent of the ratio. The large diameter peak corresponds to the capillary pore diameters. Thus, at higher w/c ratios, paste has more capillary pores in agreement with Powers et al(13).

If we combine the work of Verbeck et al(65) with that from Brunauer et al,hardened cement paste has pores with pore diameters concentrated at about 15 Å, 100 Å and larger than 550 Å (depending on w/c ratio). Verbeck et al also obtained a pore distribution by using the same method as Brunauer et al, i.e. using nitrogen absorption, they found only one maximum at about 30 Å, although the range of diameters they measured was up to 300 Å. What we can conclude is that gel pores may have diameters from about 10Å to 45Å for paste with low w/c ratio and can be up to 100Å for higher w/c ratio paste.

Finally, let us look at the effect of thermal cycles on the distribution of pore volumes. Rostasy' et al(67) reported that on cooling a cement paste to $-170\ ^{0}C$ the distribution of pore diameters between 40 Å and 500 Å showed no significant change.

However, some change was observed in the range greater than 500 Å. Following a number of cooling cycles on a particular paste, they observed that the cumulative pore volume in the range greater than 500 Å diameter had increased, whilst the cumulative pore volume within 40 to 500 Å diameter had decreased. They conclude that the effect of cooling cycles is to coarsen the structure of the pores.

4.1.5 DISTRIBUTION OF WATER

The presence of water in hydrated concrete paste has been repeatedly mentioned in previous sections. Its effects on the properties of concrete is universally agreed. However, its distribution in the paste is still not well known. The water has been conveniently divided into two arbitrary catagories; i.e. evaporable water and non-evaporable water. In more detail, the water may be categorised according to how it is being held in the paste. At present, we can firmly say that there are two extremes cases of water, one is free water while the other is chemically bonded water. In between, there is physically adsorbed water. How the

adsorbed water is being held and what is its binding energy is not clearly determined.

A moist cured concrete paste should contain water in both type of the pores. Due to the smallness of the gel pores, we can say that the water is in an adsorbed phase; whether it can easily evaporate is not known. Capillary pores which have diameters ranging from 100 Å to 10 µmetres may also contain water with a binding energy which varies according to the size of the pores. On leaving the paste in a room of 50% relative humidity, we can notice that the paste has lost some of its water. Then, on heating it at 100^{0}C, another part of the water is evaporated.

Figure 4.5 shows some work done by Verbeck and Helmuth(16) on drying a concrete paste through a various stages. The volume of water loss and the decrease in volume of the paste was measured. The ratios of the shrinkage to the volume of water loss are given in table 4.4.

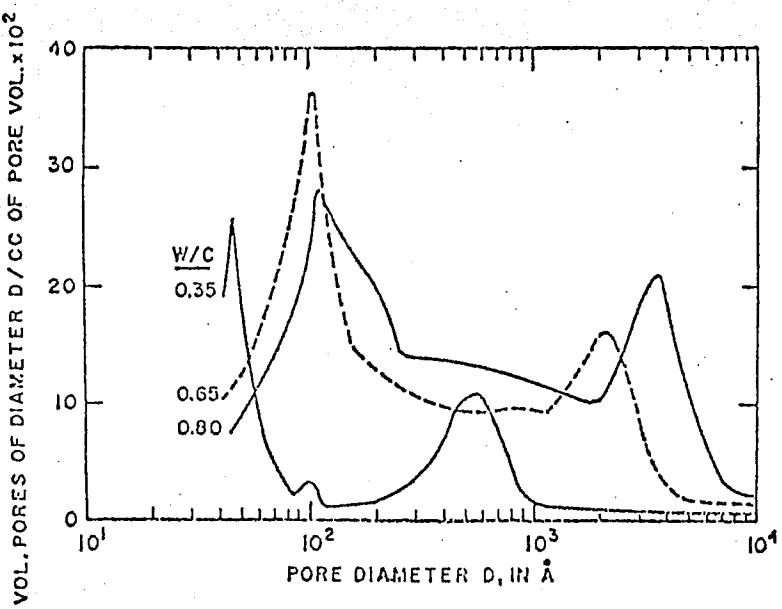

Figure 4.4: Pore size distributions of cement pastes, moist cured for 11 years, obtained with a high pressure mercury porosimeter. (Reference 16).

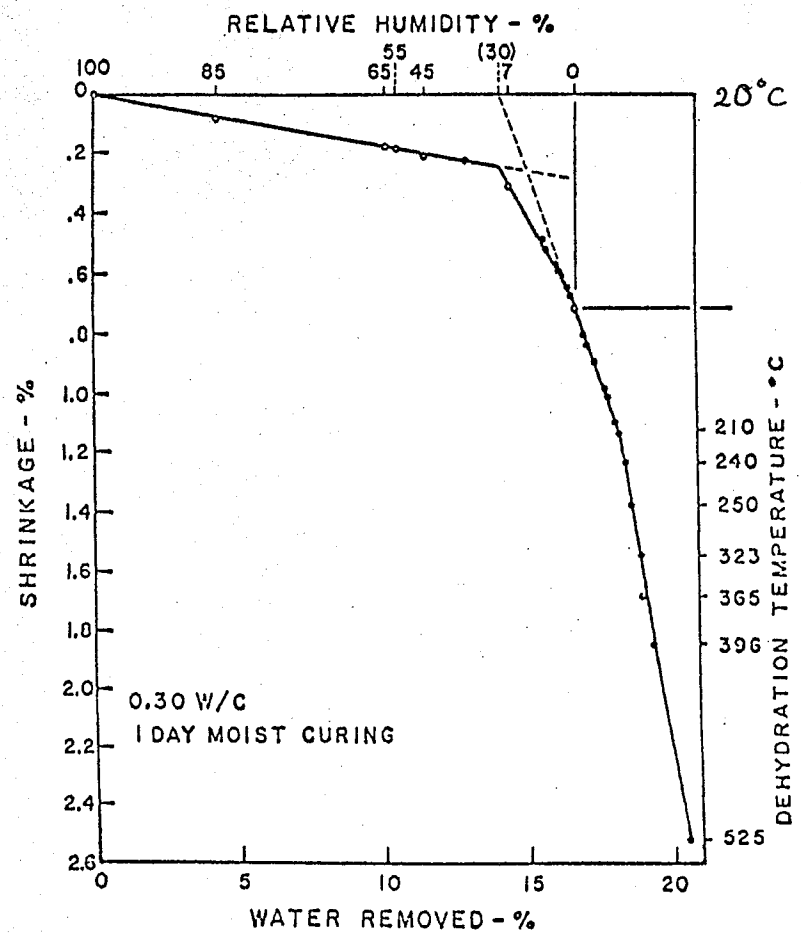

Figure 4.5: The variation of the first shrinkage of moist cured cement paste with water removed by drying in air, and dehydration at elevated temperatures. (Reference 16).

Stage	Range of humidity or temperature	Ratio $\Delta V_p / \Delta V_w$
1	100% RH to 30% RH	0.025
2	30% RH to 1% RH	0.22
3	1% RH to 200^0 C	0.40
4	200^0 C to 525^0 C	1.00

Table 4.4: Ratios of $\Delta V_p / \Delta V_w$ (Reference 16).

If we look at the table, the water loss during the first stage of drying has no significant effect on the volume of the concrete paste, i.e. the shrinkage volume is only 2.5% of the water loss.

In a more dry condition or when heated to 200 C the water loss caused the volume ratio to rise to 22% and 40% respectively. In the last stage, the drying caused the chemical bound water to decompose which may explain why the shrinkage volume is equal to the loss of water.

If we look into figure 4.5, the change between the stages is abrupt suggesting that there are different environment where the water is being held. Seligmann(20), based on his NMR results, said that the adsorbed water in the concrete paste is not evaporated if the relative humidity is less than 80%. Thus, Verbeck

and Helmuth's result suggests that the water loss in the first and second stages of drying is not the adsorbed water of the type refered to by Seligmann.

Powers(10) reported that water in concrete paste is in a state of tension due to negative hydrostatic pressure which may cause the water to tend to flow from a saturated region into a less saturated region. Thus, on drying a saturated paste, the water in the paste will flow outwards in order to equalize the hydrostatic tension. The water distribution in concrete paste under a temperature gradient is therefore always changing.

Water also redistributes itself under cooling conditions because on cooling,the temperature of a paste will vary from one point to another. Thus water in concrete paste will always be moving until it freezes.

The distribution of water between concrete paste and its aggregate is different.Powers(10) mentioned that aggregate usually holds only a little moisture under 50% relative humidity, but concrete paste under a similar humidity condition may have a degree of saturation between 40% to 90%. At 90% relative humidity, concrete paste can become fully saturated, whilst its

aggregate is still nearly dry. It can only attain full saturation if the humidity is at 100%. Therefore, in normal circumstances, the aggregates of concrete paste cannot take the water from the fine texture of the paste, unless the surrounding paste is already fully saturated. Powers also said that a similar characteristic is shown by macropores (i.e. voids, capillaries and air bubbles) in the concrete paste. A macropore can only take water from its surroundings after the concrete gel has become fully saturated.

4.2 THE THEORY OF FLUID FLOWS IN POROUS MEDIA

4.2.1 GENERAL

Moisture may be present in porous media in several phases; i.e. liquid, vapour or in the form of an adsorbed phase. If the media is exposed to low temperature and the fluid is water then ice may exist. All of these phases have some influence on the movement of the moisture in the media along with other factors such as gravity, the difference in concentration of the moisture, and the temperature gradient.

Another factor which is significant is the degree of saturation. A saturated porous solid may be assumed to have pores full of water or moisture; therefore moisture flows must be in the liquid phase only. In an unsaturated porous solid, the pores are not fully occupied by water and therefore two phase flow of the fluid may be present(57).

A primary quantity which we have to consider is the temperature gradient because, it has a great influence on changing many internal parameters in porous media. At higher temperatures, the solute concentration may easily vary from one region to

another. At low temperatures, the formation of ice crystals can exert an extra pressure on the fluid flow.

The direction of fluid flow can be in the same or the opposite direction of the temperature gradient. For example, liquid water movement under a temperature gradient will be from the cold regionsto the warmer regions because of the extra hydrostatic pressure produced during the formation of ice. However, liquid water at low temperatures also moves from a less concentrated solution in the warm regions into a more concentrated solution in the cold regions.

4.2.2 DARCY'S LAW

The theory of laminar flow through homogenous porous media is based on experiments performed by Darcy on the flow of water through filter beds.For a filter bed of thickness L and a cross section A and the depth of water above the beds of h, then the flow of water through the beds in unit time is given according to equation 4.1.

$$Q = \frac{k'A}{L}(h+L) \qquad (4.1)$$

where K' is a constant. Philip(57) has given the Darcy's law in a form as in equation 4.2 which is more meaningful.

$$q = \frac{k}{\mu} S \qquad (4.2)$$

where,

q = is equal Q/A, the macroscopic flow velocity.

S = the magnitude of the potential gradient.

μ = the viscosity of the fluid.

K = the permeability of the filter beds.

4.2.3 FLUID FLOWS MODELS IN POROUS MEDIA

A porous medium contains pores which can either be interconnected or non-interconnected. In order for a fluid to flow, the pores have to be interconnected and therefore a porous medium should contain a network of pores or capillaries. Scheidegger(68) in explaining fluid flow in a porous medium has given two basic models of a porous medium.

The first model was a parallel capillary type model. The model represents a porous medium as a

bundle of parallel capillaries which extend across the porous body from one surface to the opposite surface.The capillary diameter is constant along the flow line and only varies with different capillaries. The size distribution of the capillaries diameters is a(δ) across the surface A of the porous body.

From the law of Hagen-Poiseuille(68) for a straight circular tube of diameter δ and length h, the flow equation can be written as in the following,

$$Q = \frac{\pi\delta^4}{128\mu}\frac{\Delta p}{h} \qquad (4.3)$$

where Δp is the pressure drop and μ is the viscosity of the fluid. If the pressure gradient of the fluid flows in the x-direction is dp/dx, and the flow velocity is v, then equation 4.3 for this flow becomes,

$$v = \frac{1}{32}\frac{\delta^2}{\mu}\frac{dp}{dx} \qquad (4.4)$$

If the number of capillaries per unit cross sectional area is n, then the porosity P of the porous medium can be expressed according to equation 4.5 below,

$$P = \frac{1}{4} n\pi\delta^2 \qquad (4.5)$$

Therefore, in unit frontal area of the flow between diameter δ and $\delta+d\delta$ and thickness Δx, the quantity of fluid flowing through unit area per unit time is given as,

$$q = \frac{1}{3} P \int_0^\infty v a(\delta) d\delta \qquad (4.6)$$

where the factor 1/3 is expressing that only one-third of the capillaries are in the x-direction. By substitution of v from equation 4.4 into equation 4.6, we have,

$$q = \frac{P}{96\mu} \frac{dp}{dx} \int_0^\infty \delta^2 a(\delta) d\delta \qquad (4.7)$$

From Darcy's law for a flow with pressure gradient dp/dx, we have,

$$q = \frac{k}{\mu} \frac{dp}{dx} \qquad (4.8)$$

By dividing equation 4.7 by equation 4.8, the permeability of the porous medium can be written as in the following equation.

$$k = \frac{P}{96} \int_0^\infty \delta^2 a(\delta) d\delta \qquad (4.9)$$

Then, by defining the average capillary diameter as,

$$\overline{\delta}^2 = \int_0^\infty \delta^2 a(\delta) d\delta \qquad (4.10)$$

we can express the permeability k as below.

$$k = \frac{P\overline{\delta}^2}{96} \qquad (4.11)$$

This model has a drawback because each capillary was assumed to be straight, with a constant diameter like a tube, whilst a capillary in a true sense varies in direction and diameter along the flow.

The second model, which is called a serial type model, represents a porous medium as a body which contains very tortuous channels connecting through all the pores with one inlet at one surface and an outlet at the opposite surface of a porous body. In reality this model also is far from true but it has a good aspect in representing the capillaries in a better way. i.e. via the tortuosity of the capillaries.

In this model therefore, capillaries of different diameters are put together in series one after another. If we assume that the length of the porous

body and the length of a capillary are x and s respectively and the pressure drop over the length of the porous body is $p_2 - p_1$, then by Hagen-Poiseuille formula, the equation of mean flow velocity over each capillary is given as,

$$\frac{p_2-p_1}{x} = 32 \frac{\mu v}{\bar{\delta}^2} \frac{s}{x} \qquad (4.12)$$

where $\bar{\delta}^2$ is the average diameter of the capillaries along the direction of the flow. Rearranging equation 4.12 we have,

$$\frac{v}{\bar{\delta}^2} = \frac{1}{32\mu} \frac{x}{s} \frac{p_2-p_1}{x} \qquad (4.13)$$

If the density of capillaries per unit cross sectional area of the body is n, then the total flow q of fluid per unit area and unit time is given as,

$$q = \frac{nv\pi\bar{\delta}^2}{4} \qquad (4.14)$$

$$\text{Hence,} \quad q = \frac{n\pi\bar{\delta}^4}{128\mu} \frac{x}{s} \frac{p_2-p_1}{x} \qquad (4.15)$$

If the porosity P is equal to $(1/4)(n\pi\bar{\delta}^2)(s/x)$ for each

direction of flow, then for 3 dimensional flow P is equal to $(3/4)(n\pi\overline{\delta}^2)(s/x)$. Then rewriting equation 4.15,

$$q = \frac{P}{96}\frac{\overline{\delta}^2}{\mu}\left(\frac{s}{x}\right)^2\frac{p_2-p_1}{x} \qquad (4.16)$$

From Darcy's law the flow equation can also be written according to equation 4.17.

$$q = \frac{k}{\mu}\frac{p_2-p_1}{x} \qquad (4.17)$$

Then by dividing equation 4.16 by equation 4.17 we get,

$$k = \frac{P}{96}\overline{\delta}^2\left(\frac{x}{s}\right)^2 \qquad (4.18)$$

By introducing $\tau=s/x$ as the tortuosity factor, equation 4.18 becomes,

$$k = \frac{P}{96}\frac{\overline{\delta}^2}{\tau^2} \qquad (4.19)$$

If the pore size distribution of the capillaries is $a(\delta)$, thus a fraction of pore space $a(\delta)d\delta$ has a pore diameter between δ and $\delta+d\delta$. Let the length of this infinitesimal capillary with this diameter, be ds. This fraction of the pore space

should also equal the ratio of capillary volume of length ds to the whole volume of the capillary. We can therefore write the ratio as in the following equation.

$$\frac{\pi(\frac{\delta}{2})^2 ds}{\int_0^s \pi(\frac{\delta}{2})^2 ds} = a(\delta)d\delta \qquad (4.20)$$

But the integration of the denominator of equation 4.20 can be written as

$$\frac{\pi}{4}\int_0^s \delta^2 ds = \frac{1}{3}\frac{Px}{n} \qquad (4.21)$$

where n is the number of capillaries per unit area of the porous body and x is the length of the capillary where the pressure drop exists. Thus equation 4.20 can be simplified as,

$$\frac{\pi}{4}\delta^2 ds = \frac{1}{3}\frac{Px}{n}a(\delta)d\delta \qquad (4.22)$$

or,

$$\frac{\pi}{4}\delta^2 \tau dx = \frac{1}{3}\frac{Px}{n}a(\delta)d\delta \qquad (4.23)$$

since $ds = \tau\, dx$.

From Hagen-Poiseuille's law, the pressure drop along the infinitesimal length ds can be represented as,

$$\Delta p = \int \frac{32\mu v}{\delta^2} ds \qquad (4.24)$$

Substituting $ds = \tau dx$, we get,

$$\Delta p = \int \frac{32\mu v \tau}{\delta^2} dx \qquad (4.25)$$

For a total flow of fluid q per unit area and unit time with a velocity v, we have the relation,

$$q = \frac{n\pi\delta^2 v}{4} \qquad (4.26)$$

$$\text{or} \quad v = \frac{4q}{n\pi\delta^2} \qquad (4.27)$$

Then by eliminating v and τ from equations 4.27 and 4.23, respectively, into equation 4.25, the pressure drop Δp can be represented as,

$$\Delta p = \frac{512}{3} \frac{\mu P q x}{(n\pi)^2} \int \frac{a(\delta) d\delta}{\delta^6} \qquad (4.28)$$

From the Darcy's law,

$$\Delta p = \frac{q}{k} \mu x \qquad (4.29)$$

where k is the permeability; then by dividing equation 4.28 by equation 4.29, we get,

$$\frac{1}{k} = \frac{512}{3} \frac{P}{(n\pi)^2} \int \frac{a(\delta)d\delta}{\delta^6} \qquad (4.30)$$

To eliminate n in equation 4.30, we have a relation from equation 4.21 and replace $s/x = \tau$. We then get,

$$\frac{n\pi\delta^2}{4} = \frac{P}{3\tau} \qquad (4.31)$$

Multiplying equation 4.31 by $a(\delta)d\delta$ and integrating, we get the value of n as:

$$\frac{1}{n\pi} = \frac{3\tau}{4P} \int \delta^2 a(\delta)d\delta \qquad (4.32)$$

Then by substituting into equation 4.30, we get,

$$\frac{1}{k} = \frac{96\tau^2}{P} \{\int \delta^2 a(\delta)d\delta\}^2 \int \frac{a(\delta)d\delta}{\delta^6} \qquad (4.33)$$

Comparing equation 4.19 and 4.33, the average diameter of the capillaries is given according to equation 4.34 below.

$$\frac{1}{\bar{\delta}^2} = \{\int \delta^2 a(\delta)d\delta\}^2 \int \frac{a(\delta)d\delta}{\delta^6} \qquad (4.34)$$

The models we have discussed above were based on the capillary bundles model and the flow has been assumed to be a tube flow which follows Hagen-Poiseuille law. However, in the flow in porous media such as concrete paste, the effect of the irregularity of pores is affecting the fluid flow. Philip(57) mentioned that this factor was a limitation of models based on the capillary bundles because if the fluid flow was not continous then the fluid velocity will continously change in both magnitude and direction.

Another approach to solving the problem of fluid flows in a porous medium was done by Powers et al(58). The model was based on Stoke's law of a falling particle in a fluid which produces a drag. This drag may be developed by the falling particle through the fluid or by the flow as it goes through the granular bed where the particles are in fixed positions.

A particle falling through a large volume of fluid under gravitation should experience a net force F as given according to equation 4.35.

$$F = (\rho_s - \rho_f)\left(\frac{\pi \delta^3}{6}\right) g \qquad (4.35)$$

where,

ρ_s= the density of the solid particle.

ρ_f= the density of the fluid.

δ = the diameter of a sphere which having a same volume as the particle.

g = gravity acceleration =9.8 ms^{-2}.

If the fluid has a viscosity, the particle should experience a drag or resistance which is given by Stoke's law as in the following equation.

$$Fr = 3\pi\mu(\theta)Vd \qquad (4.36)$$

where,

$\mu(\theta)$= the viscosity of the fluid at temperature θ^0 C.

V = the velocity of the particle.

d = the drag diameter of a sphere which has the same viscous drag as the actual particle.

When the falling particle achieves a constant velocity V_s, then the net force F must equal to the drag Fr. Therefore,

$$V_s = \frac{\delta^3(\rho_s-\rho_f)g}{18\mu(\theta)d} \qquad (4.37)$$

Now,if the falling particles are in a group

of a large number of such particles in a suspension, the falling velocity of the particles should be affected by the distance between the particles. Thus, the velocity can be written as a function of the concentration of particles in the fluid as in equation 4.38.

$$V(c,\theta) = V_s f(c) \tag{4.38}$$

where f(c) is a function of the total volume of the particles. In a suspension, a clear fluid is produced above the particles as the particles settle. The rate of the clear fluid being produced is equal to $(1/A)(dq/dt)$, where A is the cross sectional area of the fluid body and q is the total number of particle flocculate at the bottom. Thus,

$$V(c,\theta) = \frac{1}{A}\frac{dq}{dt} \tag{4.39}$$

From Darcy's law the rate of settling particles is according to equation 4.40.

$$\frac{1}{A}\frac{dq}{dt} = \frac{k\Delta h}{L} \tag{4.40}$$

where $\Delta h/L$ is the hydraulic head of the fluid which can

be written as below.

$$\frac{\Delta h}{L} = \frac{(\rho_s-\rho_f)c}{\rho_f} \qquad (4.41)$$

Therefore equation 4.39 can be rewritten as follows.

$$V(c,\theta) = \frac{k(\rho_s-\rho_f)c}{\rho_f} \qquad (4.42)$$

By substitution of equation 4.37 and 4.42 into equation 4.38, we get,

$$k = \frac{\rho_f g}{18\mu(\theta)c}\left(\frac{\delta}{d}\right)^3 f(c) \qquad (4.43)$$

Function f(c) in equation 4.43 was predicted by Powers(58) according to equation 4.44 below.

$$f(c) = (1 - c)^2 \exp(-f(c)) \qquad (4.44)$$

Then equation 4.43 becomes,

$$k = \frac{\rho_f g}{18\mu(\theta)}\left(\frac{\delta}{d}\right)^3 \frac{(1-c)^2}{c} \exp(-f(c)) \qquad (4.45)$$

From an argument that the flow of very thick particles have effects from neigbouring particles, Hawksley(69)

had put a factor into equation 4.45. The factor is called the tortuosity factor $\tau(c)$ as before. Therefore,

$$k = \frac{\rho_f g}{18\mu(\theta)}\left(\frac{\delta}{d}\right)^3 \frac{(1-c)^2}{c}\tau(c)\exp(-f(c)) \qquad (4.46)$$

Hawksley found that for flocculated particles in suspension, the value of $\tau(c)$ was about 2/3.

4.2.4 THE FLOW OF WATER IN CEMENT PASTE

Cement paste is not a collection of particles similar to particles in suspension. However between particles in the paste there are spaces through which water can flow. The different characteristics of the fluid flow arise from the smallness of the spaces compared with the spaces between particles in a suspension. The fluid flow in cement paste may involve greater forces, which may be the adsorption forces. Powers et al(58) mentioned that because of these forces the viscosity of the fluid may vary from one point to another in the paste and may depend on the concentration of the particles. Therefore the viscosity can be written according to the following equation.

$$\mu(\theta,c) = \mu(\theta)\mu(c) \qquad (4.47)$$

Then equation 4.46 becomes,

$$k = \frac{B}{\mu(\theta)\mu(c)} \frac{(1-c)^2}{c} \exp(-f(c)) \qquad (4.48)$$

where, $B = \frac{\rho_f g(\delta^3/d)\tau(c)}{18}$

By taking the logarithm of equation 4.48, we get,

$$\ln(k) = -(\ln\mu(\theta) + \ln\mu(c)) + \ln B + \ln\frac{(1-c)^2}{c} - f(c) \qquad (4.49)$$

Assuming that the last 3 terms of equation 4.49 are temperature independent within a small range of temperature, then differentiating with respect to (1/T) we get,

$$\frac{d(\ln k)}{d(1/T)} = -\frac{d(\ln\mu(\theta))}{d(1/T)} - \frac{d(\ln\mu(c))}{d(1/T)} \qquad (4.50)$$

where T is the absolute temperature. According to the theory of Eyring(70) the first term of equation 4.50 is the normal activation energy of water while the second term is an energy which is related to the adsorption

phase of the water. From Powers et al(58), the first term was almost constant (10% variation) between 0^0C to 30^0C and the second term was assumed to be given by equation 4.51 with α as a constant.

$$\frac{d\ln\mu(c)}{d(1/T)} = \alpha\left(\frac{c}{1-c}\right) \qquad (4.51)$$

This is because the effect of particle concentration on the viscosity depends on the distance between the solid surfaces and hence is assumed to be inversely proportional to the local hydraulic radius. The hydraulic radius is proportional to (1-c)/c (58). Integration of equation 4.51, we get,

$$\ln \mu(c) = \frac{\alpha}{T}\frac{c}{1-c} + \text{constant} \qquad (4.52)$$

The integration constant is zero since $\lim_{c\to 0}\mu(c)=0$ and α is therefore an empirical constant. Function f(c) in equation 4.49 was assumed by Powers et al(58) according to equation 4.53 with γ is a constant.

$$f(c) = \gamma\left(\frac{c}{1-c}\right) \qquad (4.53)$$

Now substituting equation 4.52 and 4.53 into equation

4.49 we get,

$$\ln k = -\ln \mu(\theta) - \frac{\alpha}{T}\left(\frac{c}{1-c}\right) + \ln B + \ln\frac{(1-c)^2}{c} - \gamma\left(\frac{c}{1-c}\right) \qquad (4.54)$$

Rearranging equation 4.54,

$$\ln\frac{kc}{(1-c)^2} = \ln B - \ln \mu(\theta) - \left(\frac{\alpha}{T} + \gamma\right)\left(\frac{c}{1-c}\right) \qquad (4.55)$$

Equation 4.55 expresses the flow of fluid in cement paste in terms of concentration and temperature. From Powers et al using the following constant values:

$B=(1.36 \pm 0.1)\times 10^{-10}$ $\quad \alpha = 1242 \pm 133$ $\quad \gamma = 0.7 \pm 0.5$

the expression in equation 4.54 can be written empirically as:

$$k = \frac{1.36X10^{-10}(1-c)^2}{\mu(\theta)}\,\frac{}{c}\,\exp\left(-\left\{\left(\frac{1242}{T} + 0.7\right)\frac{c}{1-c}\right\}\right) \qquad (4.56)$$

The calculated values of K from equation 4.56 are compared with the observed values in table 4.5 below.

Temperature ^{0}C	K calculated $x10^{-14} ms^{-1}$	K observed $x10^{-14} ms^{-1}$
0.20	15.0	15.1
8.92	22.8	21.9
18.54	34.4	32.2
26.97	47.4	48.2

Table 4.5: Permeability of cement paste (ref.58)

From the above table, it appears that the empirical equation in equation 4.56 is well fitted with the observed values of the permeability.

4.2.5 THE FLOW OF WATER UNDER A TEMPERATURE GRADIENT

In this section we shall discuss the flow of water in concrete paste when the paste is subject to a temperature gradient below 0 ^{0}C.

Before we discuss concrete specifically, let us examine some experimental results on water flows in other porous media under a temperature gradient. Kuzmak and Sereda(76) have reported that there was no flow of water due to the temperature gradient as long as the body remained saturated. The flow began when the capillaries began to unsaturate. In their experiment a saturated gap of 250 μmetres at a temperature gradient between 0.9 ^{0}C to 49^{0}C, became unsaturated by the application of pressure. For this size of gap, a pressure of about 56 cm of water caused the water to flow as shown in figure 4.6. Under a temperature gradient, vapour distills across the gap and condenses on the cold surface, and produces a hydraulic head of about 10 cm of water which can cause the water to flow. However, this amount of pressure cannot unsaturate the gap. As the applied pressure was increased, and unsaturated the gap, the observed rate of flow had a large increase. This is because the hydraulic head was

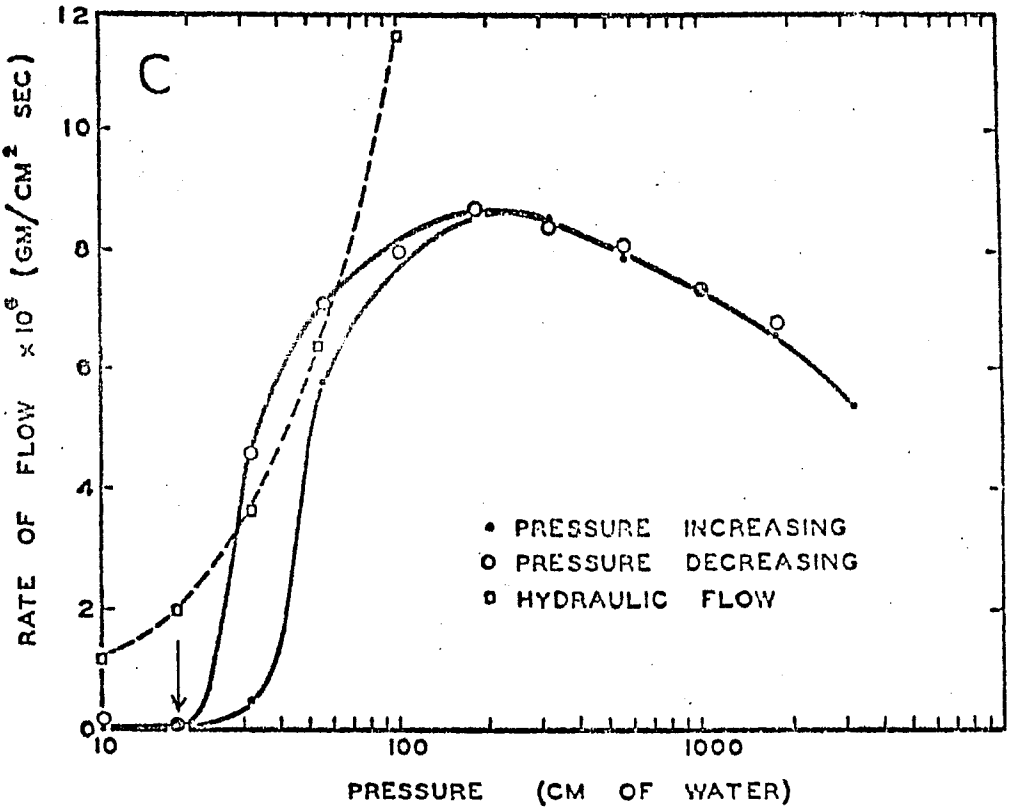

Figure 4.6: Flow of water through a gap of size 250μmetre under a temperature gradient. The pressure was used to unsaturate the gap. (Reference 76)

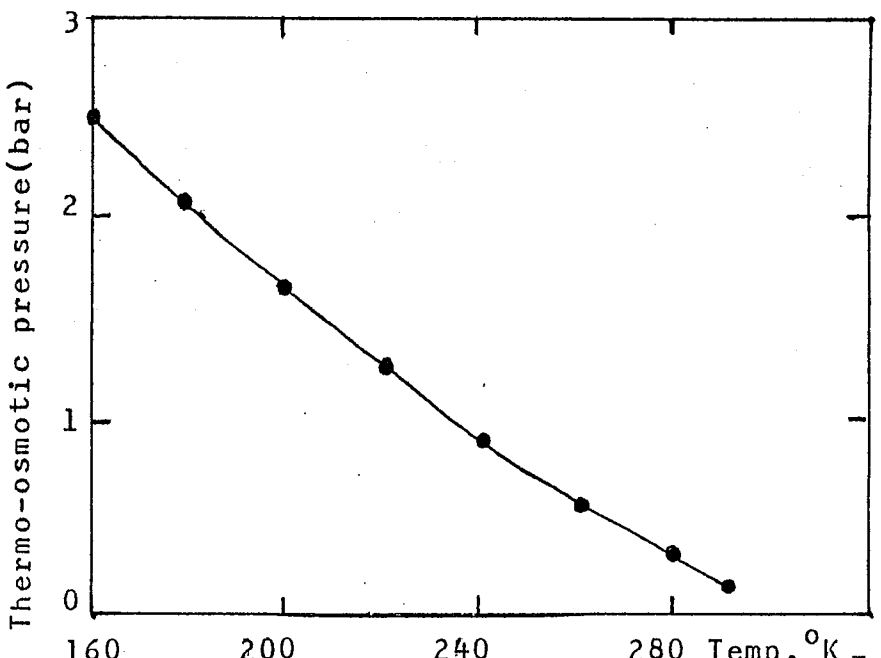

Figure 4.7: Plot of equation $\Delta p = 0.92 \log(\frac{T_2}{T_1})$

increased and acted on the flow. A maximum was reached when the gap was completely unsaturated; beyond this point the observed rate of flow decreased.

Kuzmak and Sereda also studied the movement of salt solution in a partially saturated porous medium. They observed that the movement of salt in solution in a porous medium does not depend on the temperature gradient between 0.6^0 C to 49^0C. See table 4.6 below.

Suction pressure cm of water	The rate of water flow ml/hr	Experim. rate of salts transfer under a temp. gradient.	Experimental rate of salts transfer at 27^0 C.
1050	0.2	0.0001	0.0001
20	0.2	0.0001	0.0001

Table 4.6: Transfer of salts through partially unsaturated sand.

From the above results and previous discussions on moisture distribution, water in a porous medium flows from a higher pressure region to a lower one under a temperature gradient but the transfer of

salts from one region to another does not neccessarily relate to the temperature gradient. However, due to segregation of ice, the concentration of salt solution may vary from one region to another and this produces an osmotic pressure that can cause the salt solution to move. Powers(8) suggested that under a temperature gradient, an osmotic pressure may be produced which he called a thermo- osmotic pressure.Based on discussions of the Faraday Society(77) on osmotic pressure, he gave a formula according to equation 4.57 below.

$$\Delta p = 0.92 \log (T_2/T_1) \qquad (4.57)$$

where Δp is the magnitude of the osmotic pressure produced in newton/square mm. T_2 and T_1 are absolute temperatures of the warm and cold region respectively. The plot of equation 4.57 is shown in figure 4.7. For a warm region temperature of about 300^0 K and with a temperature difference of 20 degrees, the formula predicts an osmotic pressure of about 0.06 newton/sq. mm (0.6 bar) being produced. This pressure is however very small compared with hydraulic pressures(14).

The formation of ice lenses in a restricted space such as in concrete pores will produce

hydraulic pressures that move the water front. As the temperature is lowered further, the dimension of the pores may change and this may alter the hydraulic pressure; the change of pressure will induce the water to move accordingly.

Since the freezing temperature of water in the concrete pores is distributed between $0^{0}C$ to $-40^{0}C$, the magnitude of the hydraulic pressure may also vary. Normally when a concrete paste is cooled down, the temperature of the paste varies with the distance x from the cold region of the paste. The function of temperature with distance can be expressed according to equation 4.58 below.

$$\theta = \phi(x, \theta_0) \qquad (4.58)$$

where θ_0 is the temperature at the surface of the concrete paste. The infinitesimal change of temperature $d\theta$ is therefore,

$$d\theta = d\phi(x, \theta_0)dx \qquad (4.59)$$

The change of pressure with temperature can be expressed as follows.

$$p(\theta) = p_0\psi(\theta) \tag{4.60}$$

where p_0 is the pressure at the initial condition. From Darcy's law, the flow of fluid q per unit area and unit time can be written as below.

$$q = \frac{k}{\mu}d\phi(x,\theta_0)\frac{dp}{d\theta} \tag{4.61}$$

$$\text{or} \quad q = \frac{k}{\mu}d\phi(x,\theta_0)p_0 d\psi(\theta) \tag{4.62}$$

since $dp = p_0 d\psi(\theta)d\theta$

From equation 4.28, the Hagen-Poiseuille flow equation, we have,

$$dp = \frac{512}{3}\frac{\mu Pqdx}{(n\pi)^2}\int\frac{a(\delta)d\delta}{\delta^6} \tag{4.63}$$

$$\text{or} \quad pd\psi(\theta)d\theta = \frac{512}{3}\frac{\mu Pqdx}{(n\pi)^2}\int\frac{a(\delta)d\delta}{\delta^6} \tag{4.64}$$

Substituting q from equation 4.62 into equation 4.64, we get an expression for the permeability as follows.

$$\frac{1}{k}d\theta = \frac{512}{3}\frac{Pd\phi(x,\theta_0)dx}{(n\pi)^2}\int\frac{a(\delta)d\delta}{\delta^6} \tag{4.65}$$

Then, integrating equation 4.65.

$$\frac{1}{k}(\theta_s-\theta_0) = \frac{512}{3}\frac{P}{(n\pi)^2}\int\frac{a(\delta)d\delta}{\delta^6}\int_s^L d\phi(x,\theta_0)dx \qquad (4.66)$$

where θ_s and θ_0 are the temperatures of the body at x=s and x=L respectively. Since liquid water flows from the cold region to the warm region, L is the length along the flow line between the two regions with a highest temperature difference. Equation 4.66 can be written as follows.

$$\frac{1}{k} = \frac{96\tau^2}{P(\theta_s-\theta_0)}\frac{1}{\bar{\delta}^2}\int_s^L d\phi(x,\theta_0)dx \qquad (4.67)$$

since $1/\bar{\delta}^2 = \frac{1}{(n\pi)^2}\int\frac{a(\delta)d\delta}{\delta^6}$

and $\frac{1}{n\pi} = \frac{3\tau}{4P}\int\delta^2 a(\delta)d\delta$

Now we have to find a suitable function which can represent $\phi(x,\theta_0)$. Since the function relates the temperature of concrete paste with the distance x from a cold region, it must contain the heat flux and the thermal conductivity of the paste. Parrot and Stuckes(78) have given an expression relating the temperature with distance x for a heat flow through a low diffusivity material as,

$$\theta = \frac{2Q}{\lambda} F(x,t) \qquad (4.68)$$

where Q is the heat flux, λ is the thermal conductivity of the material and the function F(x,t) depends on time and is very complex. There are many unknown theoretical parameters in the function. It can only be used in a comparative study of two or more different flows when the unknown parameters can be cancelled.

However, for heat loss from a solid cylinder of low thermal conductivity and at steady state, Pratt(79) has given the flow equation as in the following equation.

$$Q = 2\pi\lambda'\{1 + (\theta-\theta')\}x\frac{d\theta}{dx} \qquad (4.69)$$

where the thermal conductivity is assumed to vary linearly within a small temperature difference and there is no heat loss through a direction perpendicular to the direction of the flow. λ' is the thermal conductivity at an arbitrary temperature θ'. Rearranging equation 4.69 and integrating, we get,

$$\int\{1 +(\theta-\theta')\}d\theta = \frac{Q}{2\pi\lambda'}\int\frac{dx}{x}$$

$$\theta - \theta_0 = \frac{Q}{2\pi\lambda'} \ln \frac{x}{L} \qquad (4.70)$$

where $\theta' = \frac{1}{2}(\theta + \theta_0)$ and θ is the temperature at distance x from the cold region. θ_0 is the temperature at the warm region and L is the distance between the cold and warm regions. Therefore the temperature function is,

$$\theta = \theta_0 + \frac{Q}{2\pi\lambda'} \ln \frac{x}{L} \qquad (4.71)$$

In the derivation above, the value of λ', the thermal conductivity of the paste, has been assumed to decrease linearly. In fact, it has been reported(78) that from 300^{0}K to 290 ^{0}K the thermal conductivity of porous solids decrease by 50% and from 290^{0}K to 280^0 K the decrease is only 30%. This is because in porous solids there are many parameters affecting the heat flows. In the case of concrete paste, the differences of heat flows through cement gel, aggregates and water in pores have to be considered.

Taking into account all the factors, Allen and Thorne(80) have derived an expression for the thermal conductivity in concrete paste as in the following equation.

$$\lambda' = \lambda_m(2M-M^2) + \frac{\lambda_a\lambda_m(1-M)^2}{\lambda_a M+\lambda_m(1-M)} \qquad (4.72)$$

where,

λ_m = the thermal conductivity of cement gel.

λ_a= the thermal conductivity of aggregates.

M = is a factor related to the pores and is equal to $(1-(1-P)^{\frac{1}{3}})$ and,

P = the volume of cement gel per unit volume of concrete.

Allen and Thorne have calculated the values of λ_m, λ_a, M and P experimentally and these are given in table 4.7 below.

λ_m = 1.99 W/m^{0}C with 10% moisture content.

M = 0.245

λ_a = 1.21 W/m^{0}C for dolerite type aggregates.

λ_a = 1.38 W/m^{0}C for barytes type aggregates.

λ_a = 8.13 W/m^{0}C for Haematite type aggregates.

Table 4.7: (From reference 80)

Now differentiating equation 4.71 and substituting in

equation 4.67, we get,

$$\frac{1}{k} = \frac{96\tau^2}{P(\theta_s-\theta_0)} \frac{1}{\overline{\delta}^2_s} \int_{0}^{L} \frac{Q}{2\pi\lambda'} \frac{L}{x} dx \qquad (4.73)$$

and on integration of the equation, we have the permeability equation as below.

$$k = \frac{2\pi\lambda'(\theta_s-\theta_0)}{AQL \ln(L/s)} \qquad (4.74)$$

where $A = (96\tau^2)/(P\overline{\delta}^2)$ and λ' is the average value of the thermal conductivity between the distance L and s. The expression of k can be written as,

$$k = \frac{2\pi\lambda'\Delta T}{AQ \ln(L/s)} \qquad (4.75)$$

where ΔT is the temperature gradient and is equal to $(\theta_s - \theta_0)/L$.

Taking Q = 1.5 watts/square metres and $A = 1.9\times10^{14}$ m^{-2} which have been calculated from $\tau = 2/3$, P=0.25 and average pore diameter $\overline{\delta}$ = 95 Å, the average thermal conductivity of the paste, is calculated to be 1.71 watts/meter deg.C. Thus the empirical formula of the permeability is given according to equation 4.76.

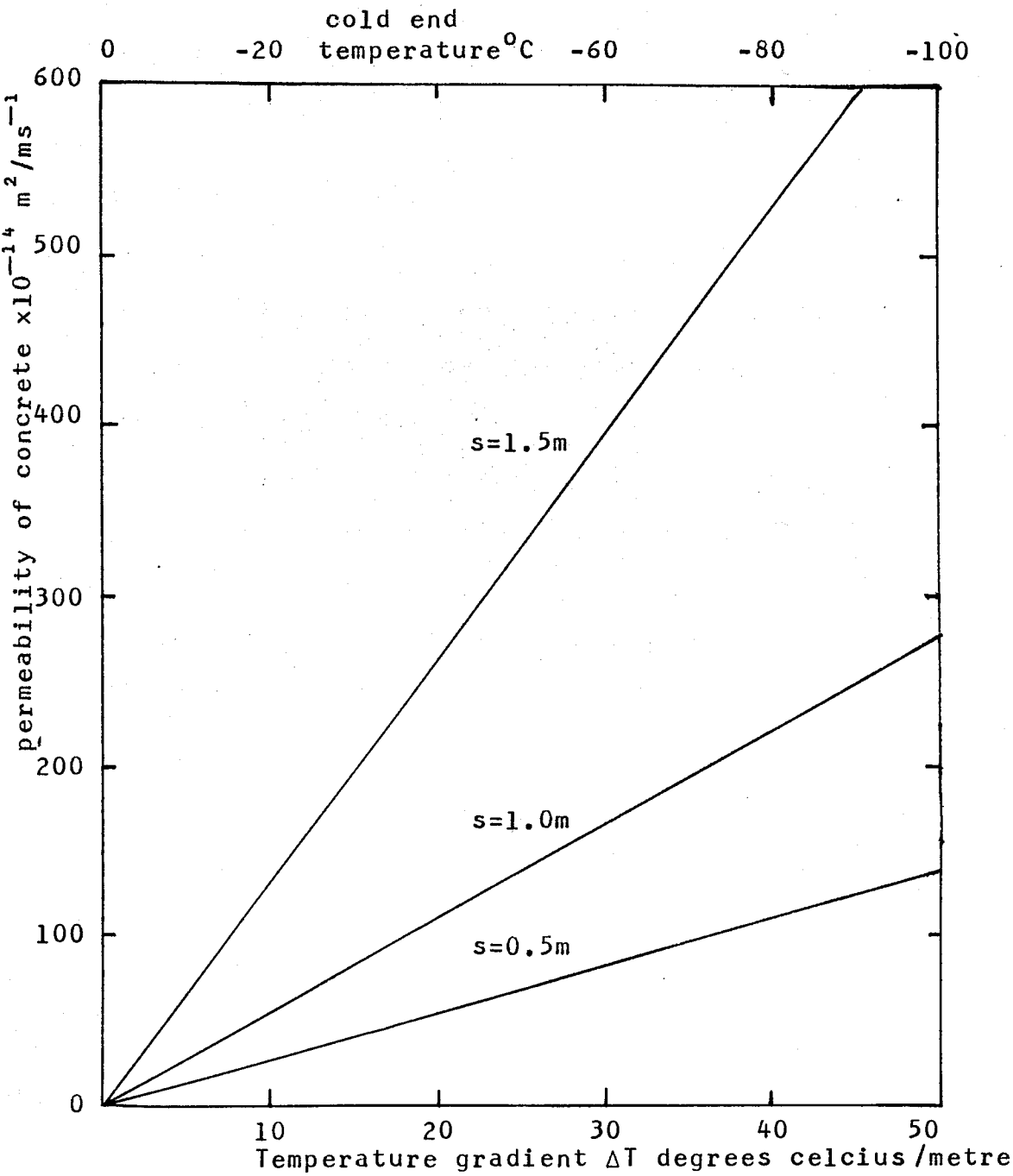

Figure 4.8: Calculated permeability of water in concrete paste from equation 4.76 for L=2metres against temperature gradient. θ_o is equals to $0^{\circ}C$.

$$k = 3.77X10^{-14} \frac{\Delta T}{\ln(L/s)} \qquad (4.76)$$

where K is in square metres per unit length and in unit time of the flow, θ_0 is at 0^0C and L is taken as 2 metres. The calculated values of K against the temperature gradient for difference values of s, are shown in figure 4.8.

According to figure 4.8, the flow of water under a temperature gradient below 0^0C, at a distance s from the cold region is increasing as s increases. The permeability of water at specific temperatures between 0.20^0C and 26.97^0C as given in table 4.5 are in the range from $15.1x10^{-14}$ ms^{-1} and $48.2x10^{-14}$ ms^{-1}. But, in figure 4.8, for a temperature gradient of 10 degrees/m., the value of the water permeability is about $130x10^{-14}$ ms^{-1}. It shows that the temperature gradient has a great effect on the flow of water.

4.3 THE FREEZING OF WATER IN CONCRETE PASTE

4.3.1 MEASUREMENTS OF HEAT CAPACITY OF CONCRETE PASTE

The enthalpy vs temperature curve for concrete paste below 0^0C contains 2 contributions, the specific heat of the concrete and the latent heat of freezing of the water.

Measurements of heat capacity $(\partial H/\partial T)$ of concrete samples below $0\ ^0$C can be done by using a cooling calorimeter which will be described in chapter 5.

The principle of the measurements is based on assuming that the heat loss by a concrete sample is proportional to its temperature drop. Figure 4.9 shows diagramatically how the heat is lost through the concentric cylindrical copper walls of the calorimeter. If the total heat loss in time interval $\Delta\tau$ is Q and the latent heat of fusion of ice is L, then the heat equation is given as follows.

$$Q = \Sigma\alpha\Delta t\Delta\tau = M\Sigma\Delta T + Lw_f \qquad (4.77)$$

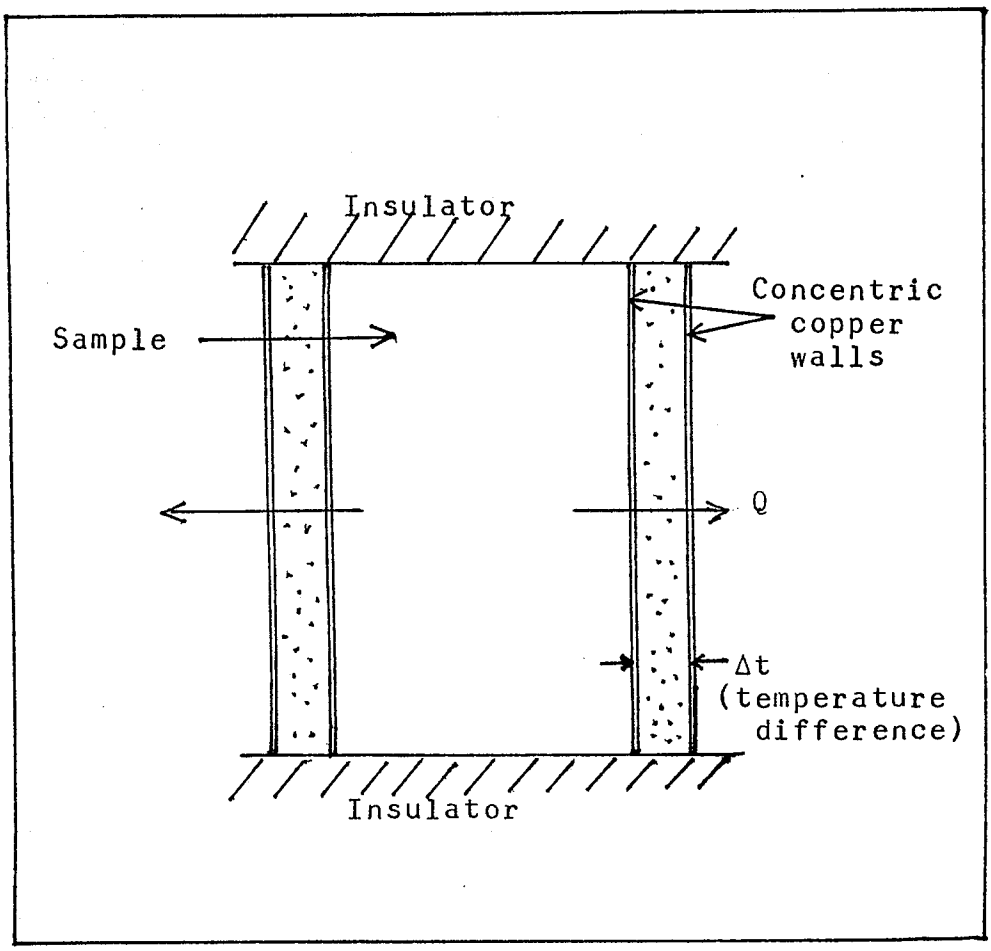

Figure 4.9 : Diagram of heat loss through the walls of the cooling calorimeter

where,

α = coefficient of heat transfer through the copper walls.

Δt= mean temperature difference between the concentric copper walls in time interval $\Delta\tau$.

M = the heat capacity of the sample and the calorimeter.

ΔT= the temperature drop of the sample in time interval $\Delta\tau$.

w_f= the weight of freezable water that freezes in time interval $\Delta\tau$.

The value of the heat transfer coefficient α was measured experimentally via a constant heat supply from a heater mounted on the inside copper wall of the calorimeter. The coefficient of heat transfer was calibrated over the temperature range 0^0 to $-80\ ^0$C. The calibration curves in figure 4.10 show that the value in a given time interval is almost constant over the temperature range. Therefore equation 4.77 can be written as,

$$\Sigma\Delta t\Delta\tau = (M/\alpha)\Sigma\Delta T + (L/\alpha)w_f \qquad (4.78)$$

To calculate the value of M, several runs

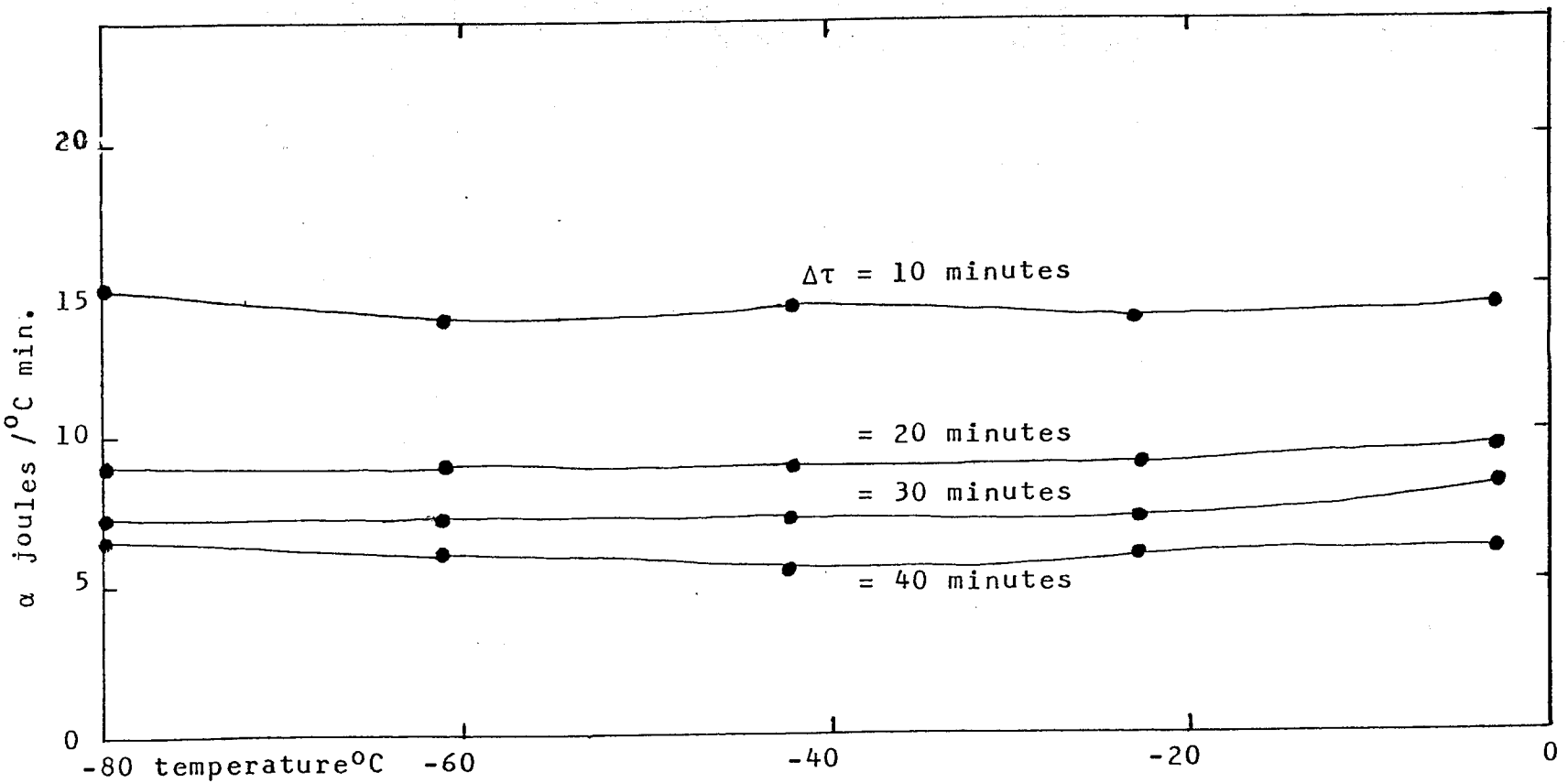

Figure 4.10: Variation of heat transfer coefficient α with temperature.

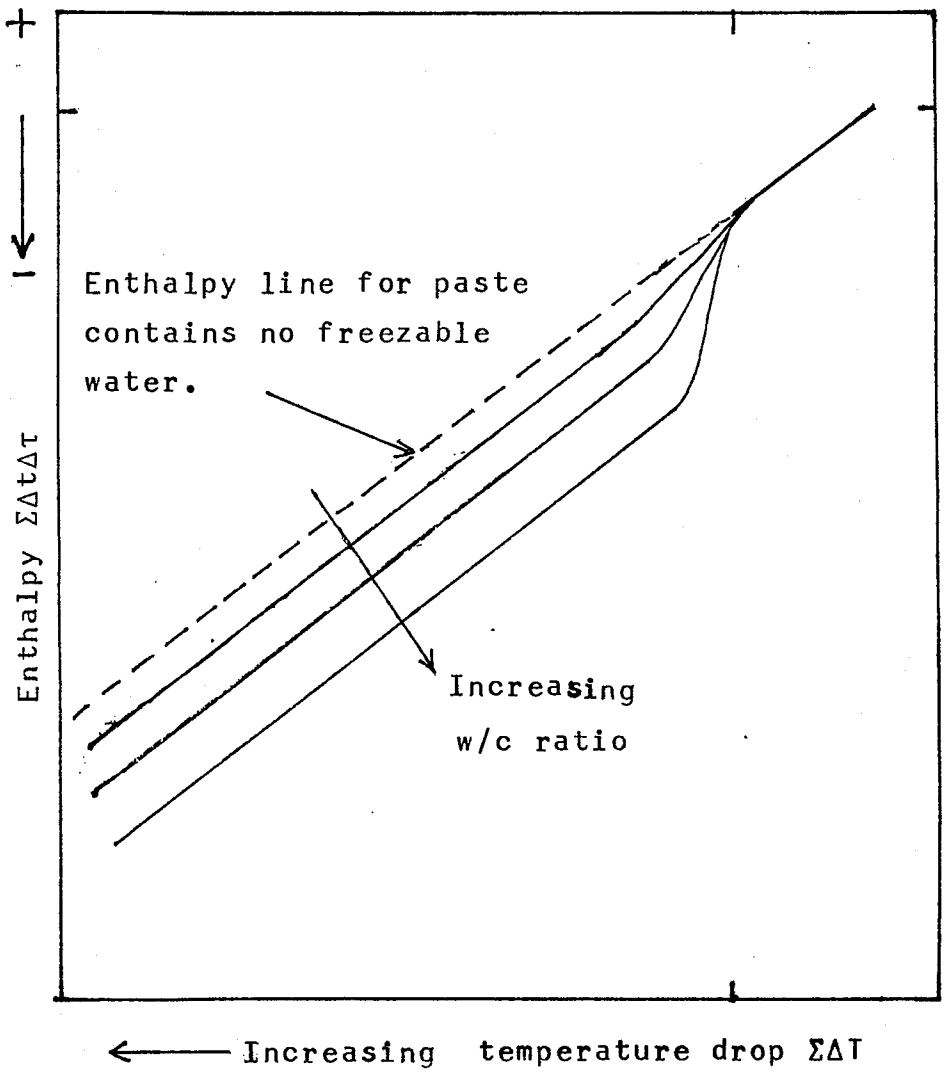

Figure4.11: The theoretical plot of equation $\Sigma\Delta t\Delta\tau=(M/\alpha)\Sigma\Delta T+(L/\alpha)w_f$

of experiments have been performed on a solid metal sample of heat capacity M_A. The heat equation of the experiments on the metal sample is given in the following equation.

$$\Sigma\Delta t\Delta\tau = \frac{(M_c+M_A)}{\alpha}\Sigma\Delta T \qquad (4.79)$$

where the second term of the heat equation in this case is zero. By plotting the enthalpy against the total temperature drop, M can be calculated ($M=M_c+M_A$).

Theoretically, if a sample is free from water, the plot of enthalpy against total temperature drop should be a straight line, but due to the latent heat of freezing of the water in the sample the curve will deviate as shown in figure 4.11.

For concrete samples with higher water-cement ratio the deviation is larger. This deviation corresponds to the value of the second term of equation 4.78. If the value of the latent heat of ice at the corresponding temperature is known, then the amount of freezable water at that temperature can be calculated.

4.3.2 FROST RESISTANCE OF CONCRETE

Concrete paste which is subject to low temperature use, may be exposed to frost action.The main reason, as we have discussed since the beginning, arises from the water content.

We Know that some of the water in concrete paste is evaporable. It has also been reported(72) that water in capillary pores can be evaporated under low relative humidity and that the paste can recover some of this water loss on resoaking it with water. Thus, a primary factor involved in frost action on the concrete paste is the degree of saturation.

The degree of saturation is defined according to equation 4.80 below.

$$s = \frac{w_f}{(w_f+a)} \qquad (4.80)$$

where w_f and a are the weight of freezable water and the volume of air per gm of sample respectively. Whiteside and Sweet(73) have reported that paste with an original degree of saturation above 0.9 is not frost resistant; and below 0.75, the paste is frost

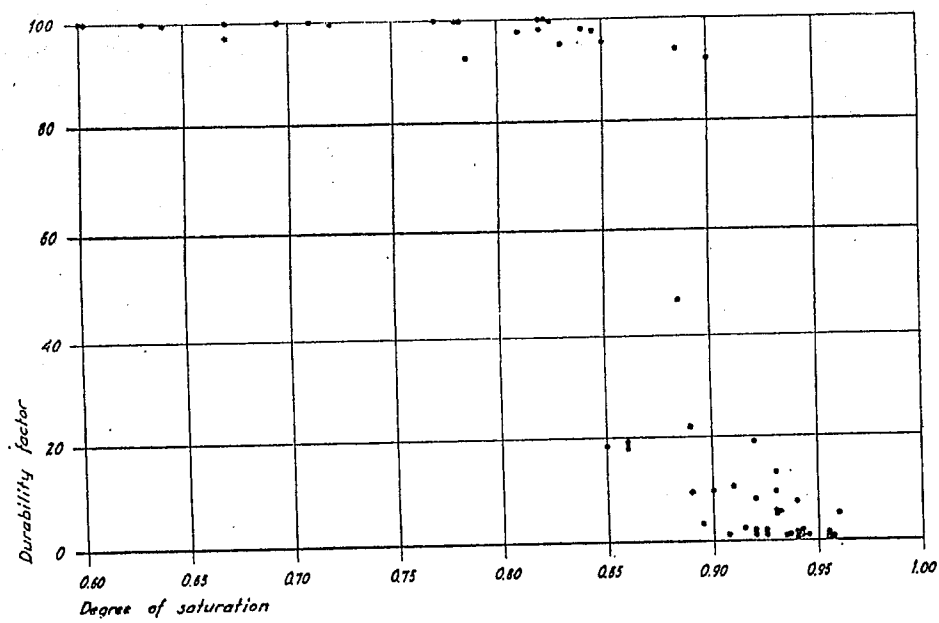

Figure 4.12: The influence of degree of saturation on frost resistance of concrete paste. (Reference 73).

resistance. Paste with original degrees of saturation between 0.75 and 0.9 is in a mixed condition. This report has been confirmed by Warris(74). Figure 4.12 shows the frost resistance of the paste against the degree of saturation which they produced. The varying degree of saturation was achieved by using partly air entrained paste and partly by drying.

Besides the water content, the air content of concrete paste also has some influence on the frost resistance. It has been reported(74) that after prolonged curing in water of both normal and air entrained concrete paste, the air voids decrease because they become partly filled with water; then the paste is subject to frost action.

Since water content in concrete paste is variable and depends on its surrounding, it is wise to examine the relation between the degree of saturation and the amount of absorbed water in concrete paste. Warris(74) made a model regarding this subject. Starting from the definition of the degree of saturation given in equation 4.80 together with equations 4.81 and 4.82 from Copeland and Hayes(75), he arrived at the relationships as in equation 4.83.

$$a = a_0 - w_a + 0.25w_n \tag{4.81}$$

$$w_f = w_t - 2.5w_n \tag{4.82}$$

$$s = \frac{w_0 - 2.5w_n}{w_0 + a_0 - 2.25w_n} + \frac{w_a}{w_0 + a_0 - 2.25w_n} \tag{4.83}$$

where,

a_0= the original volume of water content per gm weight of sample.

w_a= the weight of absorbed water per gm weight of sample

w_n= the weight of non-evaporable water per gm weight of sample.

w_0= the original water content or w/c ratio.

w_t= the weight of total water content per gm weight of sample, equal to $w_0 + w_a$.

Equation 4.83 contains two parts. For a given values of a_0 and w_0 the first part is dependent on w_n and the second part on w_a . Thus , according to this model, the degree of saturation is characterized by two factors, w_n which is related to the degree of hydration and w_a the amount of absorbed water in the concrete paste.

The frost resistance of concrete paste can also be studied by using the dilation of the paste

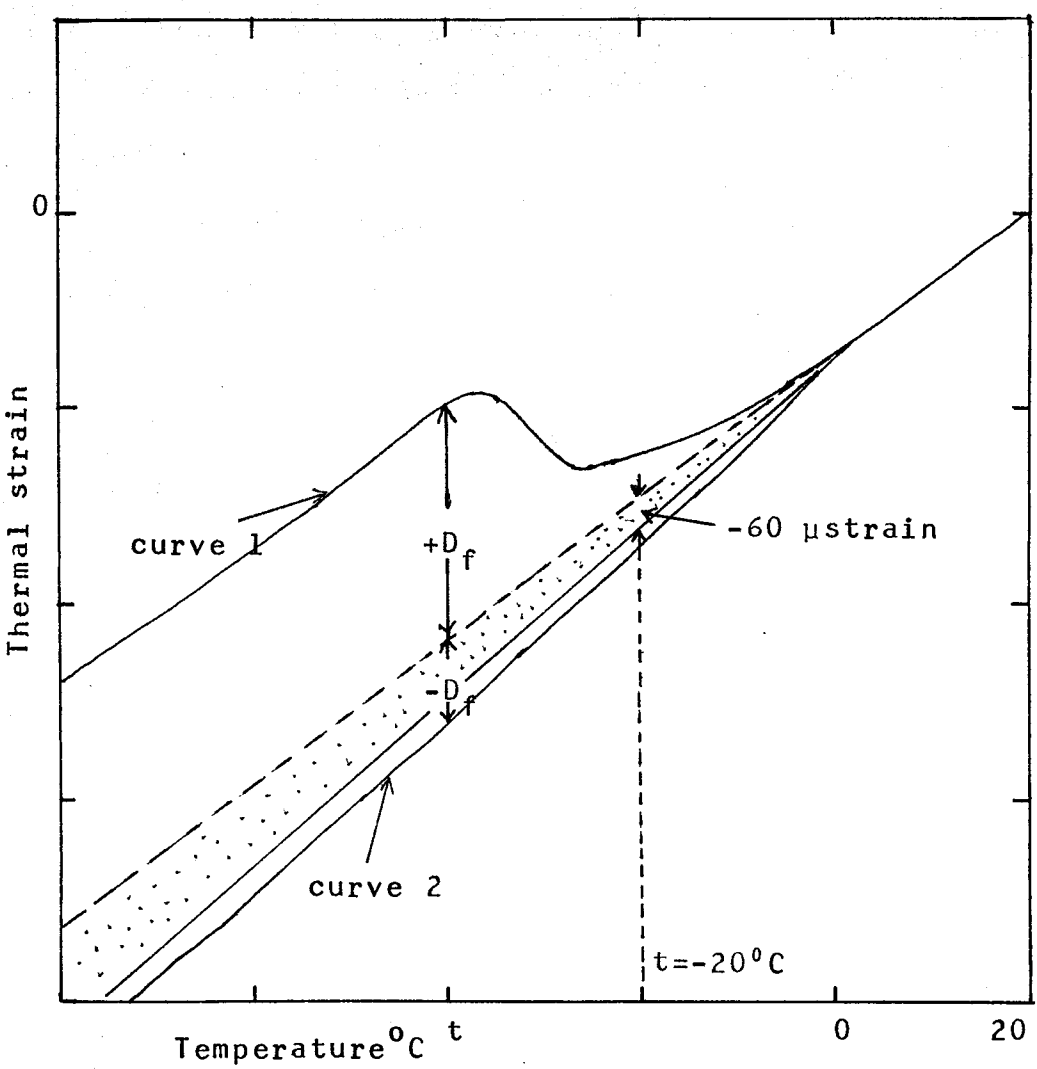

Figure 4.13: Thermal strain curves with a positive and negative dilation factor D_f at temperature t°C.

upon cooling. Vuorinen(72) has introduced a dilation factor in expressing the degree of frost resistance of a paste. He defined the dilation factor as the deviation of the contraction curve from the contraction line between 20^{0}C to 0^{0}C of a sample. Therefore, if expansion occurs below 0 ^{0}C, the factor will be positive as shown in figure 4.13 for curve 1. Conversely, if contraction occurs below 0^{0}C, the factor will be negative as for curve 2. Based on his experimental results, he concluded that a satisfactory frost resistance concrete paste can be achieved if the dilation factor is less than -60 μstrain at -20^{0}C (as in figure 4.13).

CHAPTER FIVE

EXPERIMENTS AND RESULTS

5.1 PREPARATION OF SAMPLES

All the concrete and cement samples were prepared from an ordinary Portland cement (ASTM Type I). The aggregates used in the concrete samples were from a marine type flint aggregate of about 5mm size and with smooth surface but irregular shape. The aggregates had been dried before casting. Samples with total w/c ratio 0.3 to 0.5 had a cement-aggregate ratio of 0.6 and for samples with a higher w/c ratio, the cement- aggregate ratio was 0.5.

The concrete and cement paste samples were moist-cured for at least 28 days at 20^0- 24^0C. They were then transfered into a water bath and were kept moist until several hours before experiments.

5.1.1 HARDENED CONCRETE SAMPLES

Preliminary concrete samples were cylinder with 40mm diameter and 100mm height. The average weight of the samples was 350 gm.

Later samples were 8 times heavier with diameter and height of 96mm and 200mm respectively. The average weight was 3.0 to 3.5 Kg. Samples for heat capacity measurements had w/c ratios at 0.3, 0.37 and 0.4 and for dilation samples the w/c ratios were varied from 0.3 to 0.7.

Three groups of samples for each w/c ratio were prepared. The first group was the wet or moist cured samples. These samples were kept under water at 20° to 24° C and they were taken out only for testing. However, the excess water on the surface was allowed to dry before they were put into the testing rig.

The second group were rewetted samples. After 28 days of curing period, these samples were taken out and dried in the oven at 100°C until no further loss in weight was noticed and this took about 21 days. These samples were then resoaked and kept moist as in the first group of samples.

The third group were the dry samples. They were dried as in the second group, except that they were kept dry in the oven at 35^0 C in between experiments.

5.1.2 CEMENT SAMPLES

Cement samples were similar to concrete samples. They were prepared from a mixture of ordinary Portland cement (ASTM grade- Type I) with water. Three groups of cement samples were made with water-cement ratios 0.27, 0.35 and 0.45. The samples were moist-cured at 20^0 - 24^0C for 28 days and were kept in the water bath. These samples were used for thermal strain testing.

5.1.3 AGGREGATE SAMPLES

The samples were made by cutting large flint samples into a rectangular shape of size 90x90 mm and 200 mm height. The samples were kept in a room of relative humidity 50%. These samples were used in the thermal strain experiments.

5.1.4 SAMPLES FOR NMR TEST

The size of the concrete samples was 20x4x4 mm and they were made by cutting from a large thermal strain sample with w/c ratio 0.37. Each sample was sealed in a glass tube full of water.A rewetted NMR sample was prepared by exposing the same moist-cured sample in a low humidity room for more than a week. Then it was resoaked in water before the testing were performed.

5.2 APPARATUS FOR THE HEAT CAPACITY MEASUREMENTS

The cooling calorimeter which was used in the measurements is shown in figure 5.1. Two concentric copper cylinders, each with about 1mm thickness, were embedded into two circular blocks of balsa wood at both ends. The balsa wood was used as the heat insulator, to stop the heat lost through the copper walls ends. The thermal conductivity of the balsa wood is 5.50×10^{-2} watts/m ^{0}C and is less than that for polysterene. The space in between the concentric copper walls was filled with cotton wool in order to obtain a temperature gradient between the walls. The lid of the calorimeter was also made from a balsa wood. To prevent air

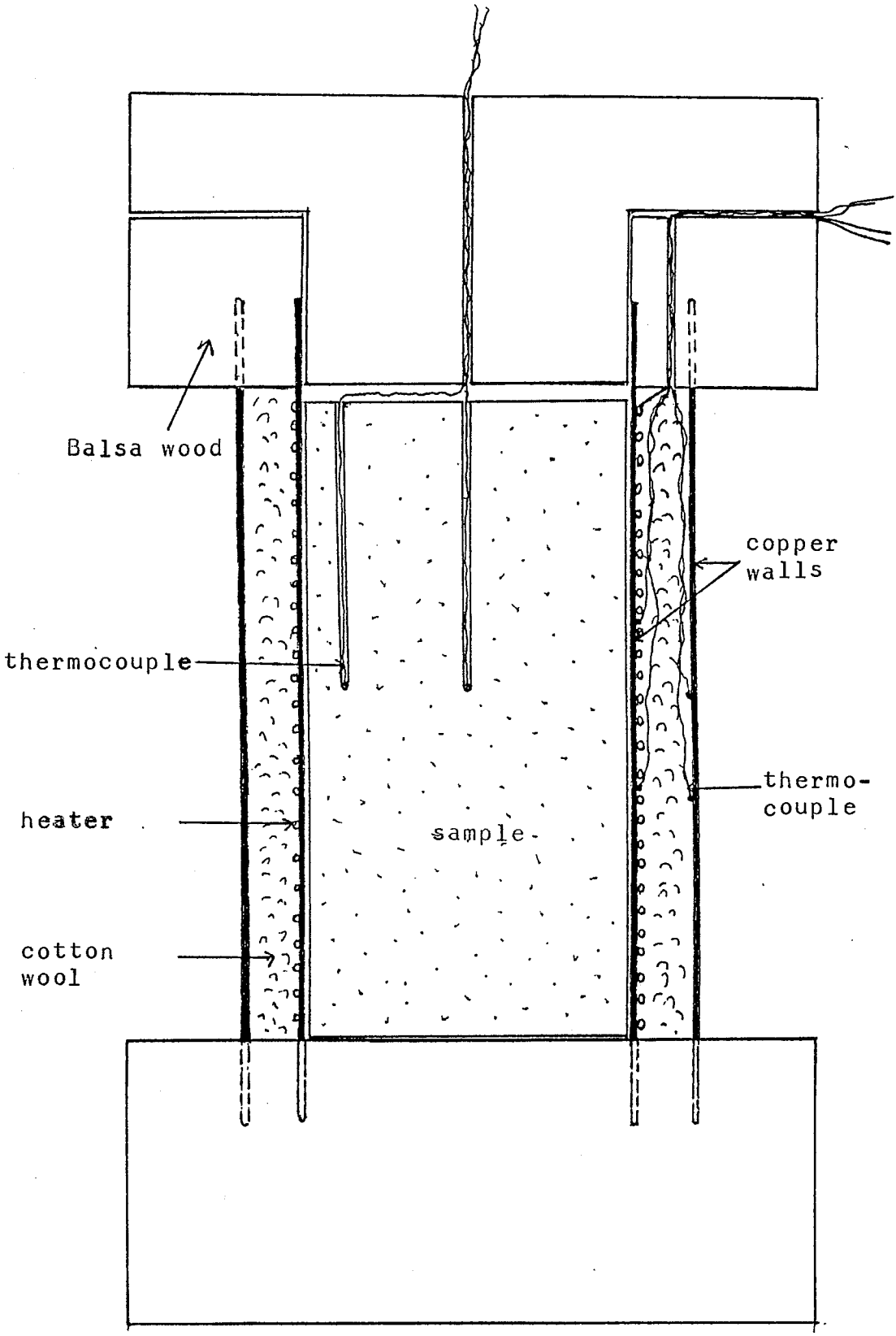

Figure 5.1: The cooling calorimeter

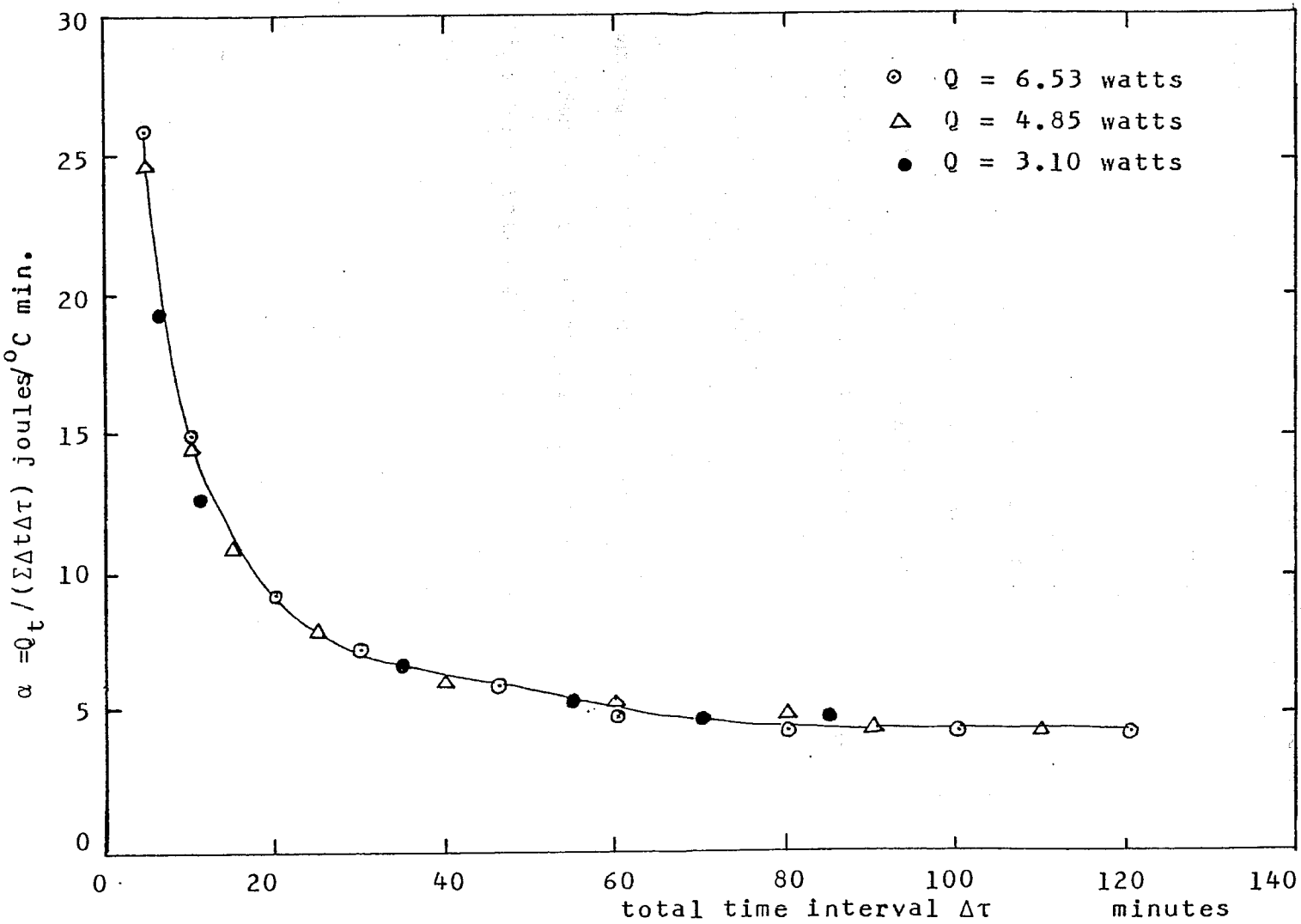

Figure 5.2: The coefficient of heat transfer α at -80°C.

convection, the lid was made a tight fit.

An earlier calorimeter had a similar set-up except that it did not have a heater coil mounted on the inner copper wall. This was because the measurement of α, the heat transfer coefficient was made by using a standard aluminium sample of known heat capacity. The value of α which was measured in this way was 8.18 J/ ^{0}C.min. Later, the heat transfer coefficient α was measured by using a constant heat supply from the heater according the following formula.

$$\alpha = \frac{\text{Total heat supply } Q_t}{\Sigma \Delta t \Delta \tau} = \frac{Q_t \Delta \tau}{\Sigma \Delta t \Delta \tau} \qquad (5.1)$$

where Δt is the temperature difference between the copper walls and $\Delta \tau$ is the time interval. The values of the heat transfer α is shown as a function of time in figure 5.2. A constant value is reached after about 90 minutes.

Calibration of the apparatus was made by cooling a standard aluminium sample of 96mm diameter and 200 mm height in the freezer cabinet which was previously maintained at -80^{0}C. The measured value of the heat capacity of aluminium agreed within 5%.

5.3 THE THERMAL STRAIN RIGS

Figure 5.3 shows the preliminary version of the thermal strain rig. This rig can only test one sample for each run of the experiment. To counter the vibration of the freezer which may affect the reading of the dilation gauge, the rig was rested on a thick rubber pad inside the freezer cabinet.

A later version of the thermal strain rig could test 4 samples at a time. It uses the same principle as the preliminary version, except that it was suspended by 4 steel coiled springs inside the freezer and it was also confined in an air-tight chamber. The setup of the apparatus is shown in figure 5.4.

A dial gauge of type Mitutoyo,model 1012-10 with a sensitivity of 0.002 mm, together with a quartz rod and a quartz tube were used to detect the dilation of the test samples.

The whole thermal strain rig was confined in a chamber to prevent vapour in the atmosphere from forming ice on the dilation apparatus when the temperature of the freezer is lowered below 0^{0}C. To avoid ice affecting the movement of the gauge, some drying agents (Silica gel and Molecular sieve) were

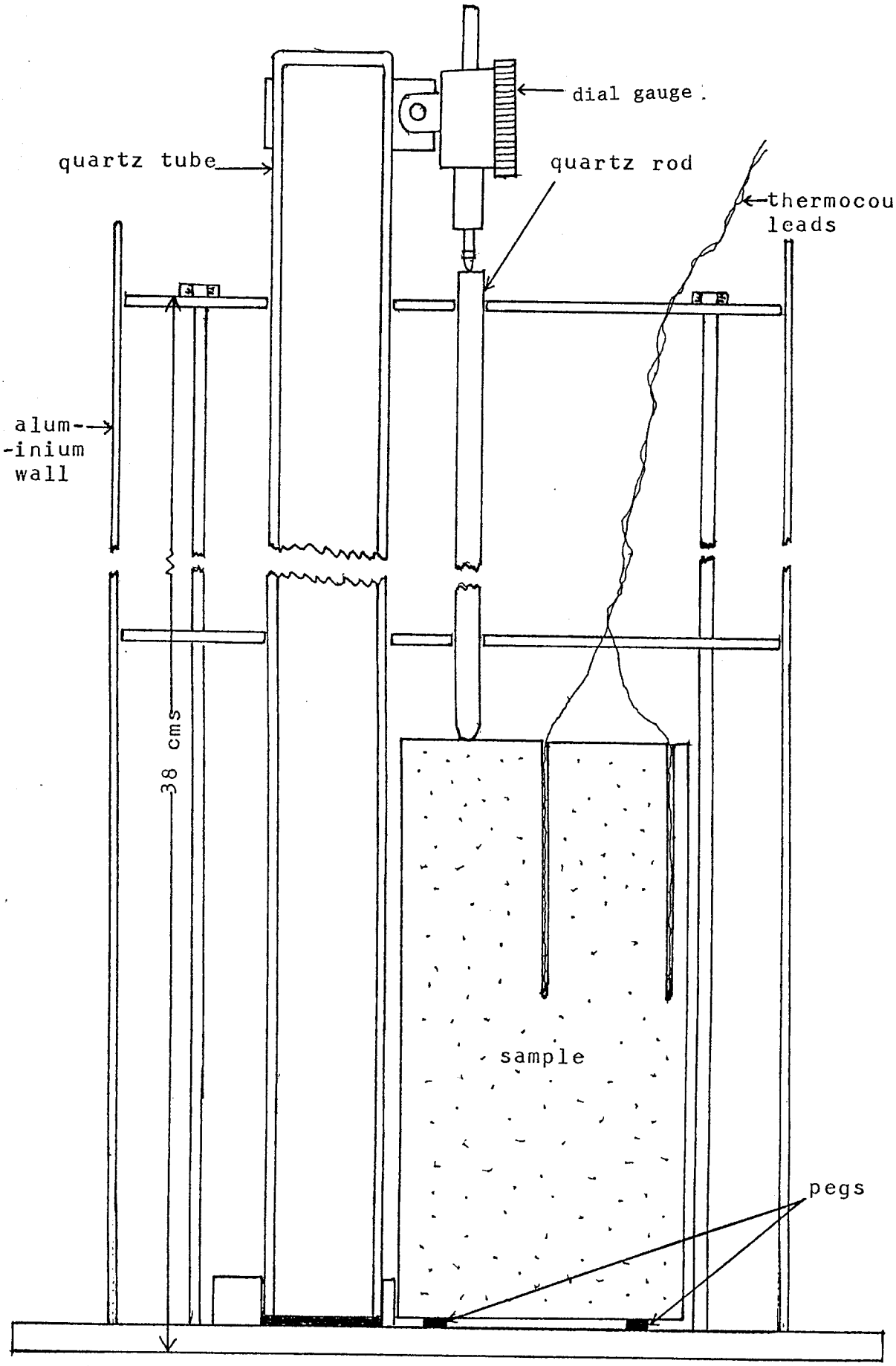

Figure 5.3: The thermal strain rig for one sample

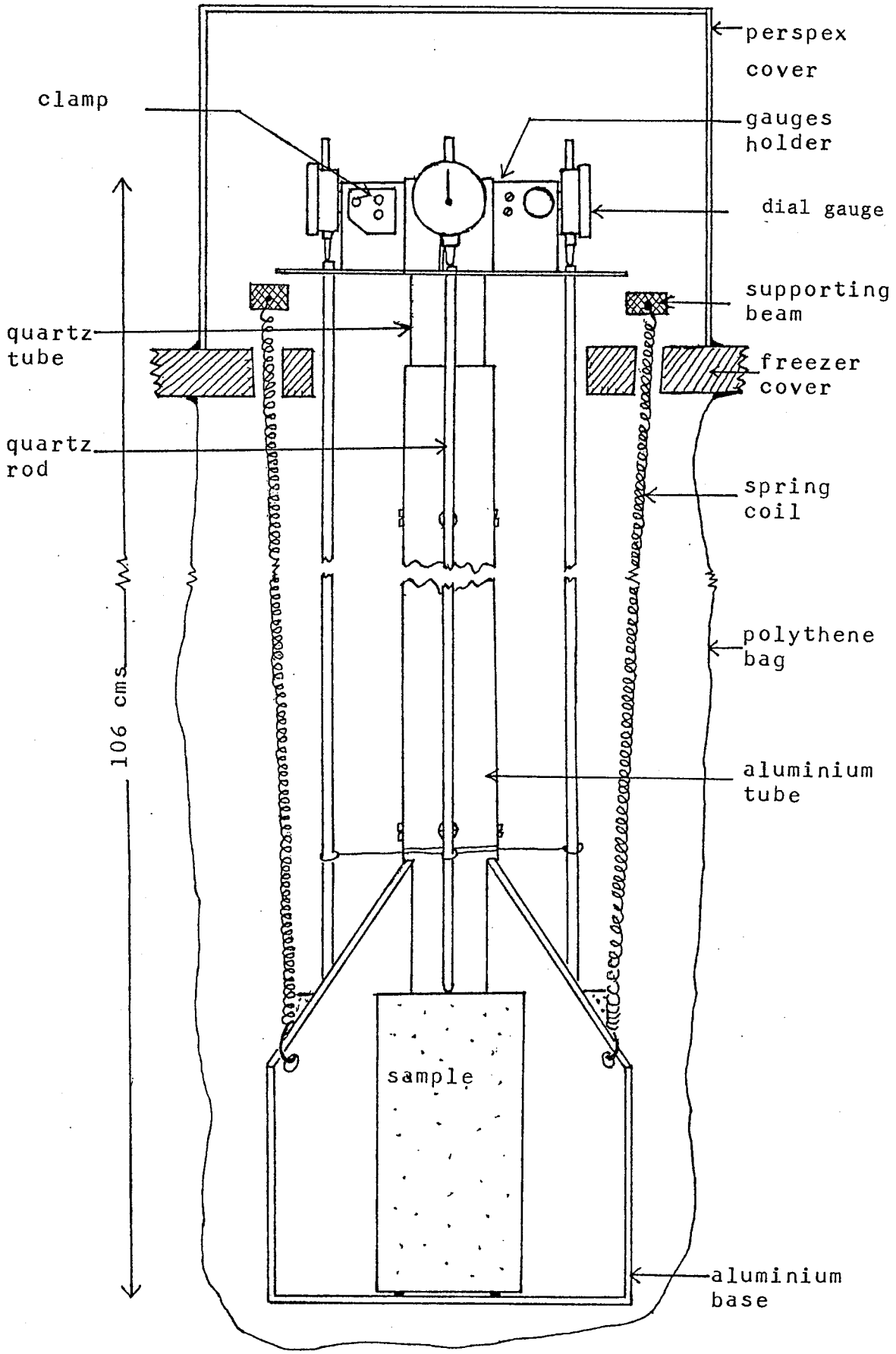

Figure 5.4: The thermal strain rig for 4 samples

suspended in small bags at the opening of the freezer lid, which is the place where the water vapour is more likely to condense.

The calibration of the thermal strain gauges was made by measuring the contraction of a standard aluminium block. The contraction curves of the one sample rig and the 4 sample rig are shown in figure 5.5 and 5.6 respectively. The data shows that the measurement of the aluminium contraction is within 5% of the published value of 22 μstrain/^{0}C.

5.4 OTHER APPARATUS

5.4.1 TEMPERATURE MEASUREMENTS

All temperature measurements have been made by using copper-constantan thermocouples with the reference point at the ice point. The thermocouples were made from standard thermocouple wires of SWG 40.

The voltage produced by the thermocouple junctions was measured by a digital voltmeter model Solatron A210 Schlumberger with a sensitivity of one μV.

For the measurement of the sample temperature , two thermocouples were placed inside the

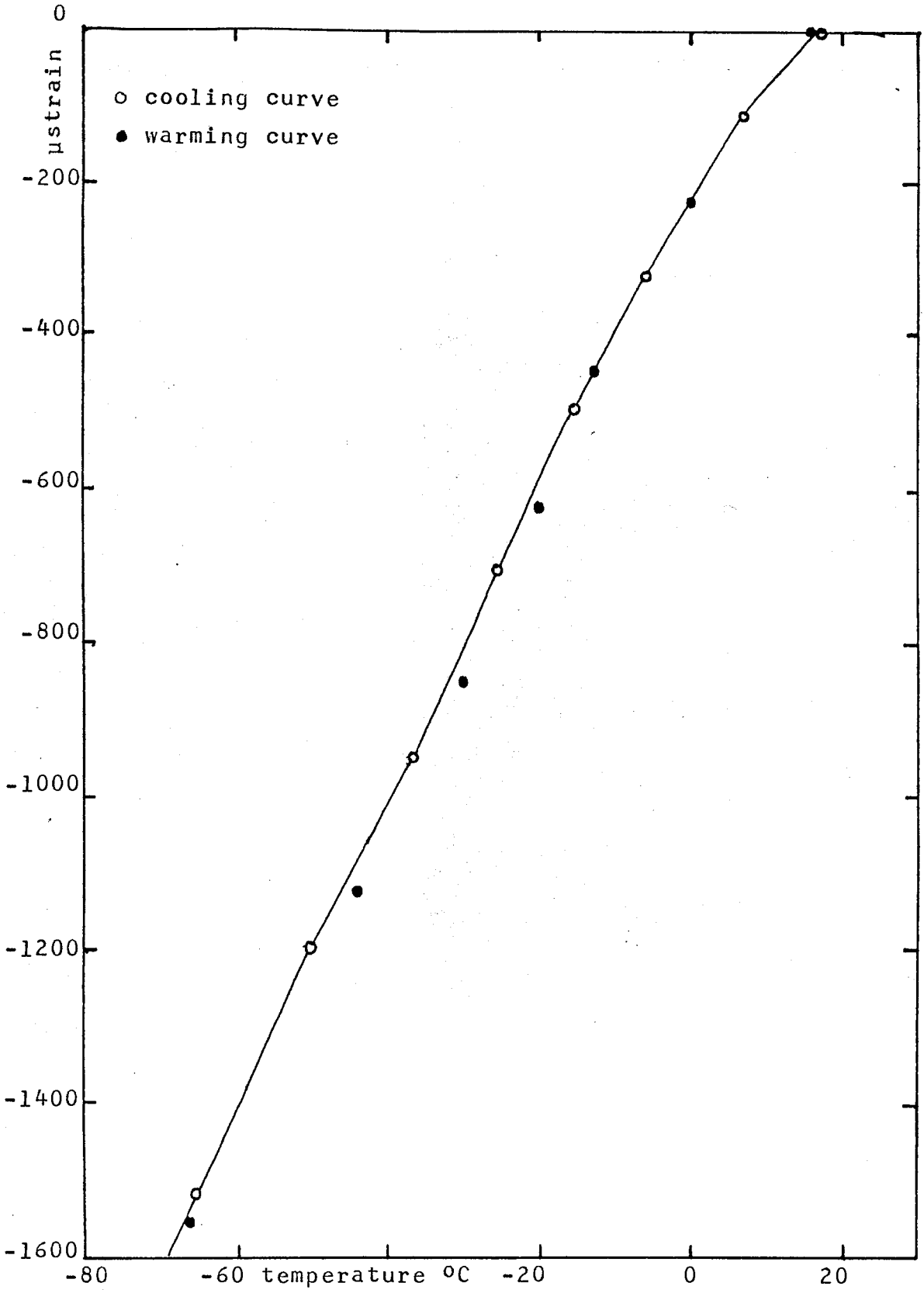

Figure 5.5: Thermal strain of the aluminium sample by using the preliminary rig.

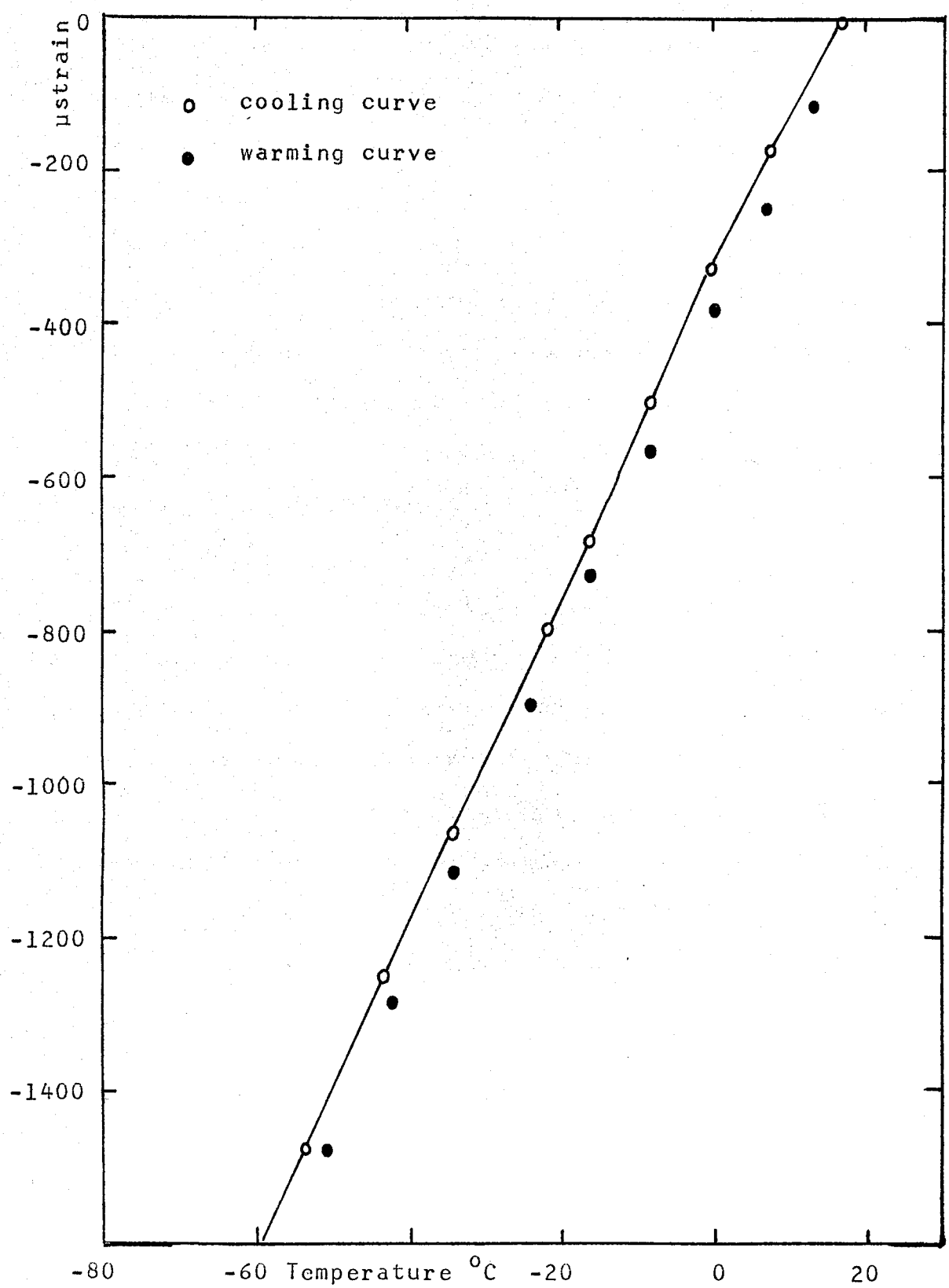

Figure 5.6: Thermal strain of an aluminium block

samples, one in a hole at the centre, the other one in a hole near the surface. In order to have a good thermal contact with the sample, the holes were filled with some vacuum grease with a quoted thermal conductivity of 168 watts/m^{0}C at 0^{0}C.

In the cooling calorimeter,the temperatures of the copper walls were also measured by thermocouples which were attached by PTFE tape (see figure 5.1).

5.4.2 COOLING CABINET

The cooling cabinet was a 2-stage deep freezer, made by Fisons Cliffco, a capability of achieving -80 ^{0}C easily. The rate of cooling from room temperature was about 0.30^{0}C per minute.

The rewarming process utilised a 1.5 kW heater connected to a voltage regulator. The maximum rate of warming was about 0.37^{0}C per minute.

5.4.3 NUCLEAR MAGNETIC RESONANCE INSTRUMENT

The instrument used in the testing of the concrete samples is a Bruker CXP 200 spectrometer with an Oxford Instruments Superconducting magnet. The

operating frequency was 200.044,444,44 MHz in a magnetic field of 4.67 tesla.

5.5 RESULTS OF HEAT CAPACITY MEASUREMENTS

To present the results, the samples have been grouped as following.

Sample A1 ... w/c= 0.30 moist-cured.

Sample B1 ... w/c= 0.37 moist-cured.

Sample C1 ... w/c= 0.40 moist-cured.

Sample A2 ... w/c= 0.30 dried to constant weight.

Sample B2 ... w/c= 0.37 dried to constant weight.

Sample B3 ... w/c= 0.37 B2 resoaked in water for more than 23 days.

Enthalpy variation with temperature for samples A1, B1, C1 and A2 are shown in figure 5.7.Figure 5.8 shows the enthalpy-temperature variation of the rewetted sample B3. The curves for the moist-cured samples show that the enthalpy of the paste decreases gradually between 0^0C and -45^0C. Below -45^0C the curves are parallel to the enthalpy curve of the dry sample A2. The enthalpy of the rewetted sample in figure 5.8 shows a sudden decrease within a small temperature range just below 0^0C. These two figures,show that the contribution of the latent heat of freezing of water in the moist-cured samples is distributed over a temperature

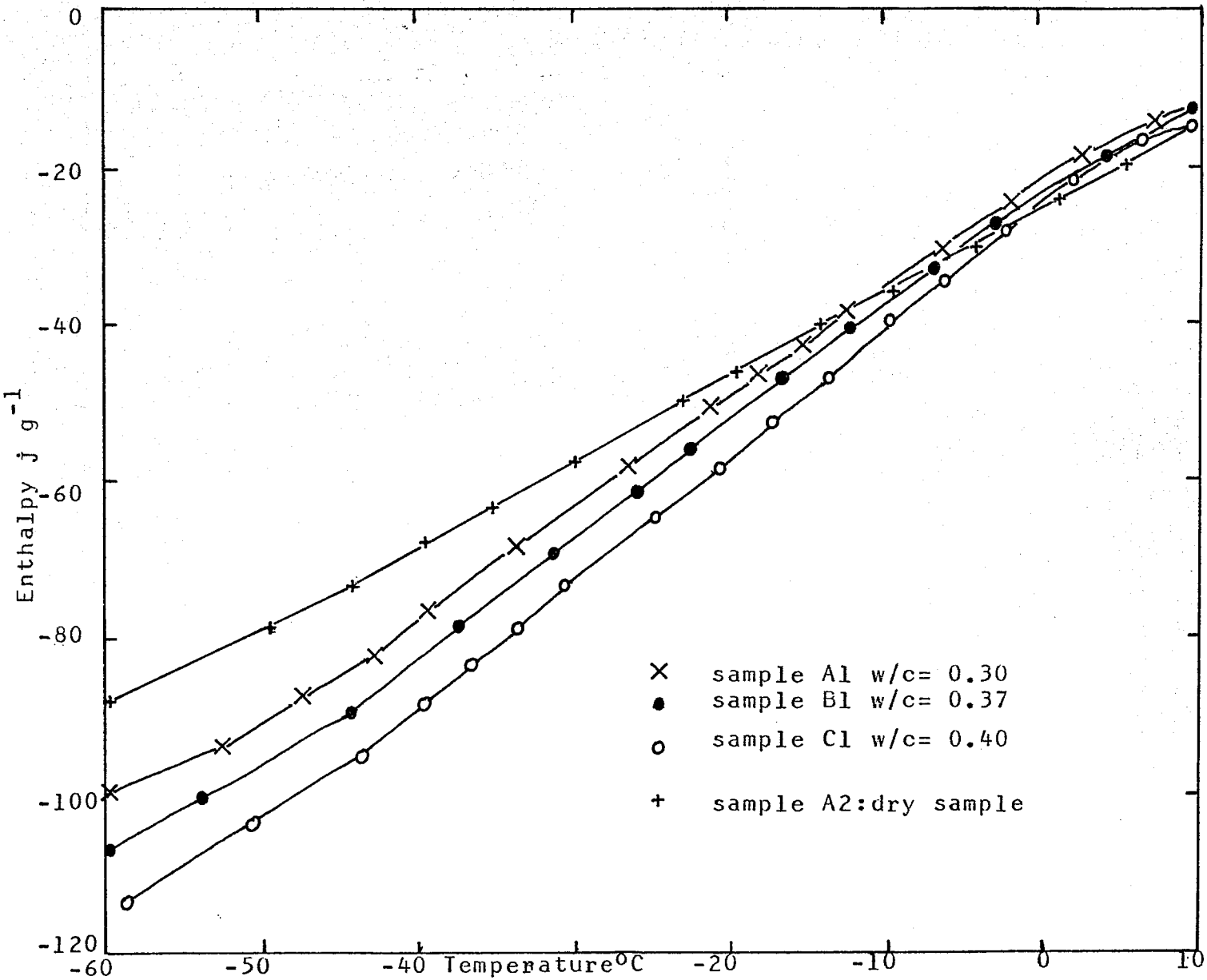

Figure 5.7: Enthalpy of concrete samples

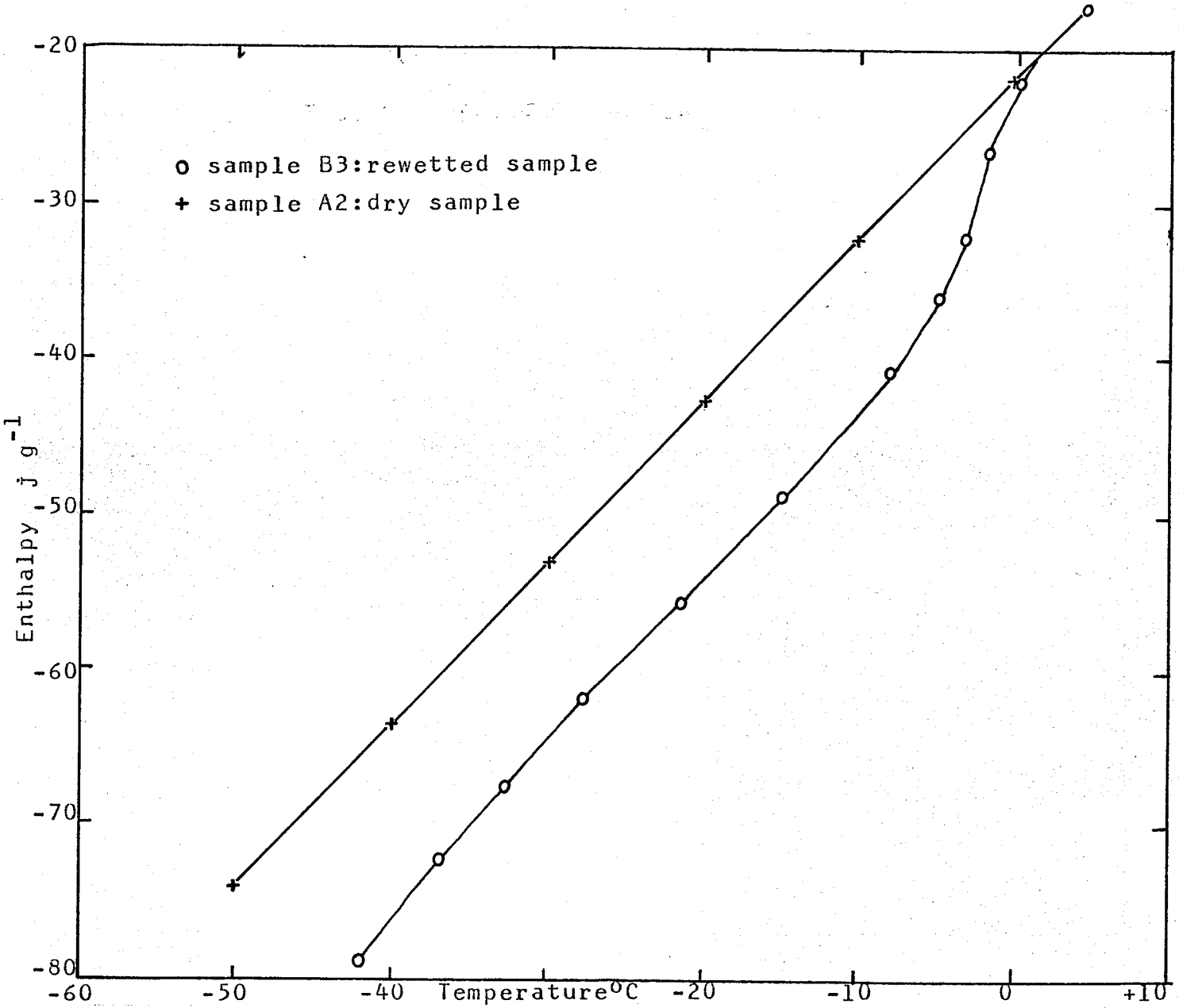

Figure 5.8: Enthalpy of a rewetted sample

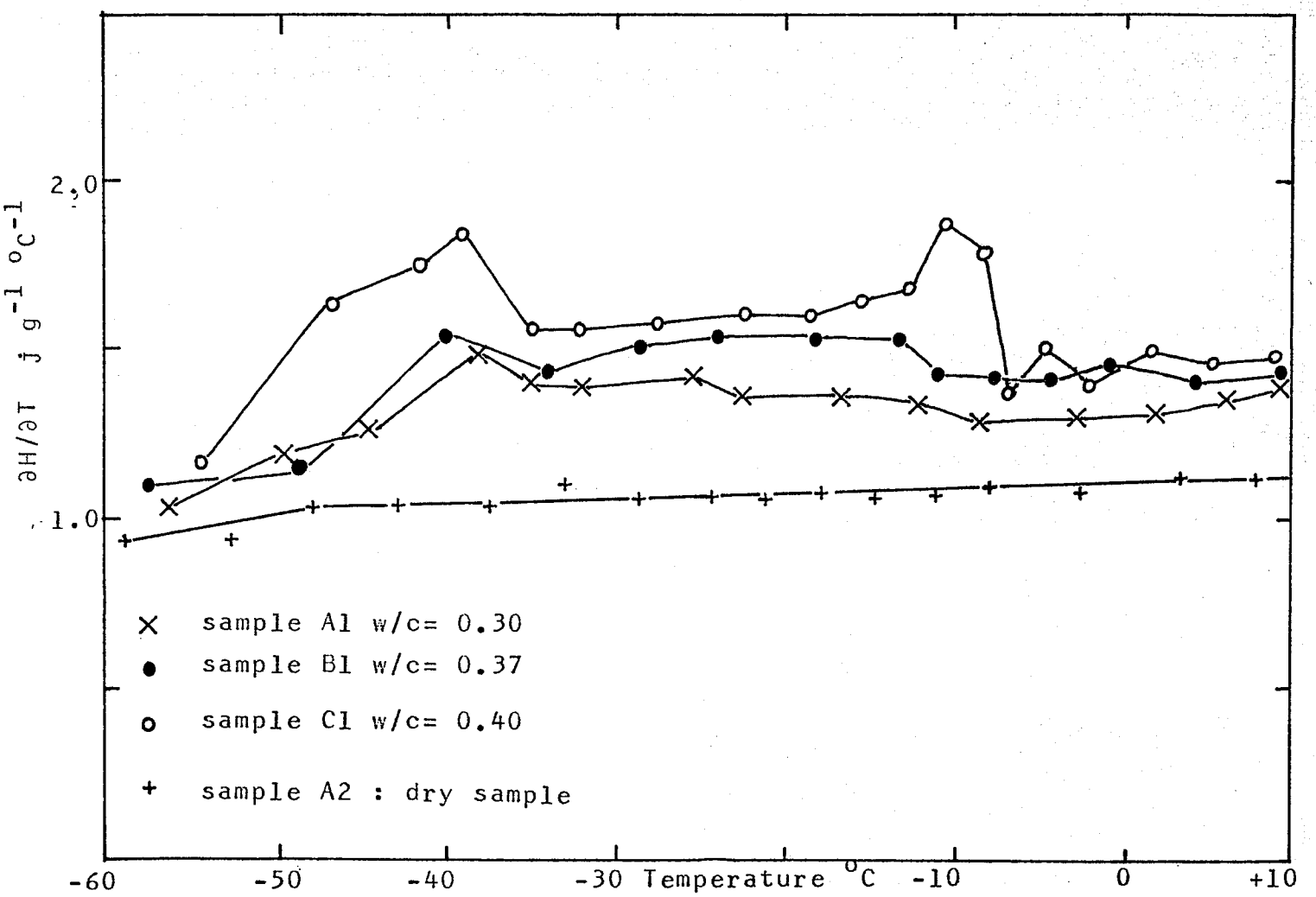

Figure 5.9: specific heat of concrete samples

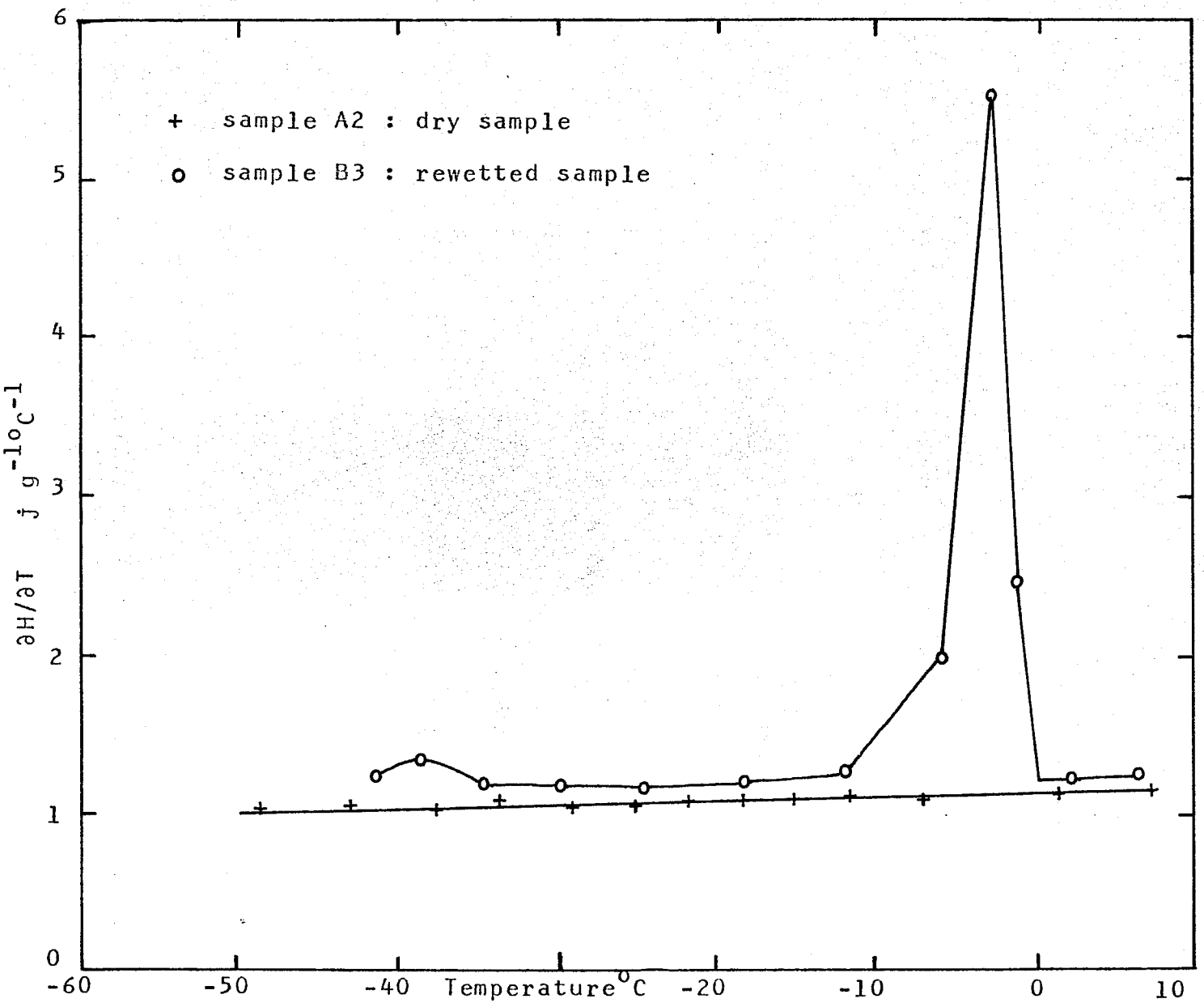

Figure 5.10: specific heat of a rewetted concrete sample

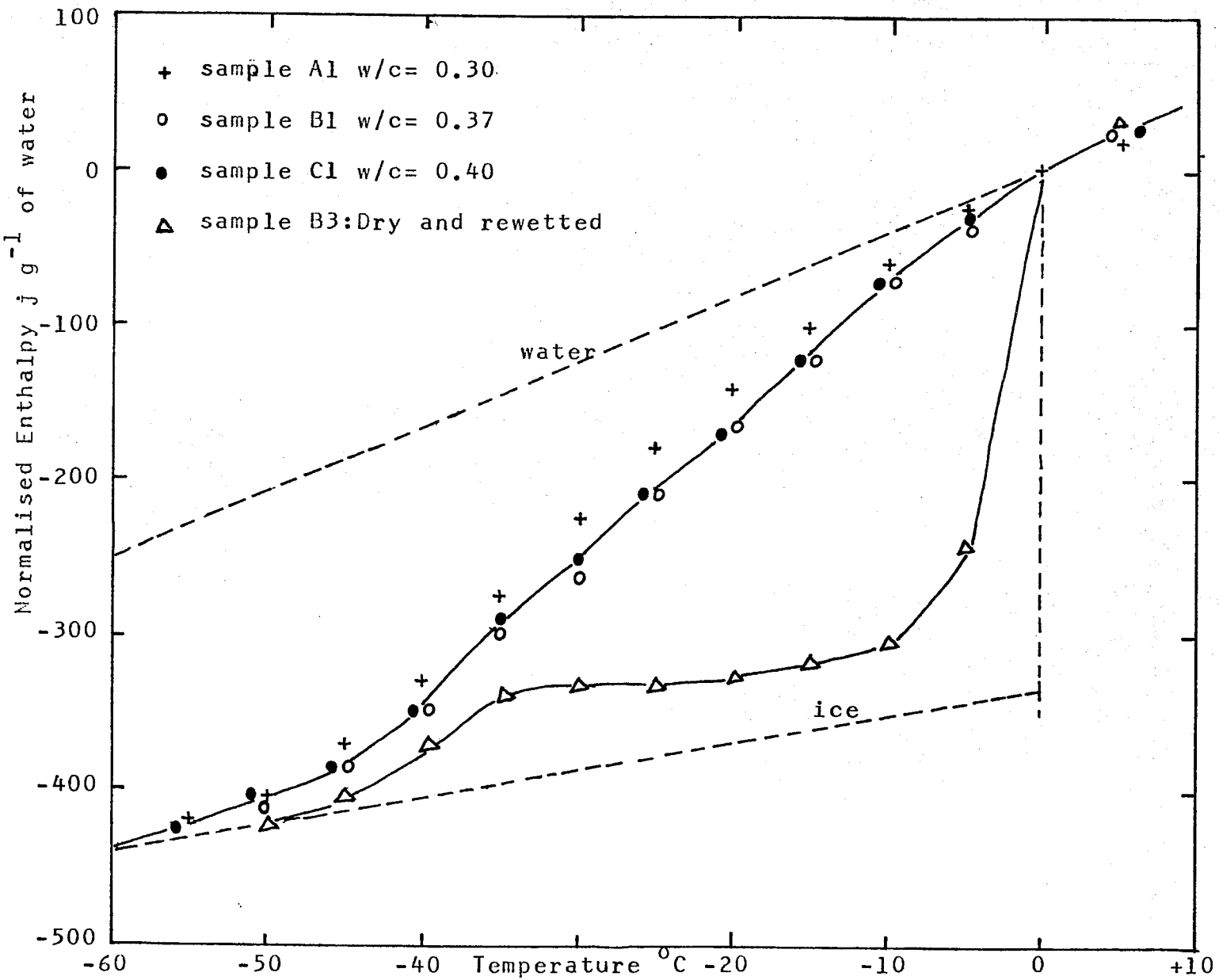

Figure5.11: Normalised Enthalpy of concrete samples

range between 0^{0} C to -45^{0} C, while in the rewetted sample, most of the water freezes just below 0^{0}C.

From the data in figure 5.7 and 5.8, values of $\partial H/\partial T$ (differential enthalpy) of the samples are plotted against temperature and are shown in figure 5.9 and 5.10 respectively. Since $c_p = (\partial H/\partial T)_p$, these differential enthalpy plots are the effective heat capacity curves. The value of c_p at each temperature interval contains the latent heat of freezing of water over that temperature interval as well as the heat capacity of the cement matrix, the aggregate and the various classes of non- chemically bound water. The curve for the dry sample A2 shown in figures 5.7, 5.8, 5.9 and 5.10 is a straight line which shows that no change of phase takes place. The values of c_p for the rewetted sample is very large within the temperature range 0^{0}C to -10^{0}C while below -10^{0}C the values of c_p are very close to the dry sample.

Figure 5.11 plots the difference in enthalpy between samples A1, B1 and C1 and the dry sample A2, to give the additional enthalpy drop associated with the freezing of the non-chemically bound water. For free water, the enthalpy change from the liquid state at 0^{0}C to the ice state at -60^{0}C is 440

joule/gm and therefore the enthalpy differences have been normalised to -440 joules/gm between 0^0 and -60^0 C. In the normalisation procedure, it was assumed that the enthalpy change of the adsorbed water in the concrete paste is the same as that of free water.

It can be seen that the normalised enthalpy plots for samples A1, B1 and C1 of different w/c ratios, are close together. On the other hand, the rewetted sample B3 shows totally different behaviour. The latent heat of freezing is largely confined to the higher temperature range with 90% above -10^0 C. The remaining 10% appears to freeze between -35^0 C and -45^0 C.

5.6 RESULTS OF NMR MEASUREMENTS

Figure 5.12 shows the effect of temperature on the NMR spectra of a moist-cured concrete with w/c ratio 0.37. The adsorption spectra show only one peak which corresponds to adsorbed water. The peak decreases with temperature, while the line-width increases from 0.49 gauss at 20^0C to 1.18 gauss at -100^0C(see figure 5.17). The shapes of the spectra do not change in passing through the freezing transition region and no sign of bulk water or ice is shown in the spectra.

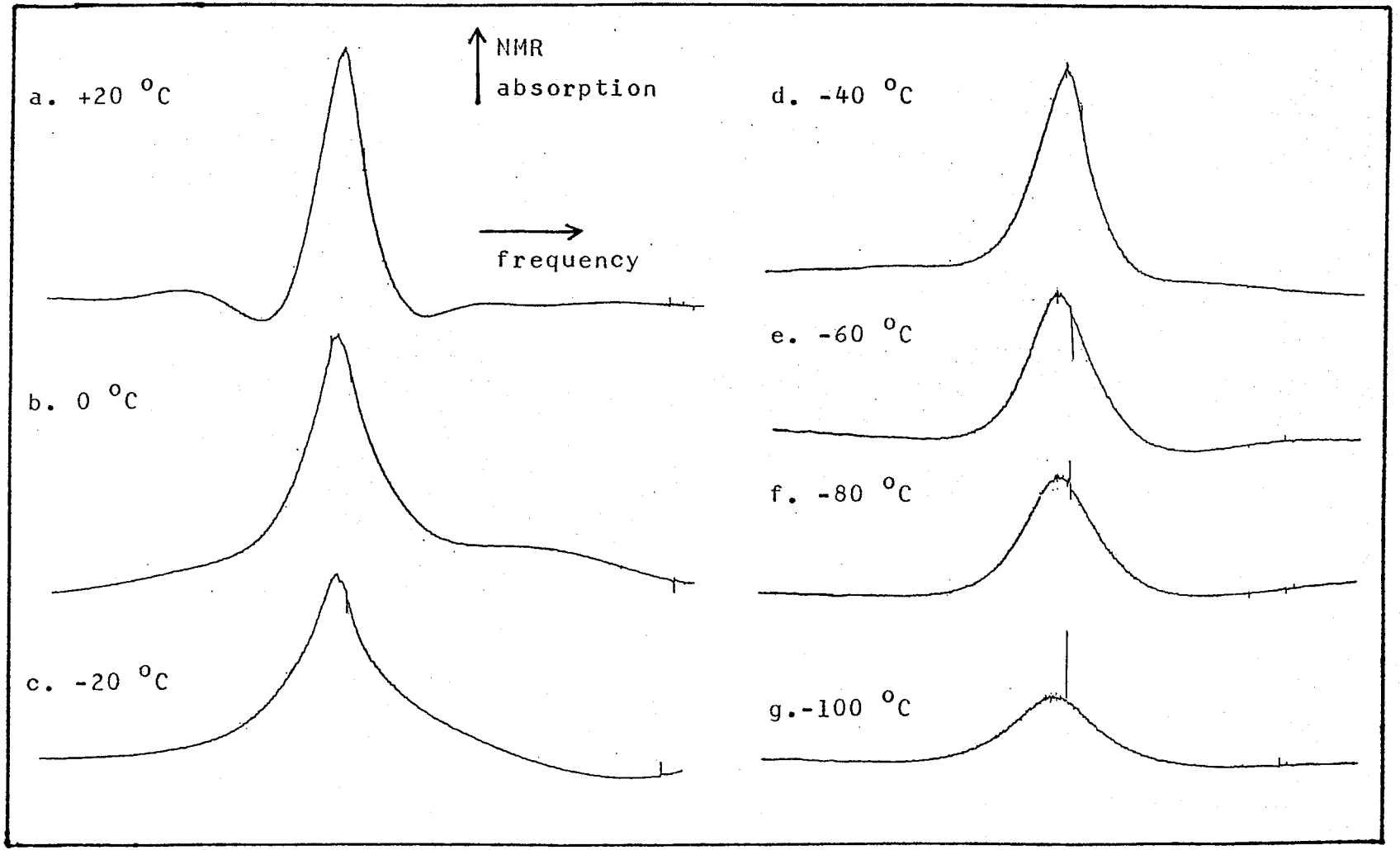

Figure 5.12: Proton NMR in moist-cured concrete w/c= 0.37
Effect of temperature

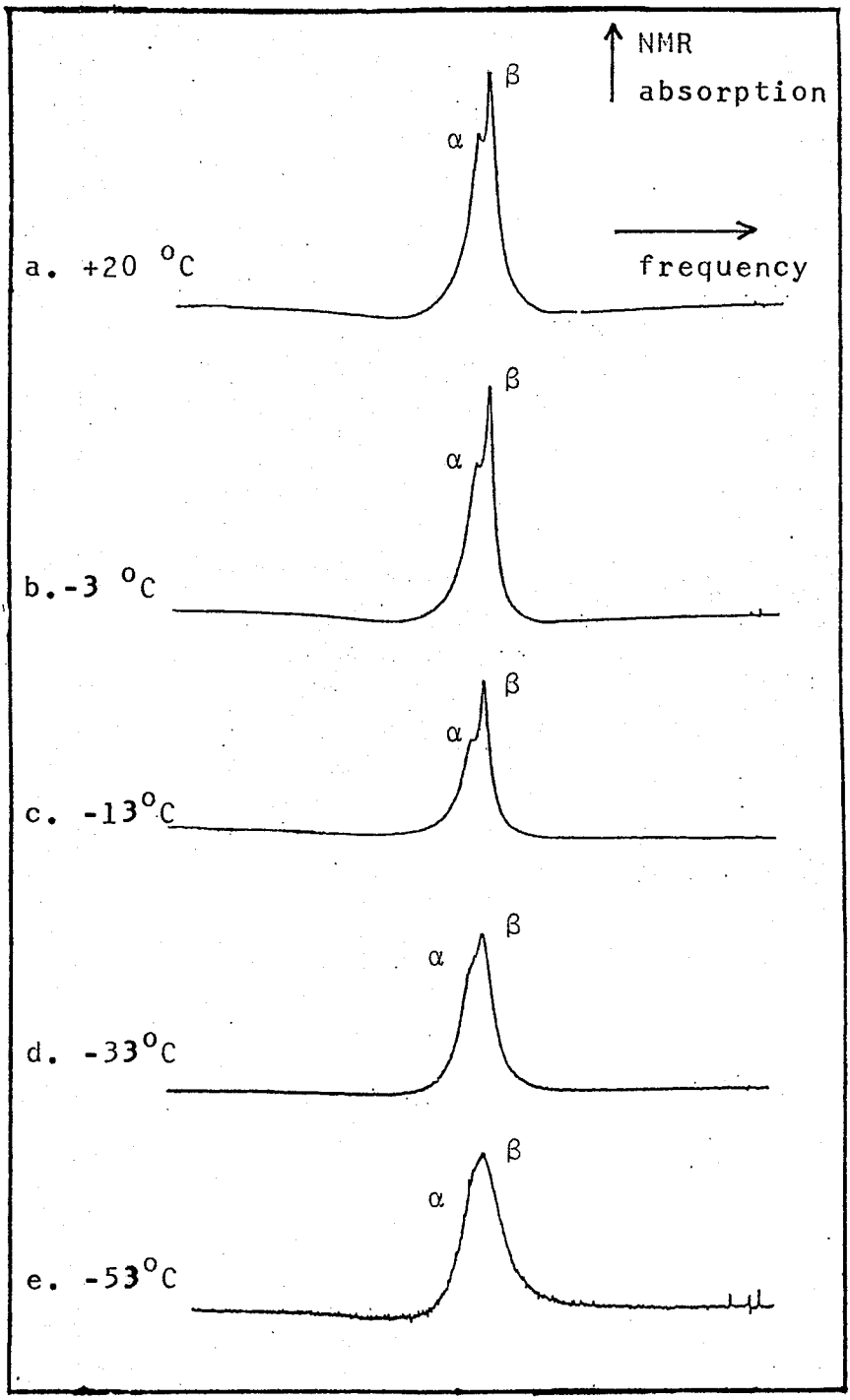

Figure 5.13: Dry and Rewetted sample
Effect of cooling

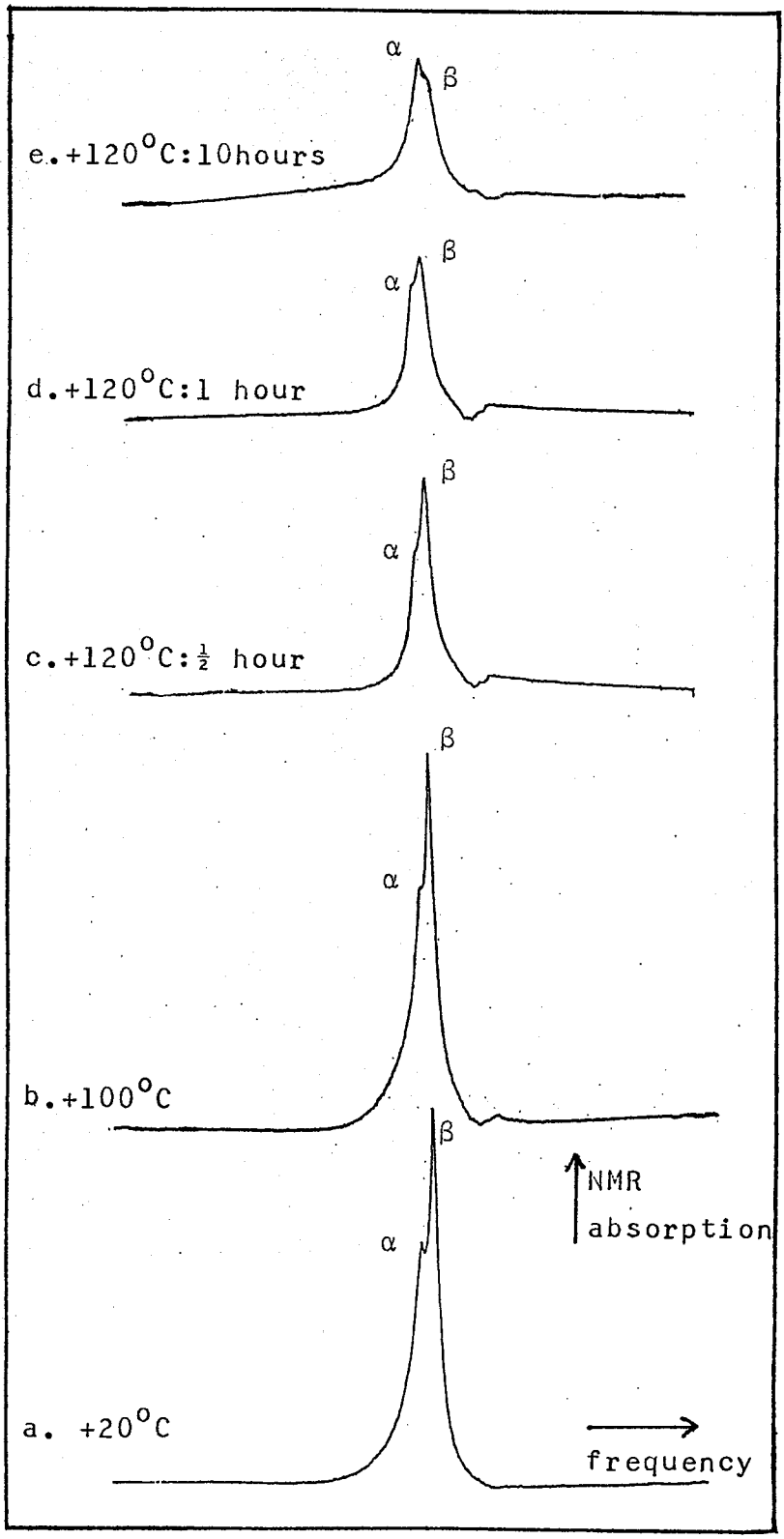

Figure 5.14: Dry and Rewetted sample
Effect of heating at 120°C

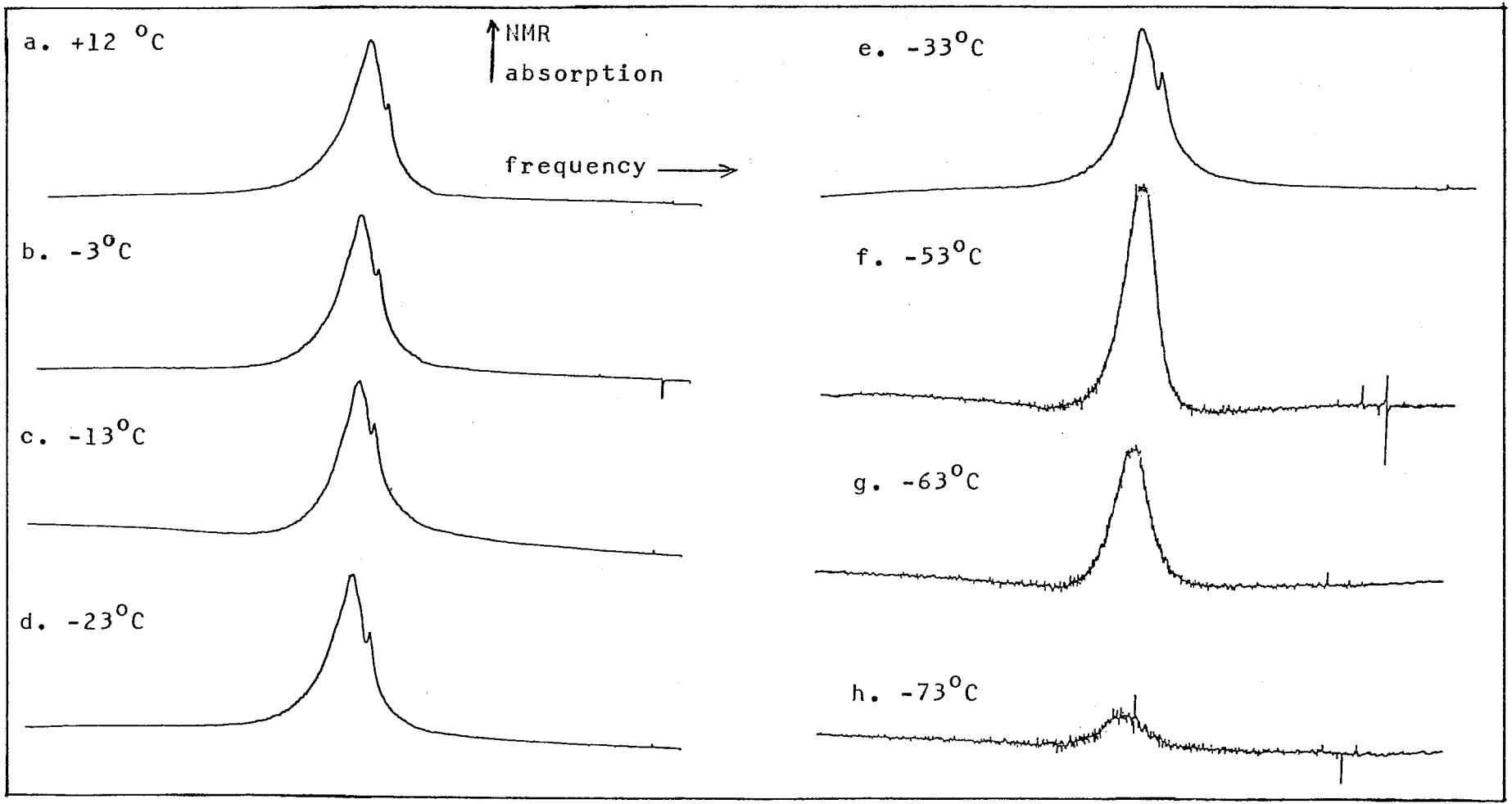

Figure 5.15: Proton NMR in a saturated moist-cured concrete sample w/c = 0.37
The effect of temperature

The rewetted sample has spectra with different characteristic and is shown in figure 5.13. A spectrum taken at 20^{0}C (figure 5.13 (a)) has two peaks α and β. The sharp line β is at a frequency of about 2.5 KHz above the main broad line α. On cooling down to -53 ^{0}C, the sharp β line has gradually disappeared into the shoulder of the α line (figure 5.13(e)). The sharp β line corresponds to the rewetting water. It is less strongly adsorbed water and freezes at a relatively higher temperature, just below 0^{0}C. On heating this sample at 120^{0}C as shown in figure 5.14,the sharp β line diminishes after 10 hours (see figure 5.14(e)). Figure 5.16 shows the relative change of the peaks α and β. The α peak which may correspond to strongly adsorbed water has shown no change after 10 hours of heating and has the same peak height from the beginning of the heating. The line-width of the rewetted sample, on heating for 10 hours has only a small increase from 0.57 gauss to 0.59 gauss (see figure 5.18).

The observed spectra of a fully saturated moist-cured concrete sample have slightly different characteristics compared with the ones in figure 5.12. The spectra, as shown in figure 5.15, have a sharp line in the shoulder of the broad line spectrum. This sharp

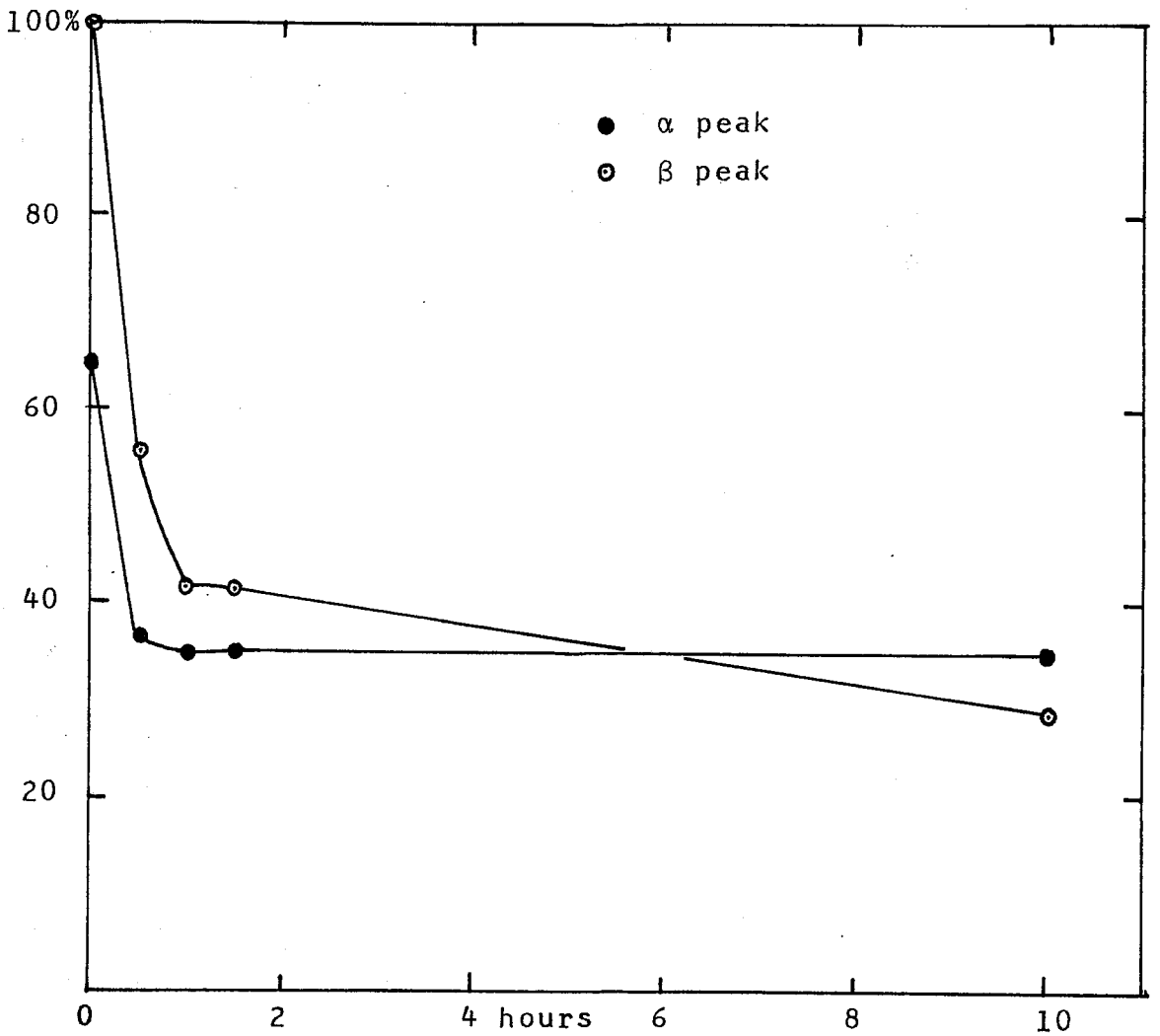

Figure 5.16: Peak height of a rewetted concrete sample baked at 120°C

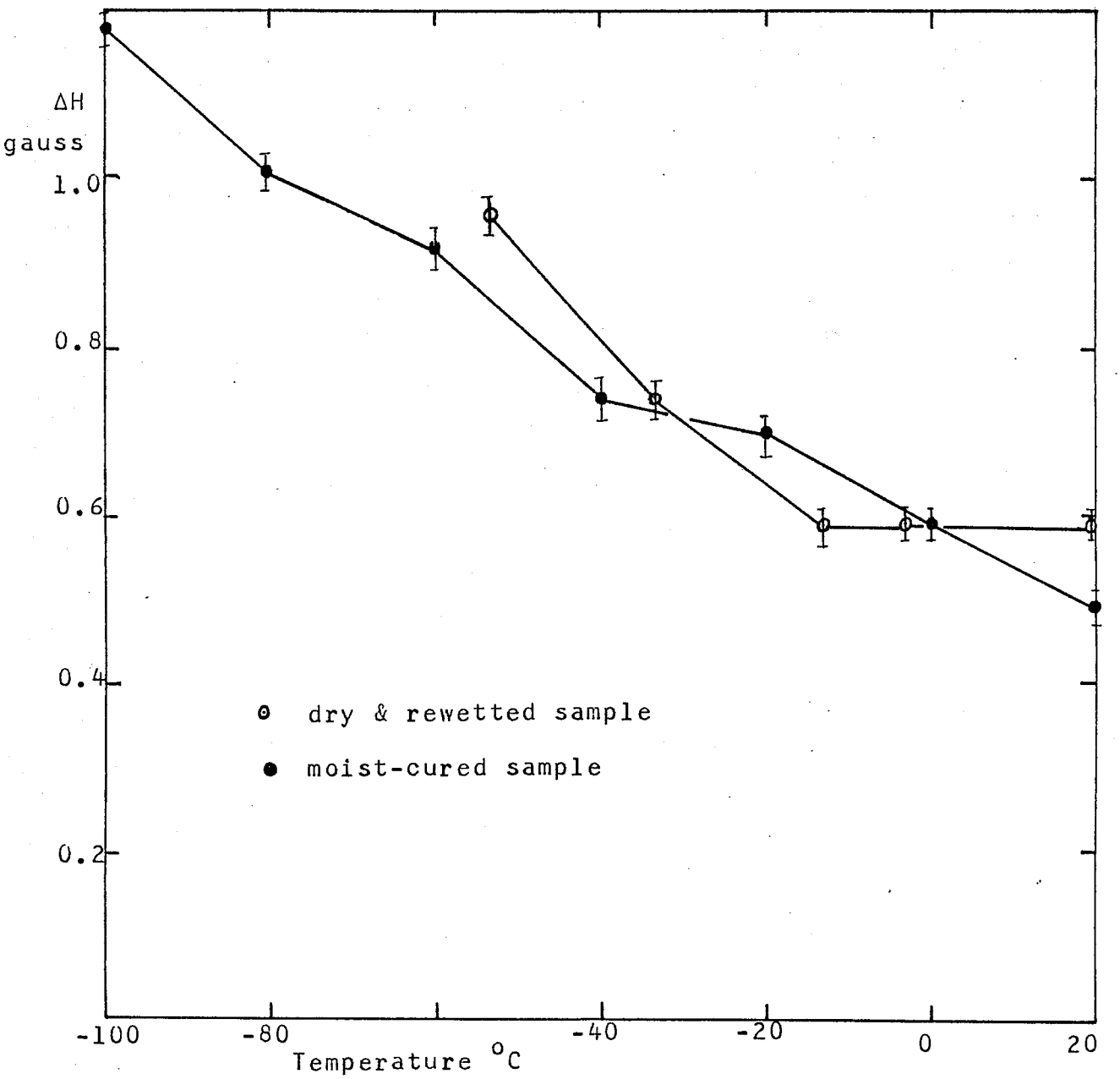

Figure 5.17: Line-width of moist-cured concrete samples
w/c= 0.37

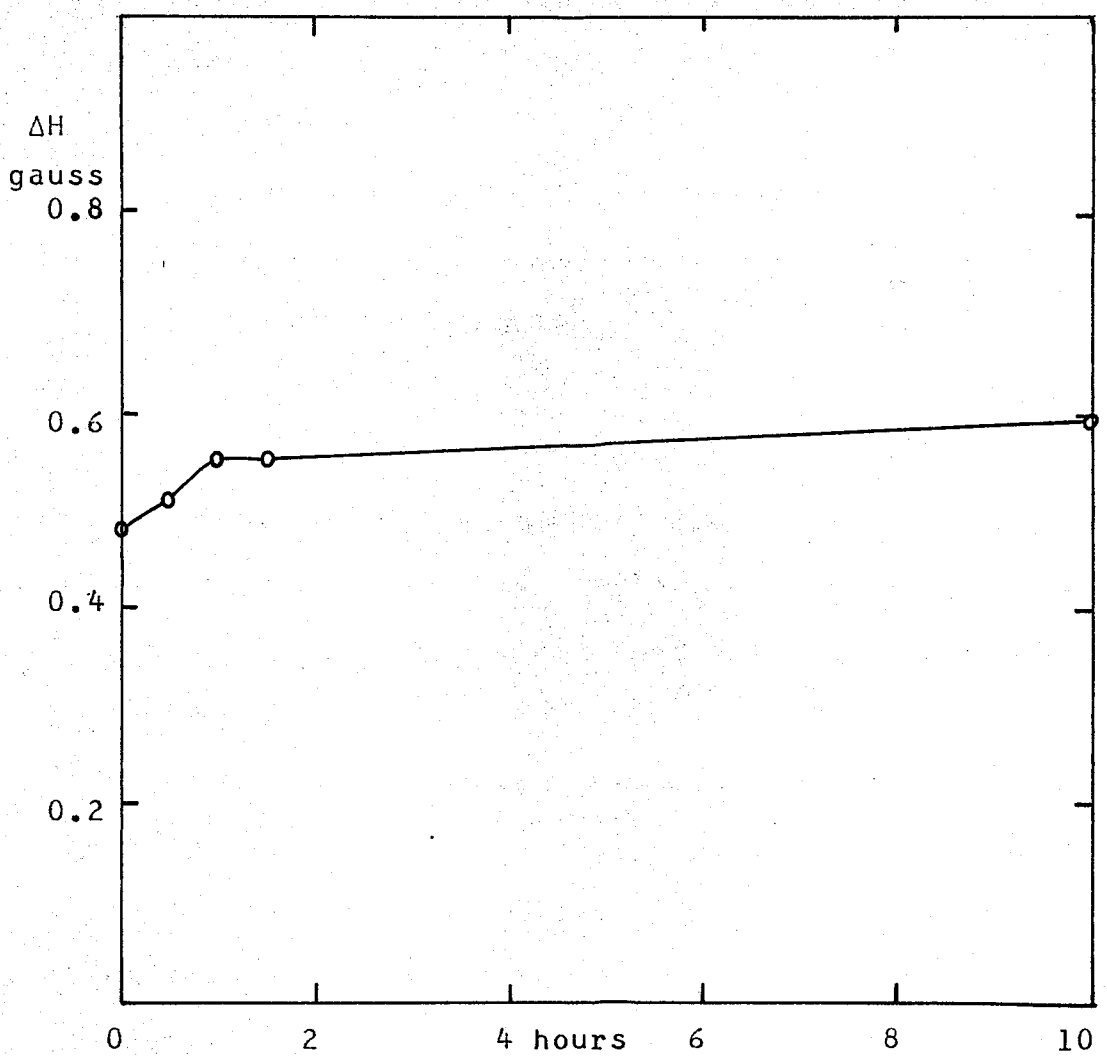

Figure 5.18: Line-width of a rewetted concrete sample baked at 120°C

line diminishes when the temperature is lowered below -38 ^{0}C. The characteristics of this sharp line are similar to the sharp β line in the rewetted sample. Further NMR studies are required to identify whether this sharp line is related to weakly bound or free water in concrete paste.

5.7 RESULTS OF THERMAL STRAIN MEASUREMENTS

5.7.1 PRELIMINARY RESULTS

Preliminary results on thermal strain have been observed on a single sample thermal strain rig. Several runs have been performed on concrete samples with w/c ratios 0.37, 0.40 and also on rewetted and dry samples. There was no problem in getting the cooling curves of all the tested samples. But to get a warming curves there was some difficulty because ice frozen on top of the sample, melted and refroze at a lower level thereby affecting the measurements. To reduce this effect, the freezer cabinet was heated up and dried out before every run of experiments. However, only a few results have been succesfully recorded with no contamination from the ice. Figure 5.19 and 5.20 shows

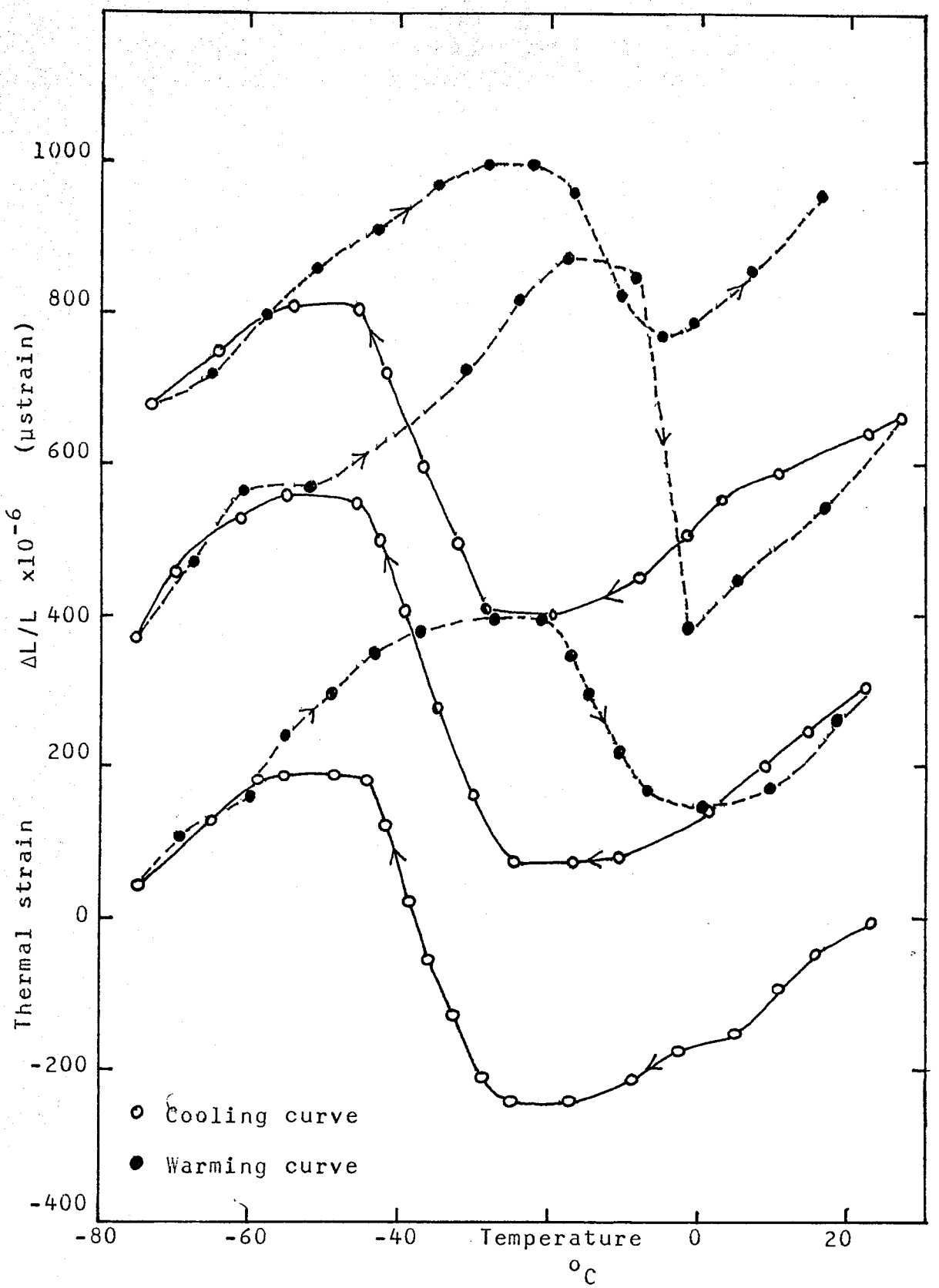

Figure 5.19: Thermal strain of a concrete sample w/c=0.37
After continous cooling cycles

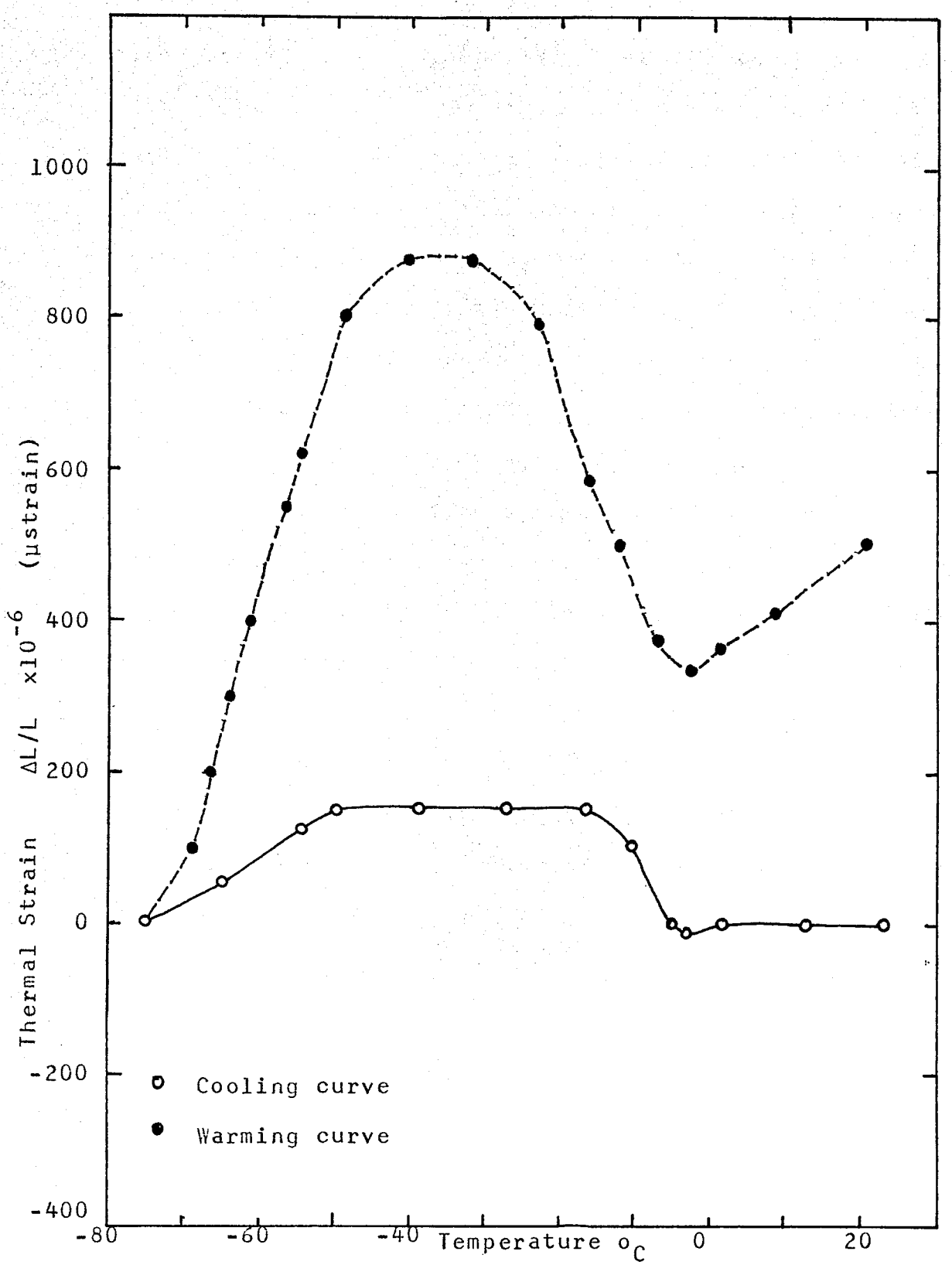

Figure 5.20: Thermal strain of a rewetted concrete sample w/c= 0.37

the results on a saturated concrete sample with w/c ratio 0.37 and a rewetted sample respectively. The results on repeated thermal cycling of the saturated sample (see figure 5.19), show that the concrete paste suffers a large thermal expansion between $-20^0$and -45^0C. On rewarming back to room temperature, the results show a hysterisis and the paste has a permanent increase in length of about 250 to 300 μstrain after each thermal cycle.

The rewetted sample had a different cooling curve compared with the saturated sample as shown in figure 5.20. The thermal strain occured between 0^0C and -15^0C and is only about 150 μstrain, which is less than half of the thermal strain suffered by the saturated sample. On rewarming to room temperature, a hysterisis occured and a permanent length increase of about 500 μstrain was observed. However, this result may be affected by contamination by ice from the atmosphere, as explained above.

5.7.2 THERMAL STRAIN OF CONCRETE SAMPLES

Samples of moist-cured concrete paste which have been tested, had water-cement ratios between 0.30

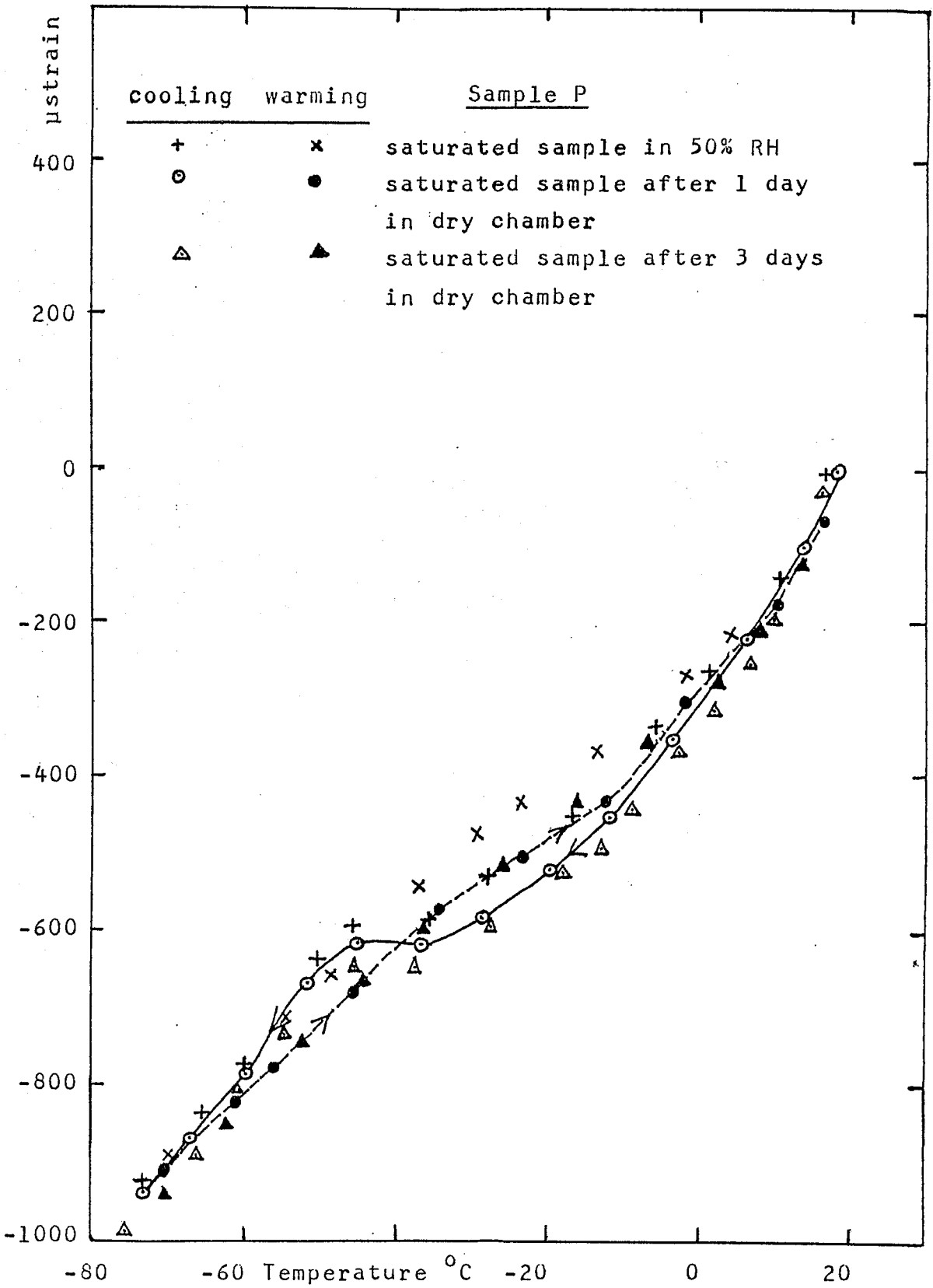

Figure 5.21: Thermal strain of moist-cured concrete samples w/c= 0.3

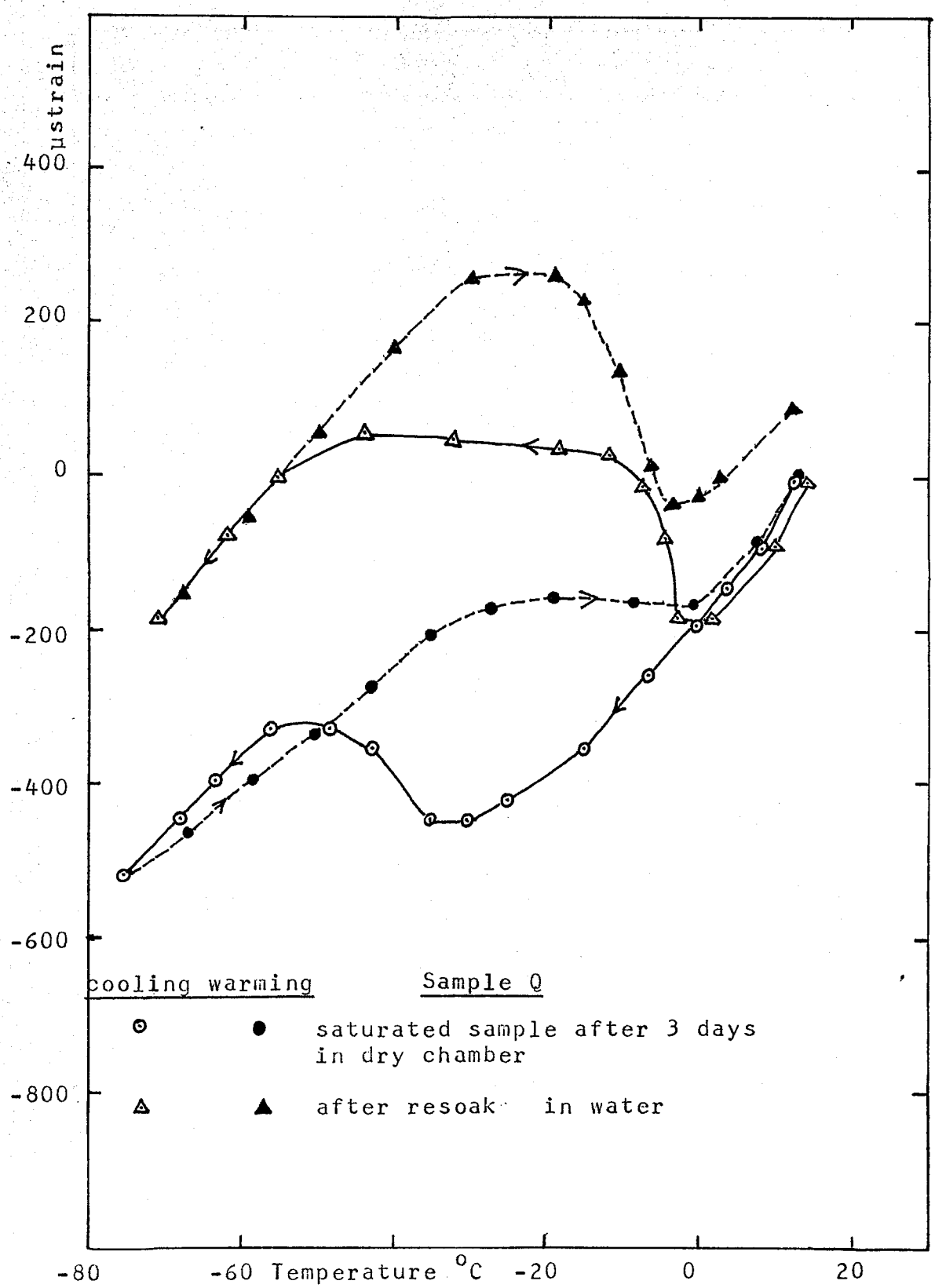

Figure 5.22: Thermal strain of moist-cured concrete samples w/c= 0.37

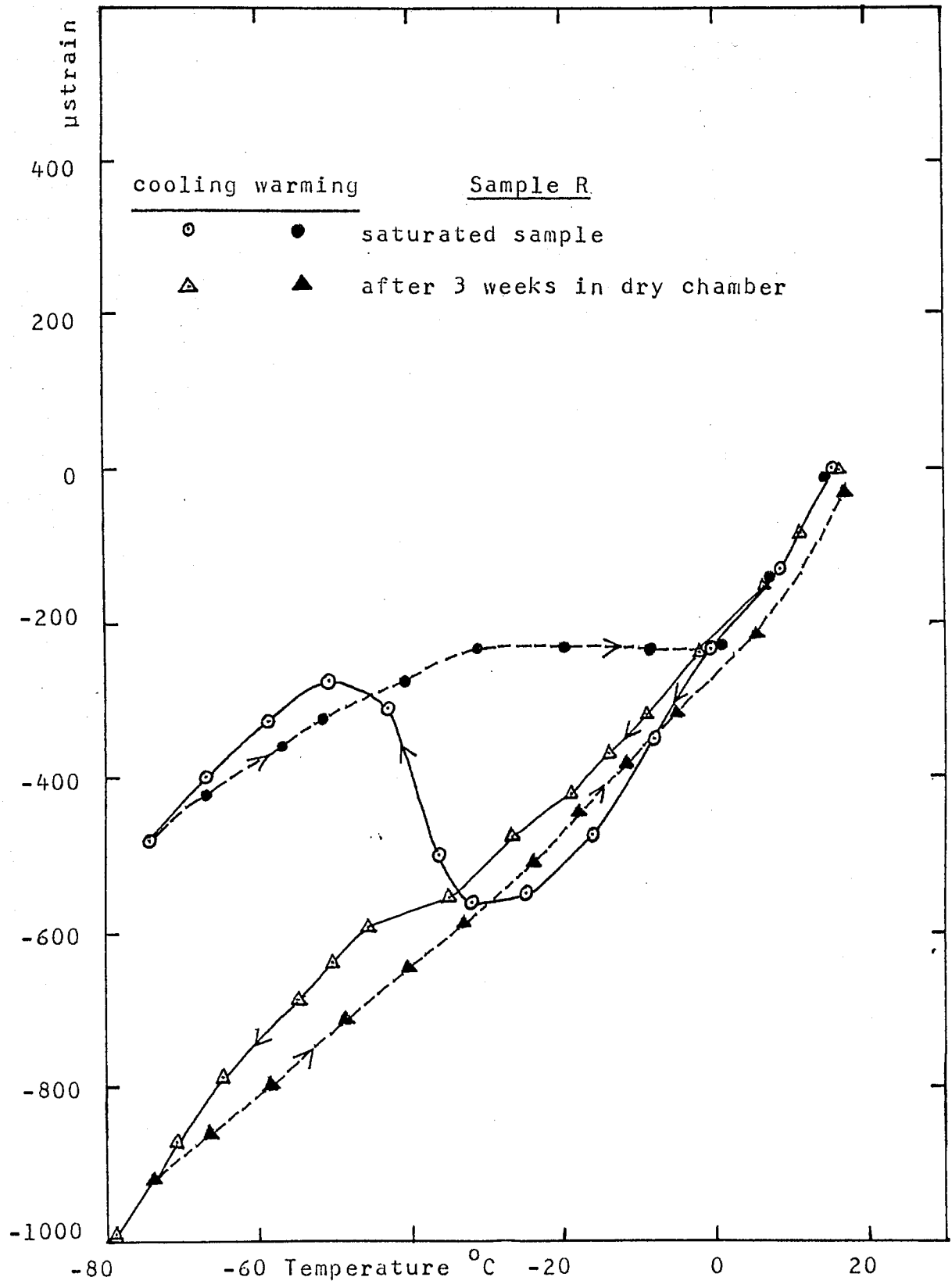

Figure 5.23: Thermal strain of **moist-cured concrete** samples w/c= 0.4

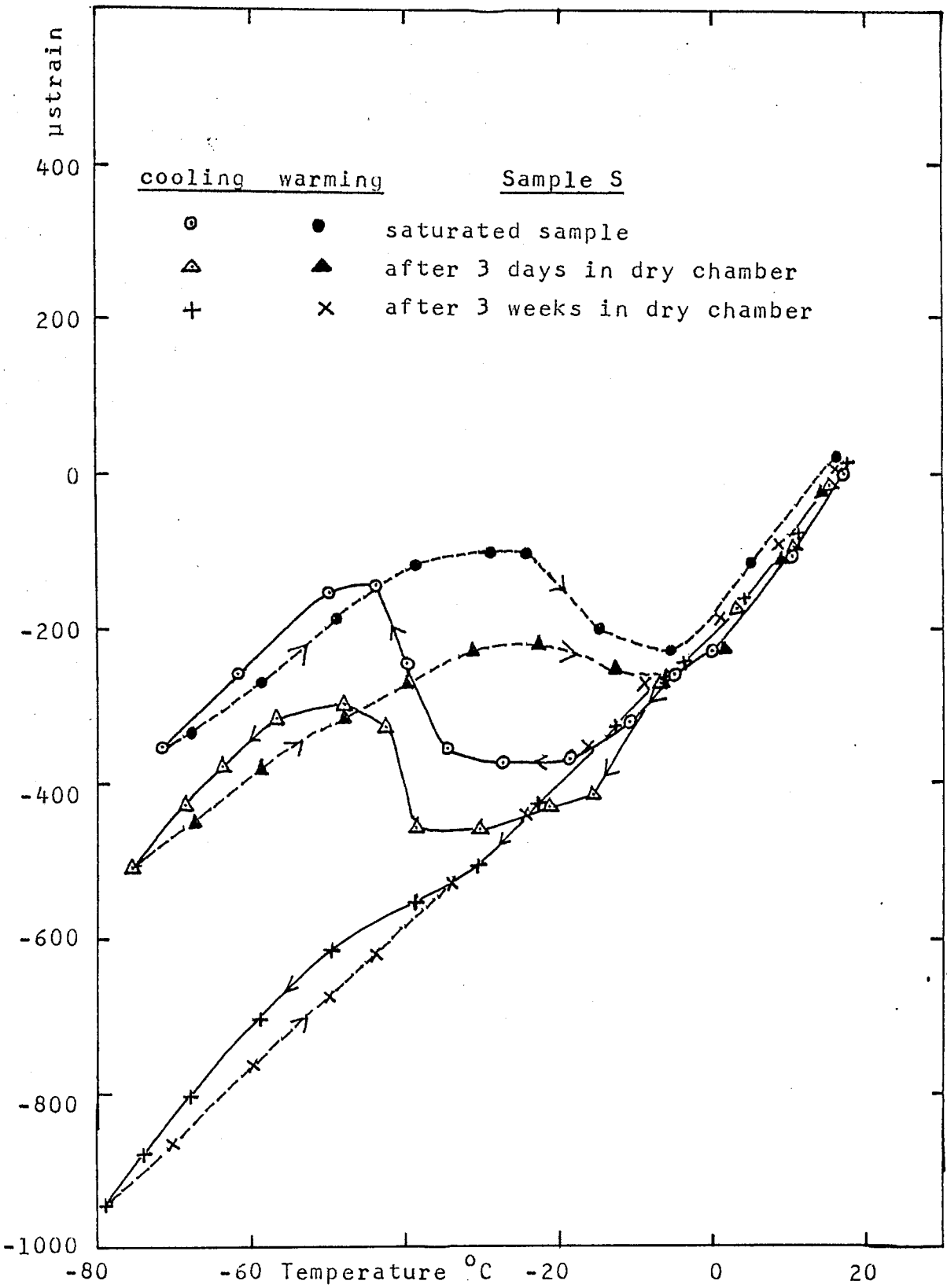

Figure 5.24: Thermal strain of moist-cured concrete samples w/c= 0.5

to 0.70. In the presentation of the results, samples are described as below.

Sample P ... w/c 0.30 - saturated moist-cured sample.

Sample Q ... w/c 0.37 - saturated moist-cured sample.

Sample R ... w/c 0.40 - saturated moist-cured sample.

Sample S ... w/c 0.50 - saturated moist-cured sample.

Sample T ... w/c 0.60 - saturated moist-cured sample.

Sample U ... w/c 0.70 - saturated moist-cured sample.

Sample V ... w/c 0.37 - heated to constant weight and rewetted.

Sample W ... w/c 0.40 - heated to constant weight after curing.

The following observations of thermal strain of the concrete paste have been performed in a confined chamber as has been discussed in section 5.3. Therefore, there was no effect of ice.

Figure 5.21, 5.22, 5.23 and 5.24 show thermal strain on samples P, Q, R and S respectively, each with different degrees of saturation. The water content in the concrete paste was varied by leaving the samples in a dry chamber for different specific periods. For sample P, this variation of water content has no significant effect on the thermal strain characteristic

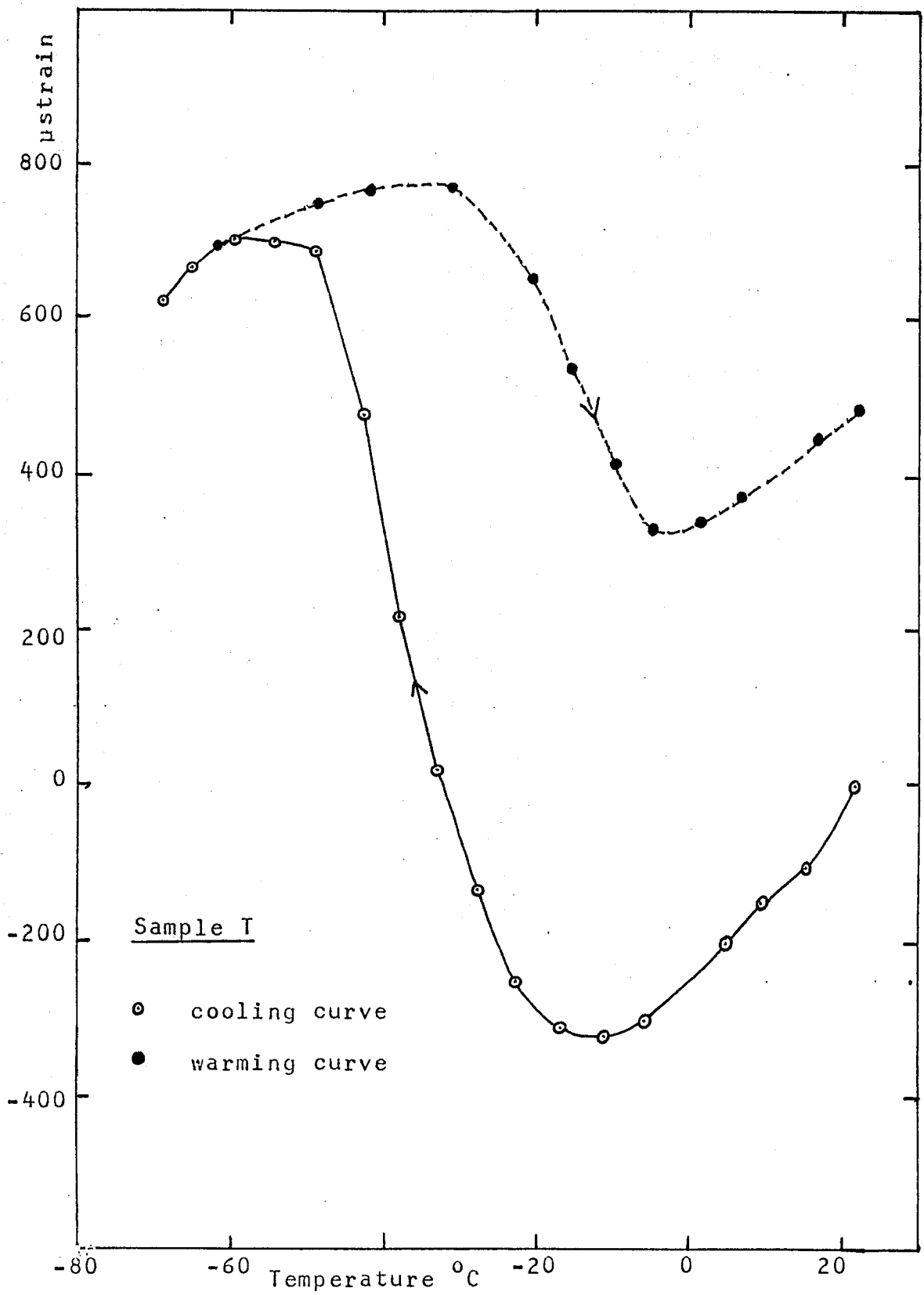

Figure 5.25: Thermal strain of a **moist-cured** concrete sample w/c= 0.6 (saturated)

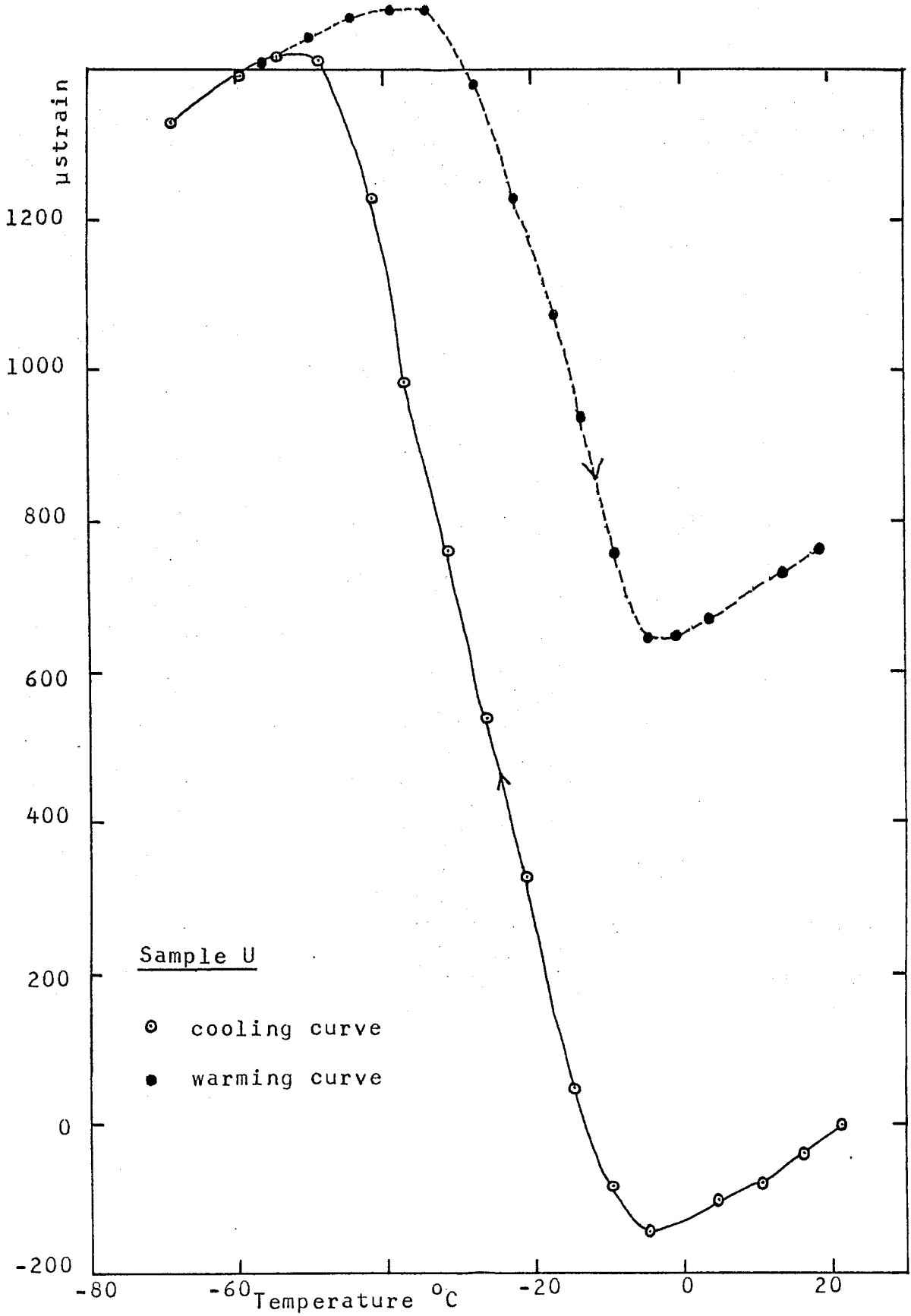

Figure 5.26: Thermal strain of a **moist-cured concrete** sample w/c= 0.7 (saturated)

of the sample. The only obvious change of the curve gradient is between -35 ^{0}C and -45 ^{0}C (see figure 5.21). Comparing the curves with the one for the dry sample W in figure 5.30, it can be seen that sample P suffers some dilation between these temperatures (-35^0 to -45^0 C) due to the evaporable water at 100^0 C.

For samples Q, R and S (w/c 0.37,0.4 and 0.5), leaving the saturated samples in the dry chamber has changed the characteristics of the thermal strain curves as shown in figure 5.22, 5.23 and 5.24. After 3 weeks of drying in the dry chamber (low humidity chamber),the thermal strain curves of samples R and S (see figure 5.23 and 5.24) have the same characteristics as sample P in figure 5.21. On resoaking the sample as for sample Q (see figure 5.22), the thermal strain curve has a similar shape to the one for the rewetted sample in figure 5.20. The increase in contraction on cooling from 0^0 to -45^0 C due to the water evaporation after 3 weeks in the dry chamber is about 300 μstrain to 450 μstrain for samples R and S.

On rewarming of these samples, with the exception of a resoaked sample Q, no permanent change of length was observed.

However, samples T and U (w/c of 0.6 and

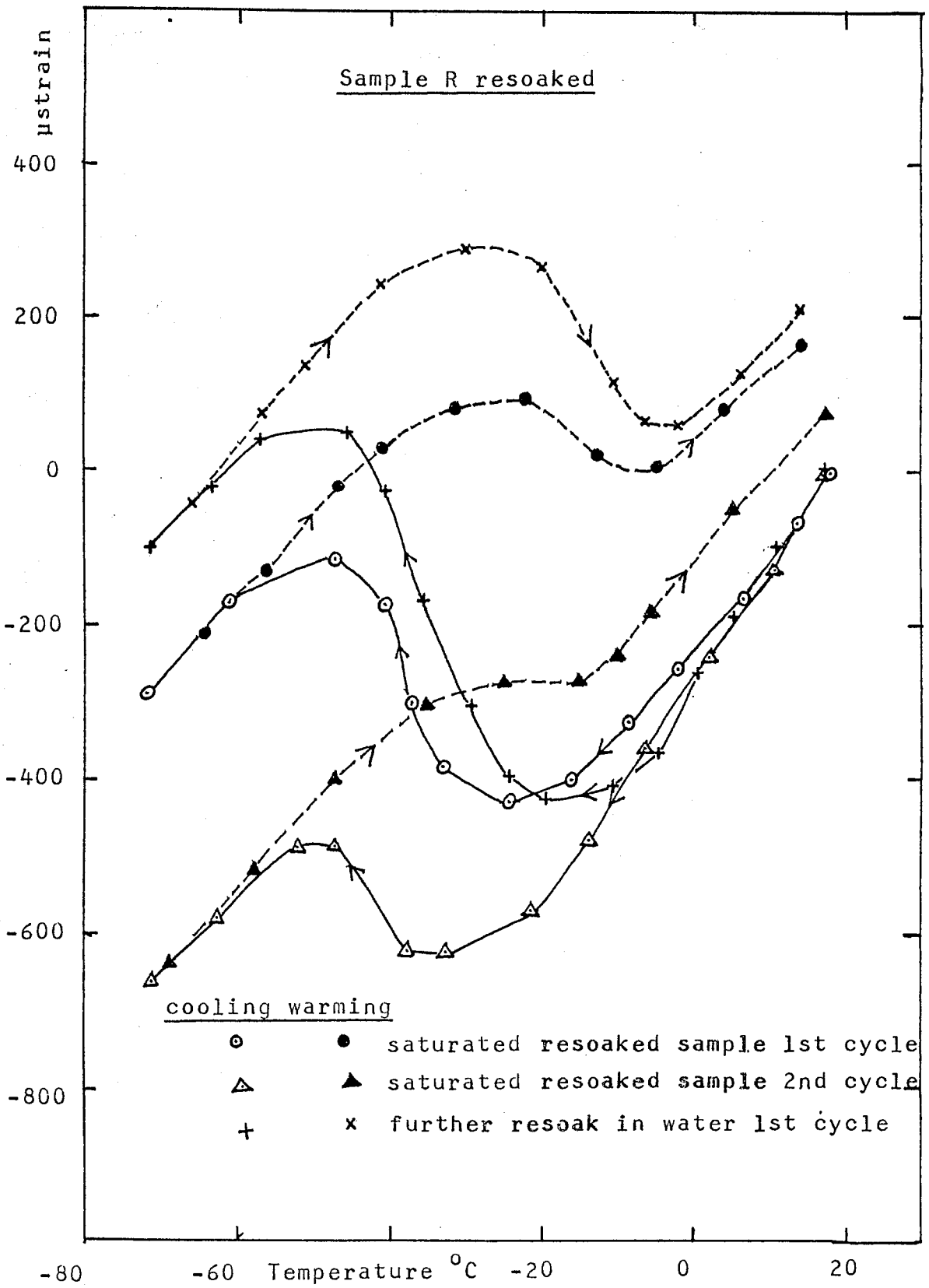

Figure 5.27: Thermal strain of resoaked concrete samples w/c ratio 0.4, after repeated cooling cycles

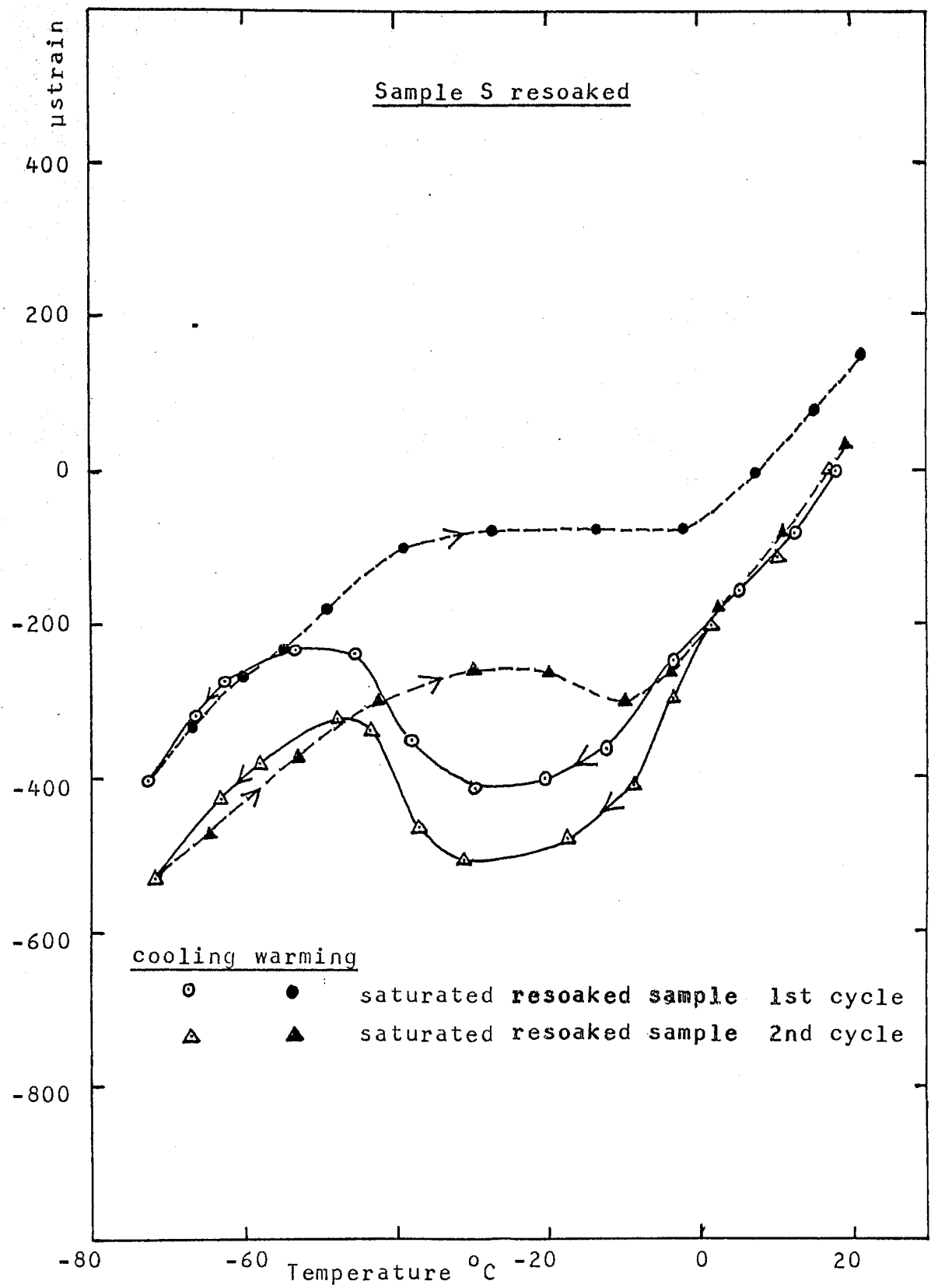

Figure 5.28: Thermal strain of resoaked concrete samples w/c= 0.5 after repeated cooling cycles

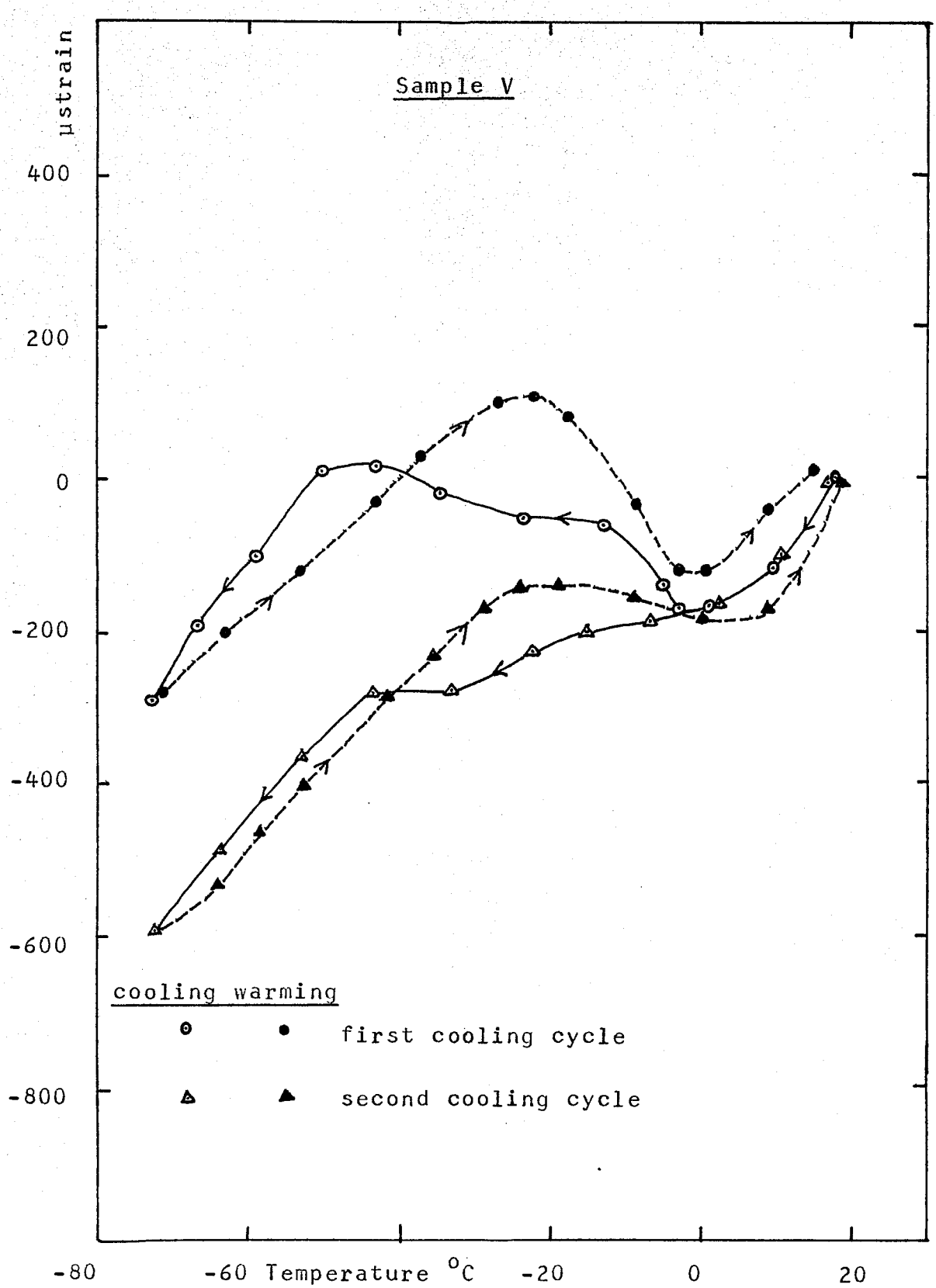

Figure 5.29: Thermal strain of rewetted concrete samples w/c= 0.37 after repeated cooling cycles

0.7) have suffered a permanent change of length of between 500 μstrain to 800 μstrain after one thermal cycle (see figure 5.25 and 5.26). It should be noted that these samples with higher water-cement ratio take a long time to mature. In this experiment these samples had been cured for 28 days only. After one thermal cycle samples T and U were found to be cracked and no further experiments could be carried out on them. This cracking did not happen to samples P, Q, R and S.

After the above experiments had been performed samples R and S were put back in a water bath and soaked for several weeks before being tested again. Figure 5.27 and 5.28 show the thermal strain of the resoaked samples R and S after repeated thermal cycles. After the first thermal cycle, both resoaked samples R and S showed a permanent change of length, but this permanent expansion was less after the second thermal cycle. On further resoaking sample R, as has been shown in figure 5.27, the permanent expansion occured again. However, if we compare the thermal strain curves of the resoaked samples of R and S in figure 5.27 and 5.28 with a rewetted sample (sample V) in figure 5.29, there are some differences. The thermal expansions suffered by sample R and S were large and occurred between -20^0C and

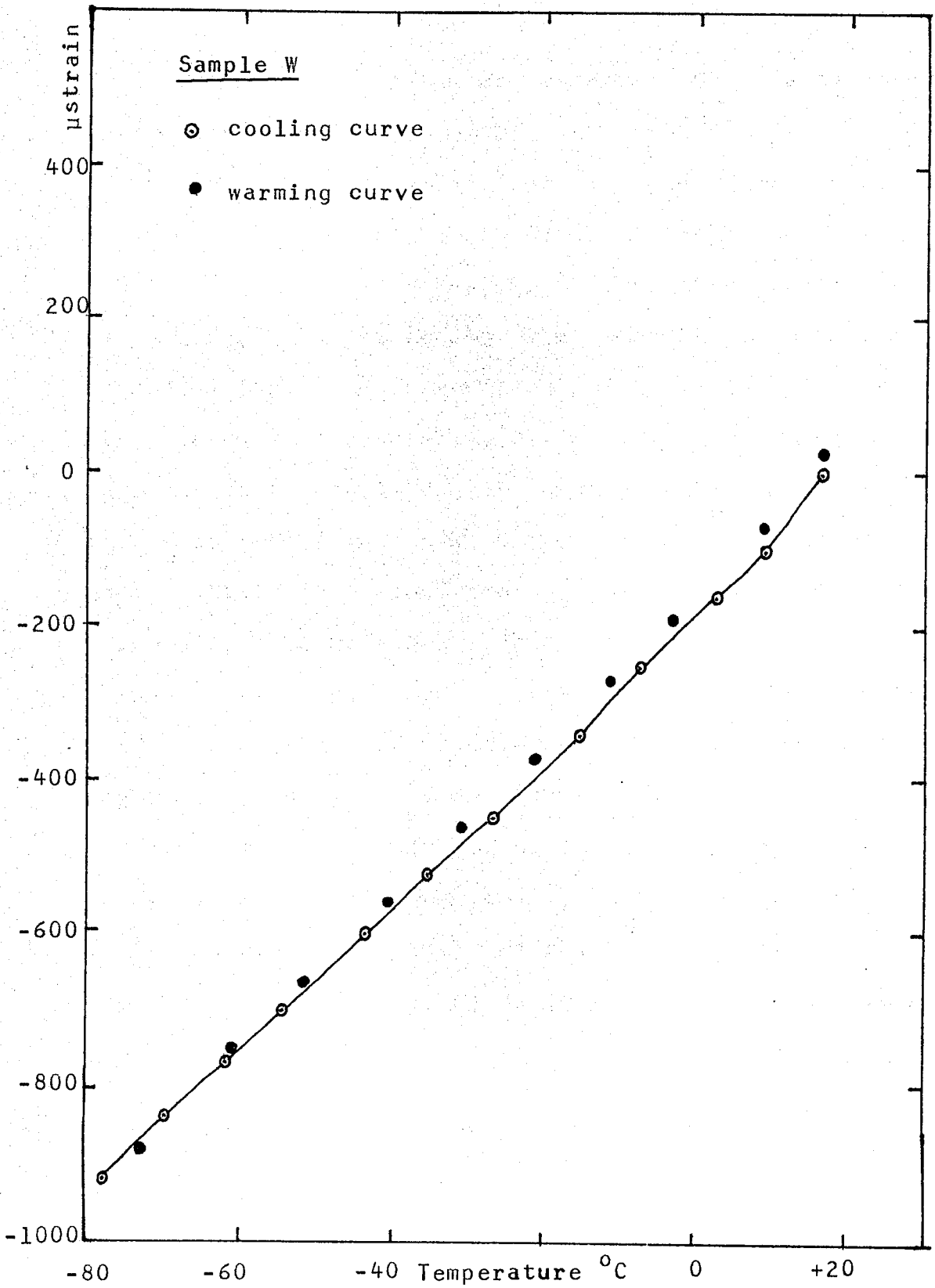

Figure 5.30: Thermal strain of dry concrete.

-45 ^{0}C, whereas, the thermal expansion of the rewetted sample occurred almost immediately below 0^{0}C.

The following figures, from figure 5.31 to 5.37 show the coefficient of dilation of the concrete samples against temperature. The dilation coefficient is defined as equal to the thermal strain/degree celcius. The values were calculated from the thermal strain curves of samples P, R, S, V and W and show the maximum positive value of the dilation coefficient occurs between about -20^{0} C and -45^{0}C. The figures also show that the positive dilation decreases with decreasing saturation of the samples. Comparing these curves with the one for a rewetted sample in figure 5.36, shows that the rewetted sample V, suffers a large expansion between 0 ^{0}C and -10^{0}C, which does not occur in the moist-cured samples. However, the rewetted sample shows some expansion on cooling between -20 ^{0}C and -45^{0}C which shows that the rewetted sample still has some water with similar characteristic to moist-cured concrete paste.

The coefficient of dilation during the rewarming process, has little variation between the samples. The maximum expansion occurs at about -20^{0}C as shown in figure 5.33, 5.35 and 5.37. However, the

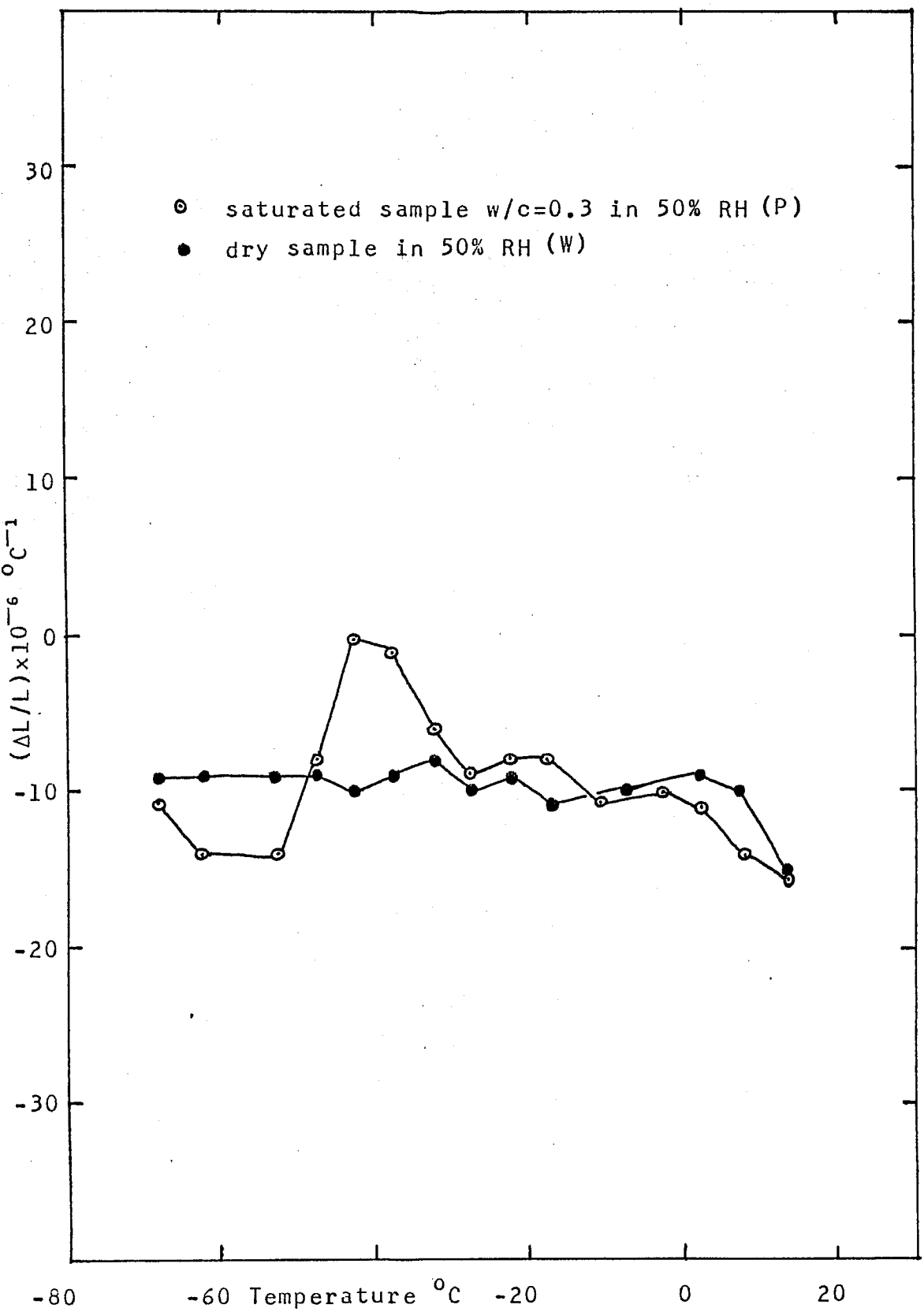

Figure 5.31: Temperature variation of dilation coefficient of moist-cured concrete samples

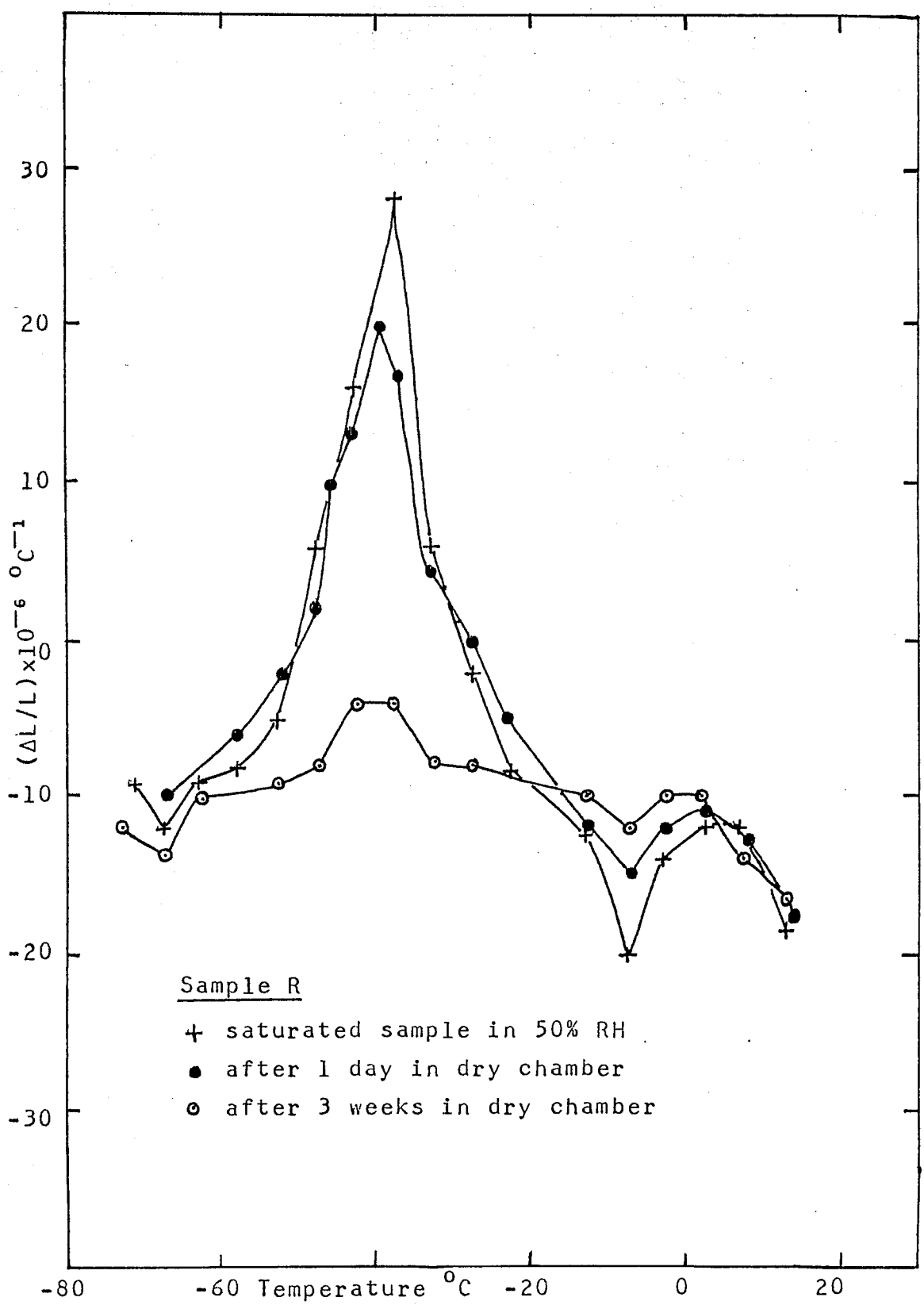

Figure 5.32: Temperature variation of dilation coefficient of moist-cured concrete samples w/c= 0.4 during cooling

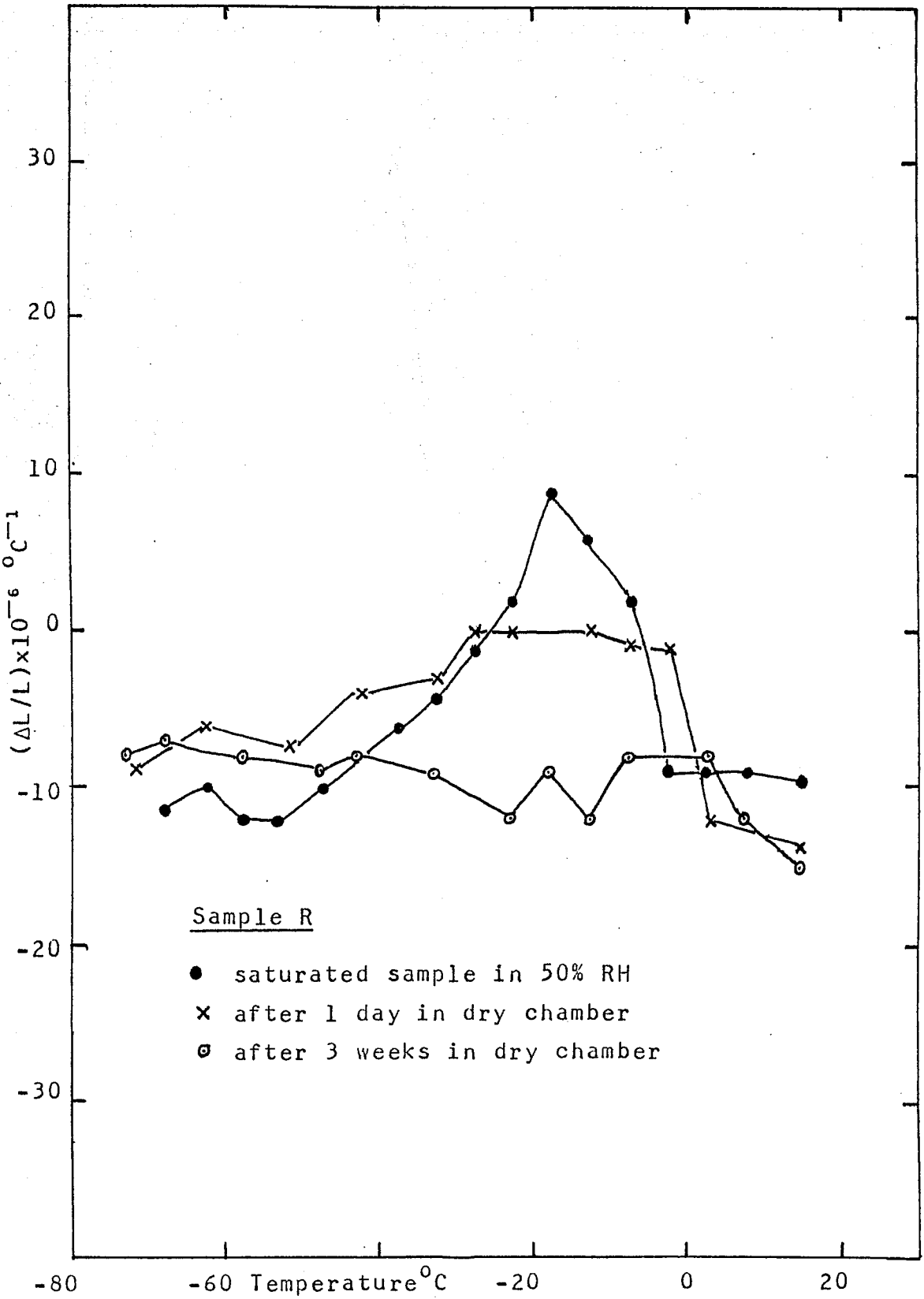

Figure 5.33: Temperature variation of dilation coefficient of moist-cured concrete samples w/c= 0.4 during warming

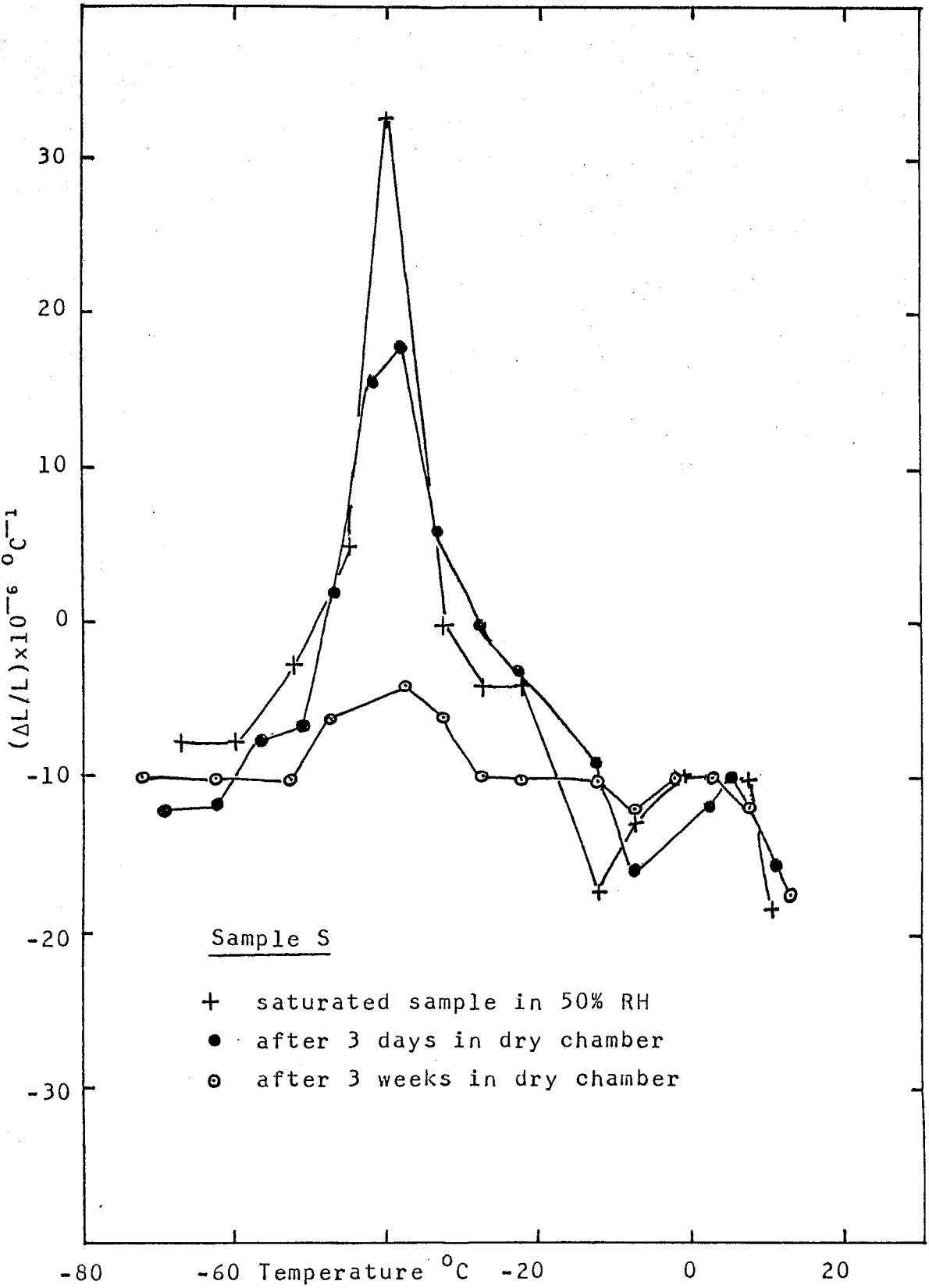

Figure 5.34: Temperature variation of dilation coefficient of moist-cured concrete samples w/c= 0.5 during cooling

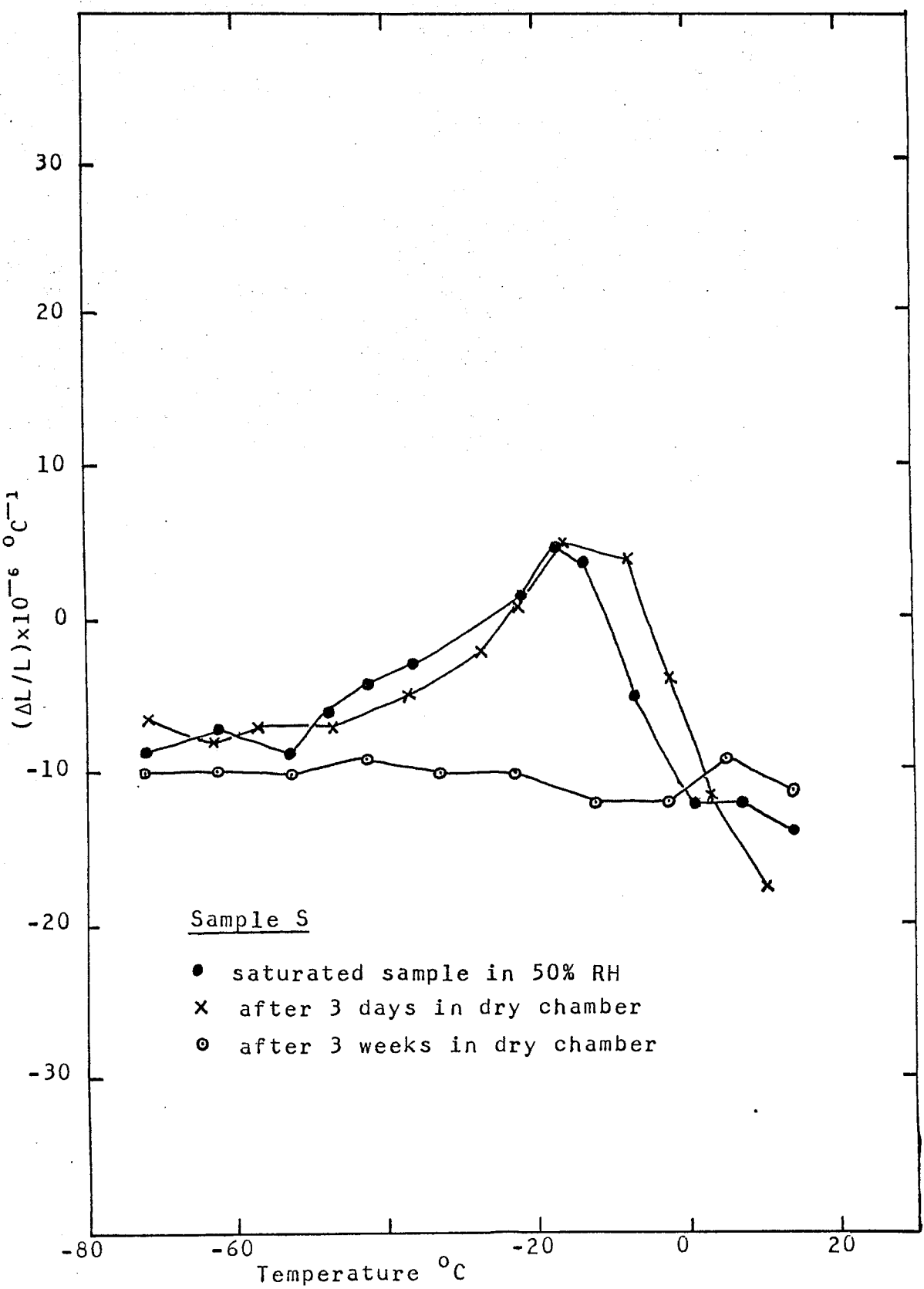

Figure 5.35 : Temperature variation of dilation coefficient of moist-cured concrete samples w/c= 0.5 during warming

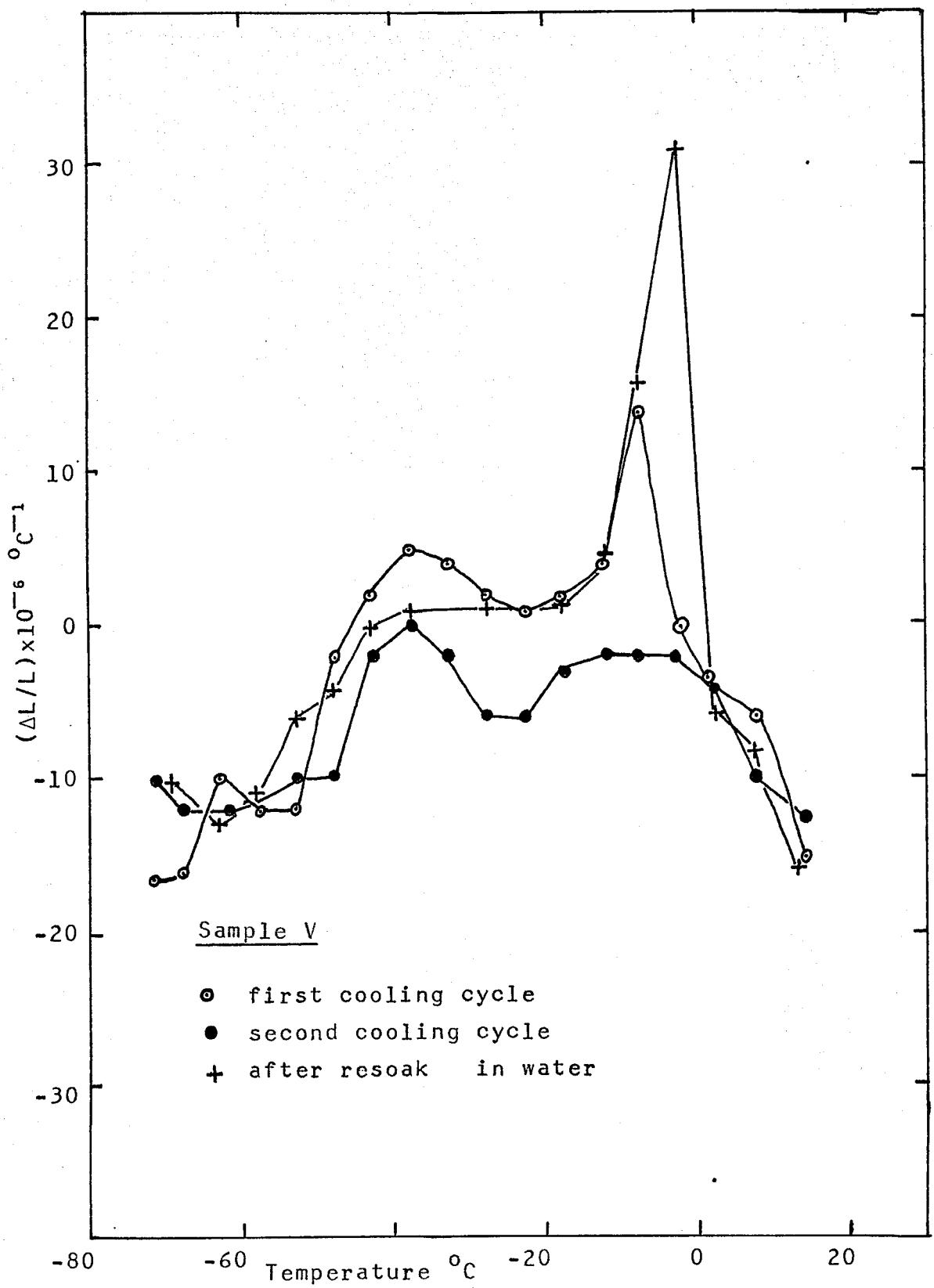

Figure 5.36: Temperature variation of dilation coefficient of rewetted concrete samples w/c= 0.37 during cooling

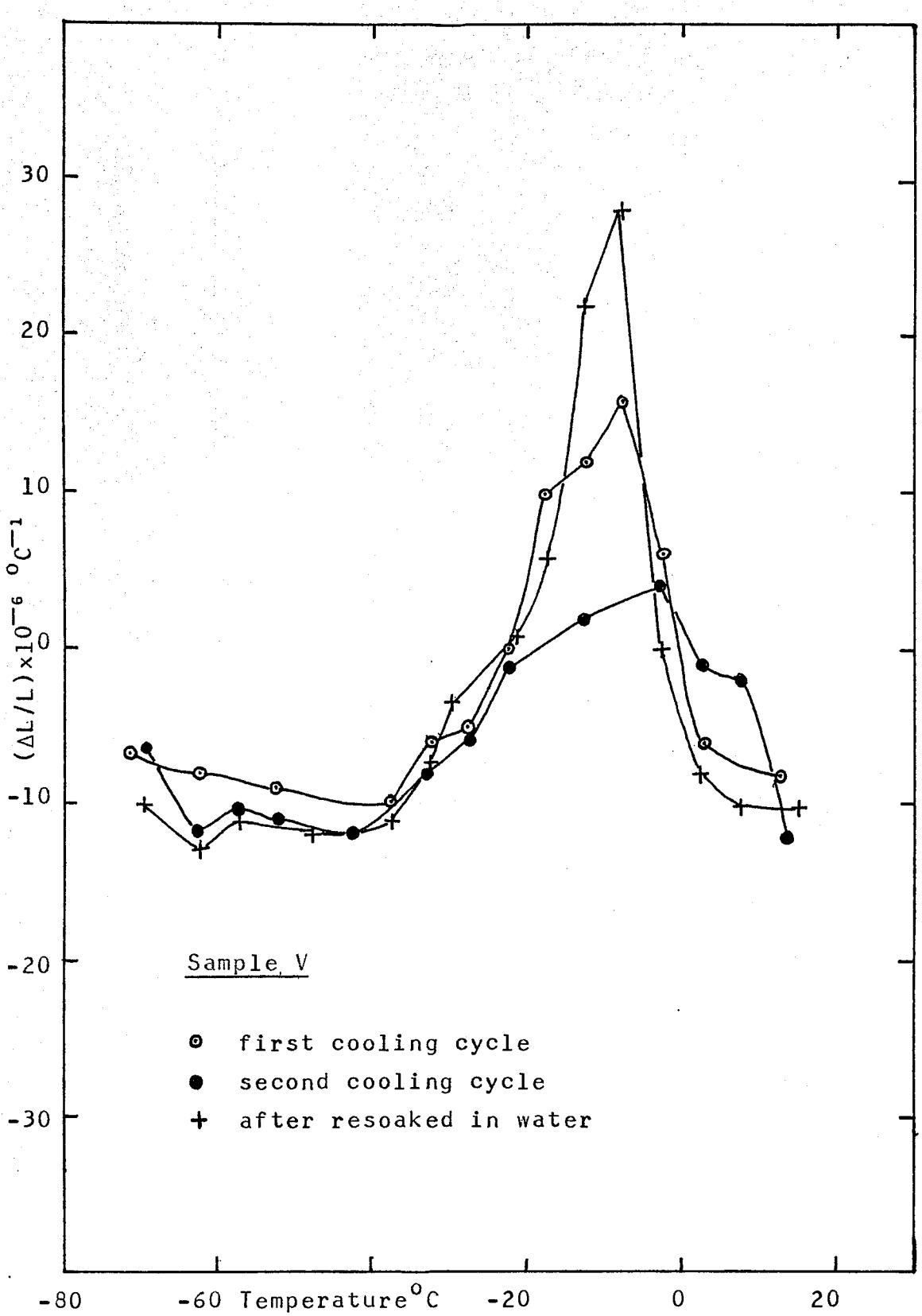

Figure 5.37: Temperature variation of dilation coefficient of rewetted concrete samples w/c= 0.37 during warming

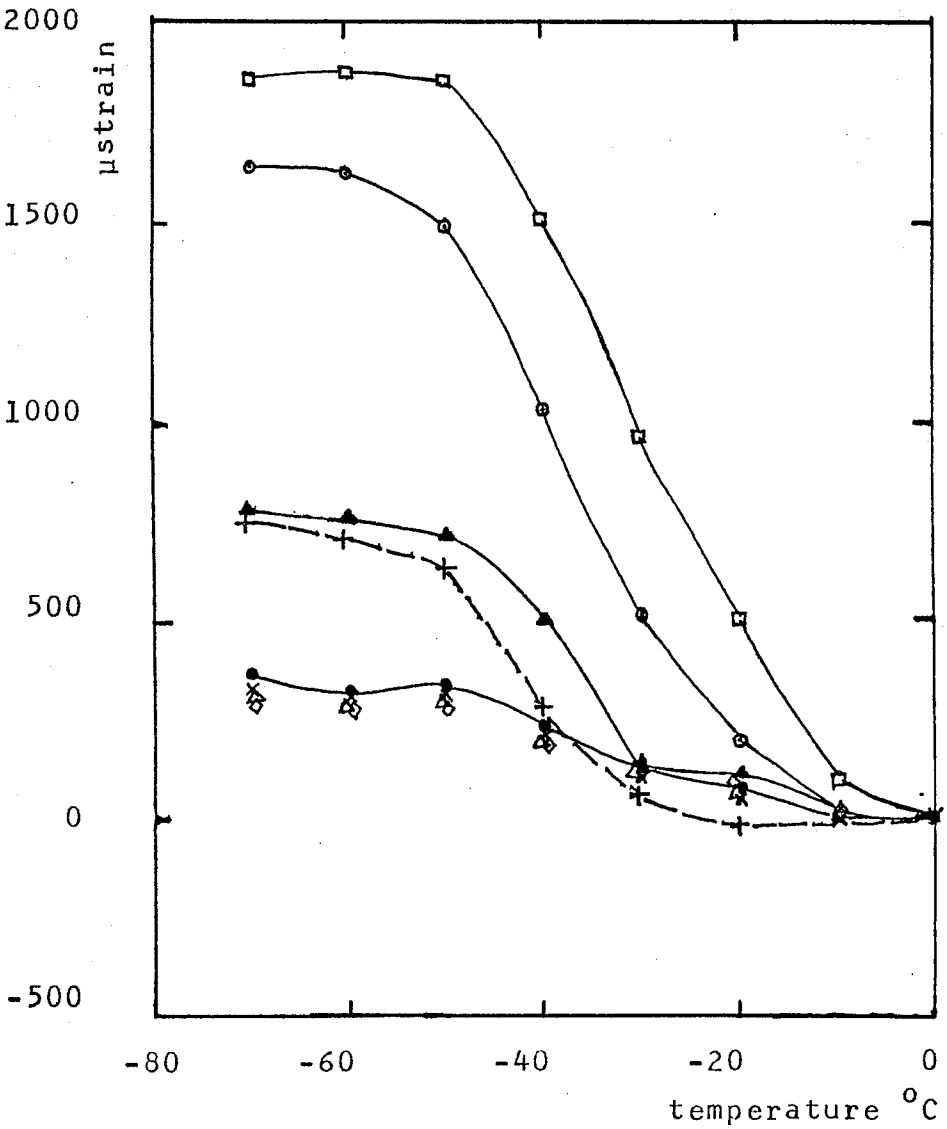

Figure 5.38: Dilation factors of the concrete samples.

× - w/c=0.3 saturated sample.
● - w/c=0.3 after 3 days in dry chamber.
\+ - w/c=0.4 saturated sample.
△ - w/c=0.4 after 3 weeks in dry chamber.
▲ - w/c=0.5 saturated sample.
◇ - w/c=0.5 after 3 weeks in dry chamber.
⊙ - w/c=0.6 saturated sample.
□ - w/c=0.7 saturated sample.

rewetted sample has a larger expansion than with the moist-cured one.

There is another difference between the moist-cured and the rewetted samples. The height of the maximum in the rewarming curve of the saturated moist-cured sample is smaller than that of the peak of the dilation coefficient during cooling. However, the peaks for the rewetted sample have the same height in both the cooling and the rewarming processes.

Figure 5.38 shows dilation factors (as defined previously in section 4.3.2) of the concrete samples with w/c ratios 0.30, 0.40, 0.50, 0.60 and 0.70 respectively. All samples show positive dilation factors with the highest w/c ratio yielding the highest value. After 3 weeks of drying in a low humidity chamber, the dilation factors of the 0.40 and 0.50 w/c pastes have the same values as the 0.30 w/c paste.

5.8 OTHER RESULTS

5.8.1 THERMAL STRAIN OF CEMENT PASTE

Three saturated moist-cured cement samples with water-cement ratios of 0.27, 0.35 and 0.45 respectively, have been tested. The thermal strain curves of the samples are shown in figure 5.39. On cooling, only the sample with w/c ratio 0.45 showed a large thermal expansion of about 1400 μstrain, followed by a net contraction on warming back to 0^0C. The other two samples showed no expansion in passing through the ice nucleation temperature. After the experiment, all the cement samples had been found to be cracked. These results are therefore not reliable, but are included to indicate the strange behaviour observed.

5.8.2 THERMAL STRAIN OF AGGREGATE SAMPLES

Figure 5.40 shows the thermal strain of aggregate samples cut from large flint stones picked out of the marine aggregate. All of the six samples contracted differently ranging from about 100 μstrain to 1000 μstrain at -50^0C. Only sample 2 showed an expansion

in passing through the -40 ^{0}C to -45 ^{0}C temperature interval. On the other hand, samples 4 and 6 showed an abrupt contraction in passing this temperature interval.

5.8.3 THERMAL STRAIN OF INDIVIDUAL COMPOUNDS

Silicon dioxide and calcium hydroxide powder have been mixed with different amounts of water and tested. These compounds are residues of the cement hydration and might be present in the concrete paste. The pastes were cooled down and the observed contractions are plotted in figure 5.41. The curves show that the pastes have a large contraction on cooling to -80^{0} C; about three times that of a low w/c concrete paste, and approaching the thermal contraction of ice.

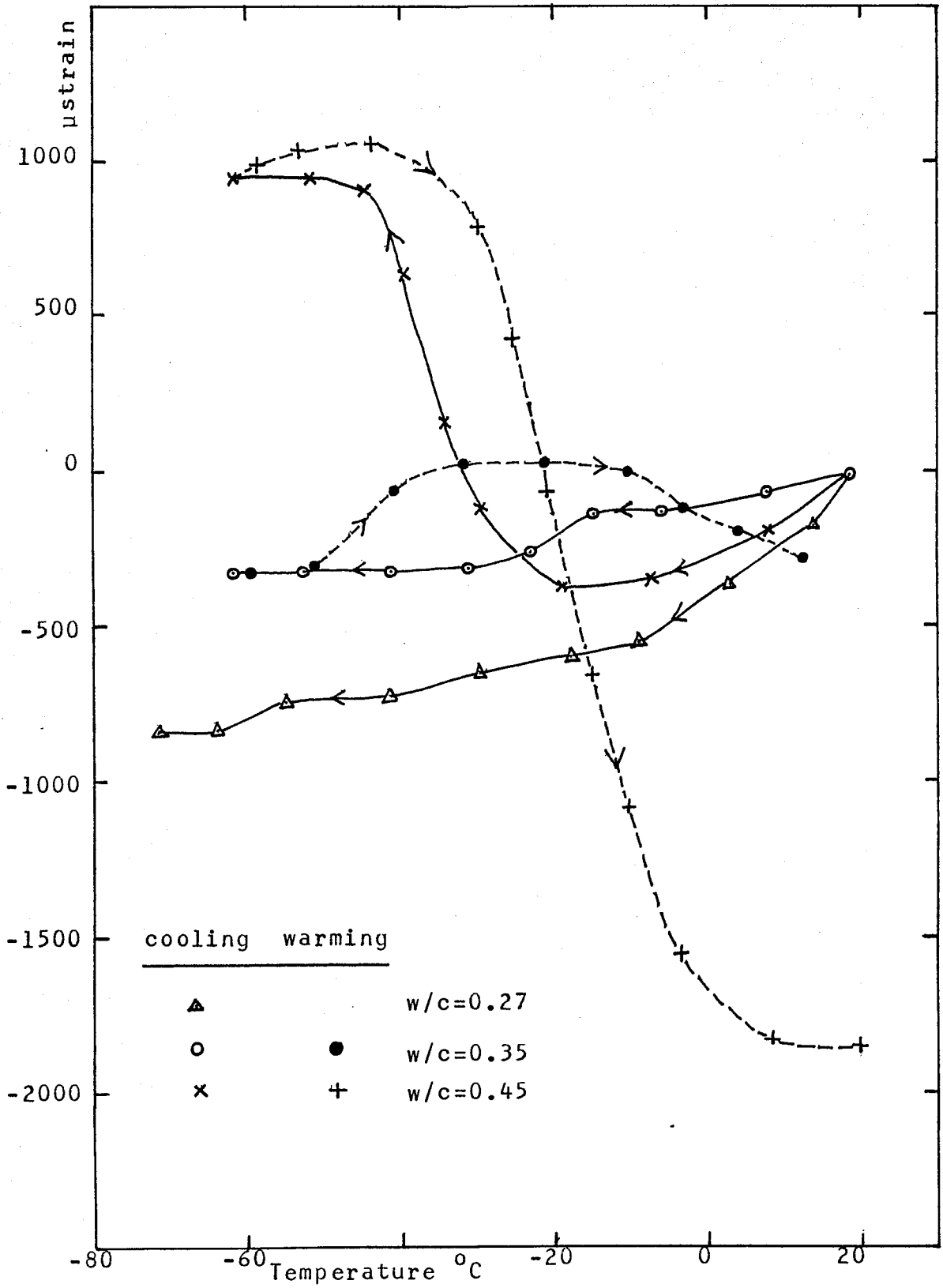

Figure 5.39: Thermal strain curves of cement samples

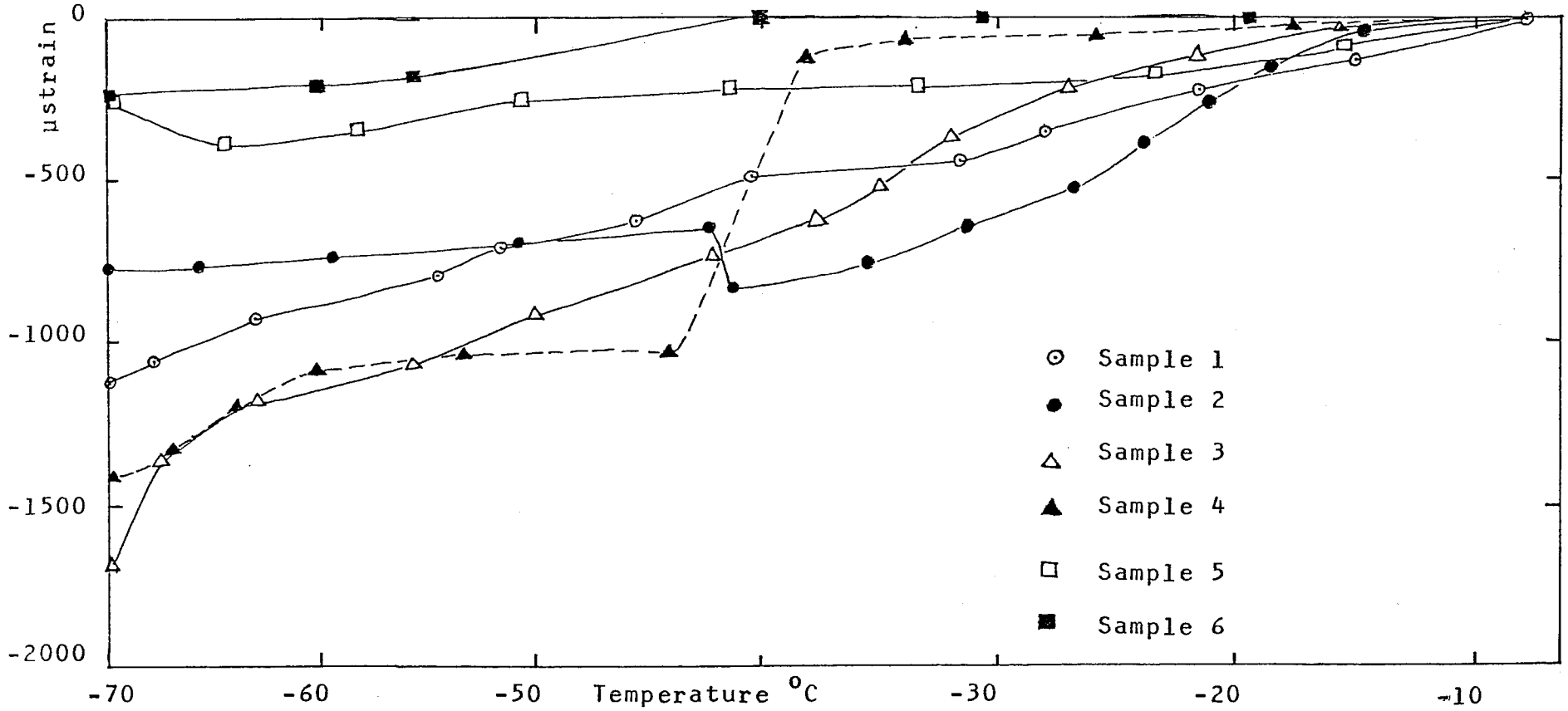

Figure 5.40: Thermal strain of aggregate samples. All samples are flint stones.

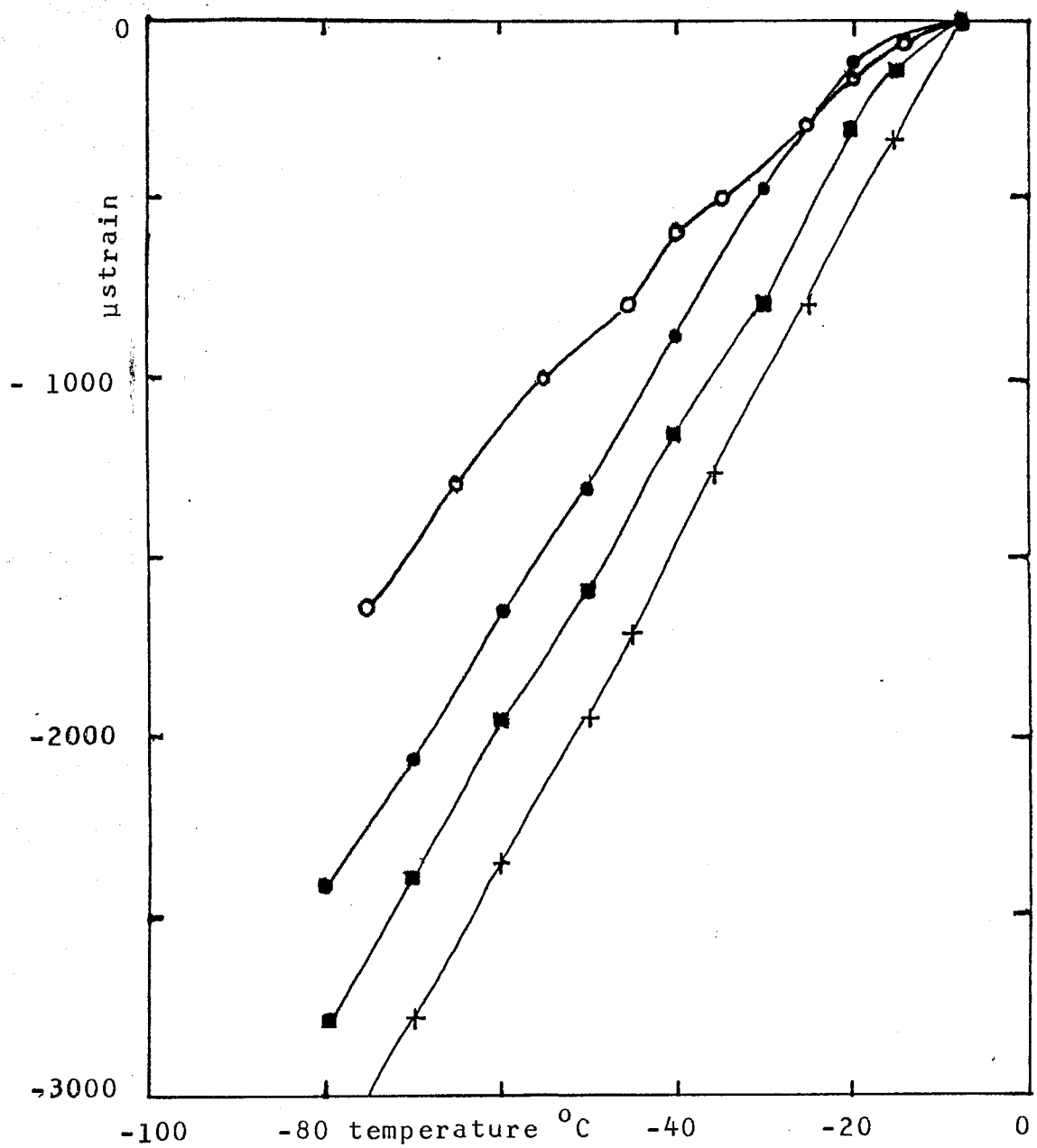

Figure 5.41: Thermal strains of individual compounds ● - SiO_2 paste with 1:6 parts of water; ■ - SiO_2 paste 1:9; o - $Ca(OH)_2$ paste 1:2; + - ice.

CHAPTER SIX

DISCUSSIONS

6.1 INTRODUCTION

This chapter begins with discussions of the results. Analysis of the results is concentrated on the effect of water in the concrete paste. From the experimental results, a schematic classification of the different types of water, with different binding energies, is postulated.

6.2 ANALYSIS OF HEAT CAPACITY RESULTS

On cooling down a concrete paste, the heat capacity consists of the heat capacities of the concrete matrix, the non-evaporable water, the evaporable water, air in the voids and the latent heat of freezing of the water. The contribution from the heat capacity of air in the voids is small and negligible.

Water lost in low humidity conditions and during drying at 100 ^{0}C can be considered as the evaporable water. Thus, the enthalpy and $(\partial H/\partial T)$ curves

in figures 5.7, 5.8, 5.9 and 5.10 for the dry sample are the curves for the concrete matrix plus the non-evaporable water. The difference between the enthalpies of the concrete samples from the curve of the dry sample is assumed to be the enthalpy of the evaporable water, including its latent heat of freezing. The curve for the dry sample is almost a straight line, which suggests that no freezing of water with associated latent heat takes place in that sample.

The enthalpy-temperature curve of the rewetted sample in figure 5.8 at a temperature below -10^0 C, is parallel to the curve of the dry sample with a difference of ΔH of 11 J/gm. for the sample. As we have discussed in section 4.3.1, this difference is due to the latent heat of freezing. Since the deviation of the curve only occurs above -10^0 C, therefore, water in the rewetted concrete sample freezes above $-10\ ^0$C with an enthalpy equal to 11 J/gm. If we assumed that the amount of water frozen within 10 degrees below $0\ ^0$C is w_f, and take the average latent heat of freezing of pure water between 0^0 C and -10^0 C to be 300 J/gm(29), therefore,

$$300w_f + c_p\Delta T(w_e - w_f) = 11 \qquad (6.1)$$

where w_e is the sample weight of the evaporable water, measured to be 6.5%. For the value of c_p equal to 4.2 J/g^{0}C, we get from equation 6.1, that the amount of water frozen within the range of temperature is 3.2%.

The curve of $(\partial H/\partial T)$ in figure 5.10, for the rewetted sample shows that there is some water which does not freeze above -10 ^{0}C. The enthalpy of this remaining water equals the area between the curves in the figure between -10^{0}C and -40^{0}C, which is 4.5 J/gm. Therefore,

$$wc_w\Delta T + 0.032c_i\Delta T + wL = 4.5 \qquad (6.2)$$

where c_w and c_i are the specific heats of water and ice respectively. w is the weight of water freezing between -10 ^{0}C and -40 ^{0}C. For c_w=4.2 J/gm^{0}C, c_i=1.96 J/gm^{0}C (from figure 4.2) and the latent heat of freezing at -40^{0}C of 240 J/gm.(29), then w is equal to 0.7%. This amount is about 10% of the total evaporable water in the rewetted paste.

Water in samples A1, B1 and C1 do not freeze in the same way as water in the rewetted sample. The enthalpy curves shown in figure 5.7, show that the water freezes gradually between 0^{0}C and -45^0 C. Thus the

enthalpy observed is a mixture of latent heat and the specific heat capacity of the supercooled water. The area under the curves in figure 5.9 give the values of the enthalpy change. To calculate the amount of water frozen in these samples in a same way as the rewetted water, is erroneous because the latent heat of freezing varies between 0^0C to -45^0C. From figure 5.11, if each gramme of sample contains x gm of freezable water, then the enthalpy due to the latent heat of freezing, and to cooling from 0^0C to -60^0C is 440x J/gm. The total enthalpy change ΔH of each gramme of sample can then be expressed as,

$$\Delta H = 440x + (1-x)\Delta h \qquad (6.3)$$

where Δh is the enthalpy of the dry sample. x can therefore be calculated from equation 6.3. The values of x are tabulated in table 6.1 below.

Concrete sample	w/c ratio	Percentage of water(x)	% of evaporable water (y)	x/y
A1	0.30	4.5	6.0	0.75
B1	0.37	5.9	8.7	0.68
C1	0.40	7.2	8.8	0.82
Rewetted	0.37	3.2	6.5	0.49

Table 6.1: Percentages of freezable water in concrete samples.

From these data, it is concluded that about 75% of the evaporable water in moist-cured samples is frozen between 0^0C and $-60\ ^0$C. But in the rewetted sample, only half of the evaporable water freezes within this temperature range.

Also the freezable water freezes in a similar manner for the 3 samples, indicating that it is in a similar physical state.

6.3 ANALYSIS OF NMR RESULTS

Besides the chemically bound water, the NMR spectra of moist-cured concrete samples show that the paste contains physically adsorbed water (see figure 5.12). However, if the sample is made fully saturated,

as shown in figure 5.15, there is a sign of free or loosely bound water in the moist-cured sample. The sharp line in each of the spectra of the sample is similar to the sharp line of the rewetted sample and diminishes on cooling.

Figure 5.17 compares the line-width of a moist-cured concrete sample with the line-width of the rewetted sample. The line-width of the moist-cured concrete sample increases proportionally with decreasing temperature but the line-width of the rewetted sample remains unchanged between $0\,^{0}C$ to $-20\,^{0}C$. Below $-20^{0}C$, the line-width increases to values which are higher than those of the moist-cured sample. These results therefore support the conclusions from the heat capacity measurements. The formation of ice in the moist-cured concrete paste occurs over the temperature range from $0\,^{0}C$ to $-45\,^{0}C$, whereas the rewetted water freezes within a small temperature range near $0^{0}C$.

On heating the rewetted sample at $120^{0}C$, the rewetted water is evaporated, leaving only the non-evaporable water. This water is tightly bound, and does not evaporate at $120^{0}C$ over a period of 10 hours. This is shown by the very small change of the line-width over this period of heating (see figure 5.18). Comparing

the areas under the absorption spectra of the rewetted sample at room temperature (figure 5.14 a.) and after 10 hours at 120^0 C (figure 5.14 e.), indicates that the amount of non-evaporable water in the rewetted concrete sample is about half of the total amount of water in the paste at 20^0C.

All of the NMR results show no sign of bulk ice. The observed broad line spectra is due to the chemically and physically adsorbed water. The loosely bound water or free water found in the rewetted sample may also be present in a fully saturated concrete sample. This water is easily evaporated in low humidity conditions.

6.4 ANALYSIS OF THERMAL STRAIN RESULTS

The preliminary results showed that the concrete paste suffered a permanent expansion after each cooling cycle.The moisture condition around the samples was not controlled and possibly the local relative humidity was more than 80%.

Results in later experiments showed that samples with w/c ratios less than 0.5 on a first time cooling do not show the permanent expansion. Further, if

they are not exposed to moisture or resoaked in water, these samples do not suffer a permanent expansion after subsequent cooling cycles (see figure 5.21, 5.22, 5.23 and 5.24). In this study however, samples with 0.6 and 0.7 w/c ratio showed a permanent expansion during the first cooling cycle. This is because these samples contain free water or loosely bound water as in the rewetted sample because they were not fully cured in the standard 28 days curing time.

Figures 5.27 and 5.28 show the thermal strain of dry moist-cured concrete samples which had been resoaked in water for more than a week after a thermal cooling cycle. Both samples showed a permanent expansion on this occasion. On repeating the cooling cycle on the same samples, the permanent expansion becomes less. This characteristic has been found similar to the rewetted sample, except that the rewetted water in the dry and rewetted concrete paste freezes at higher temperatures. It is concluded that there is a possibility that some of the water absorbed during the resoaking escapes from the samples on cooling.

We conclude that the evaporable water in as-made moist-cured concrete paste has a stronger binding energy compared with the absorbed water that goes

into the sample on resoaking. However, this absorbed water has a stronger binding energy than the water held in a dry and rewetted sample. Water in the dry and rewetted sample appears to be similar to water that is absorbed into the paste after only one or two days of resoaking. This is shown in by figure 5.22 for sample Q.

By definition, drying a concrete paste at 100^0 C to constant weight, drives out all the evaporable water. Some, but not all of this evaporable water is lost by exposing the moist-cured concrete paste in a low humidity condition at 20^0 C. On resoaking, this lost water is recovered, but this water does not, now have the same binding energy as the original evaporable water.

According to the discussions in section 4.1.4, the effect of the cooling cycle is to coarsen the pores and therefore increase the distribution of larger pores. Water in the larger pores is less strongly bound and freezes at higher temperatures and this explains why the absorbed water of the resoaked (after freezing) paste has a weaker binding energy.

Figure 5.32 (sample R w/c =0.4) and figure 5.34 (sample S w/c=0.5) show that the dry samples have similar dilation coefficients of $-10 \times 10^{-6}\ ^0C^{-1}$, except

in the region -25° to -45°C where the dilation coefficient peak to approximately zero. This behaviour is also similar to that shown in figure 5.31 (sample P w/c=0.3), for the saturated moist-cured sample. On the other hand, the positive peaks in dilation coefficient around -40^{0} C for the saturated samples are clearly due to the evaporable water which is lost by drying at room temperature.

The dilation coefficients of samples R and S also show a small negative peaks at about -10^{0}C, which does not happen in sample P, the rewetted sample and the dry sample. This decrease is larger for a sample with a higher degree of saturation. There are two possible explainations. First, the formation of ice lenses in moist-cured concrete paste at temperatures near 0^{0}C, does not expand the paste, since the voids volume may be enough to accomodate the extra volume of the ice. Water movement may be encouraged, either as liquid movement arising from changes in solute concentration, or as vapour due to local temperature differences, and the associated vapour pressure differences, produced by cooling. Thus water moves out from the gel spaces into the frozen water regions in the larger pores and this causes the paste to contract. As the temperature is lowered further, the ice lenses

increase and when there is no more void to accomodate them, further freezing of water makes the sample expand.

The second possibility is that when ice lenses form in the concrete pores, the hydraulic pressure may force some of the loosely bound water to escape from the sample surface and therefore the gel space surrounding the frozen part has a higher water content. Hence this water moves out to the frozen area and the paste contracts. However, if this assumption is true, then the rewetted sample should have a smaller value of dilation coefficient in the range from $0\,^{0}C$ to $-10\,^{0}C$, since it contains more loosely bound water. In fact, the peak values of dilation coefficient of the rewetted sample at $-10\,^{0}C$ is the same as that of the saturated moist-cured samples; i.e. $30 \times 10^{-6}\ {}^{0}C^{-1}$. Therefore, we conclude that if there is some water escape during cooling, it must be very little and is not a major reason for the contraction of the paste. It should be noted that time dependent changes of the dilation coefficients would be expected if water movement during cooldown was important. Further thermal strain measurements need to be carried out at different cooling rates.

All moist samples showed hysterisis on rewarming. This may be due to ice segregation. During cooling, water in the pores freezes between $0^{0}C$ and $-45^{0}C$, due to the smallness of the pores and also to some extent because of the depression of the freezing point as the concentration of the solute increases. On rewarming the paste, the ice melts at a higher temperature, because it is now in a more pure state.

Following the discussions in section 4.3.2, on dilation factor, the concrete samples which have been tested have either zero or positive dilation factors and their dilation factors increase as the temperature decreases. The values of the factors for the samples are tabulated in table 6.2 below. Some of them were plotted in figure 5.38.

		Temperature ^{0}C						
Samples	w/c	-10	-20	-30	-40	-50	-60	-70
P(s)	0.30	0	40	110	210	310	300	320
P(3d)	0.30	0	70	130	230	340	320	360
R(s)	0.40	-20	-20	60	280	630	700	740
R(3w)	0.40	30	60	120	200	270	300	320
S(s)	0.50	30	110	130	500	710	760	780
S(3w)	0.50	30	80	100	180	250	290	290
T(s)	0.60	30	190	500	1030	1480	1610	1620
U(s)	0.70	90	490	960	1500	1850	1880	1860

(s) - saturated. (3d) - after 3 days in a dry chamber. (3w) - after 3 weeks in a dry chamber.

Table 6.2: Dilation factors of the concrete samples. in μstrain.

This data shows that after leaving the moist-cured concrete samples with w/c ratio 0.4 and 0.5 in a dry chamber, the samples have dilation factors similar to the saturated moist-cured concrete with w/c ratio 0.3.

It is concluded that the degree of saturation affects the thermal behaviour of the concrete.

Water which is affecting the thermal strain characteristics of the concrete is easily evaporated at temperatures below 100 ^{0}C. There are several indications that this water comprises about 75%

of the total evaporable water for w/c of 0.4 and 0.5. However a sample with low w/c ratio does not appear to have this kind of water.

6.5 EFFECTS OF AGGREGATES AND OTHER SUBSTANCES

We have used only one type of aggregate made from flint stone. Our samples had unduly different thermal strain curves which suggests that the internal structures of the aggregates are different. On cooling, they showed contraction only, with values between -200 μstrains to -1200 μstrains at -60 ^{0}C. If the results truly represent the thermal contraction of the aggregates in the concrete , then further studies are needed to evaluate the importance of aggregate on the properties of concrete below 0^{0}C.

Calcium hydroxide and silicon dioxide compounds may be present in a low w/c ratio concrete because an inadequate supply of water in the hydration process may result in some of the compounds being unreacted. Results show that these compounds, if present in the concrete , do not contribute to the thermal strain of concrete during cooling.

6.6 WATER IN CONCRETE

Water in concrete has several types of binding. Apart from chemically bound water and free water, concrete also contains adsorbed water with variable degrees of binding and this energy of binding is probably closely related to the pore size distribution.

Rewetted water in a dry and rewetted concrete has a very weak binding energy and is closely similar to free water. The binding energy does not depend on how long the concrete has been immersed in water.

After the concrete has been exposed to a thermal cycle, absorbed water in a moist-cured concrete , has a different characteristics compared with the original water content of the paste. The absorbed water has a reduced binding energy somewhere between the binding energy of the original evaporable water and the rewetted water in the rewetted concrete.

Since both rewetted samples and the resoaked moist-cured concrete samples have shown a permanent expansion, after thermal cycling, it is concluded that the absorbed water is responsible for the

permanent expansion.

Collecting together all the experimental results, it is possible to produce a simplified classification of the different types of water and their binding energy in concrete. Figure 6.1 plots binding energy against evaporable water content. Three block lines are drawn to indicate the different distributions of water content with binding energy suggested from the results between moist-cured, rewetted and resoaked samples. In all cases, about 25% of the evaporable water is more strongly bound and is only released at 100 ^{0}C; this water is not responsible for dilation on cooling, or for the permanent expansion after thermal cycling. The absorbed water with low energy of binding, appears to be largely responsible for thermal strain effects in fully cured concrete.

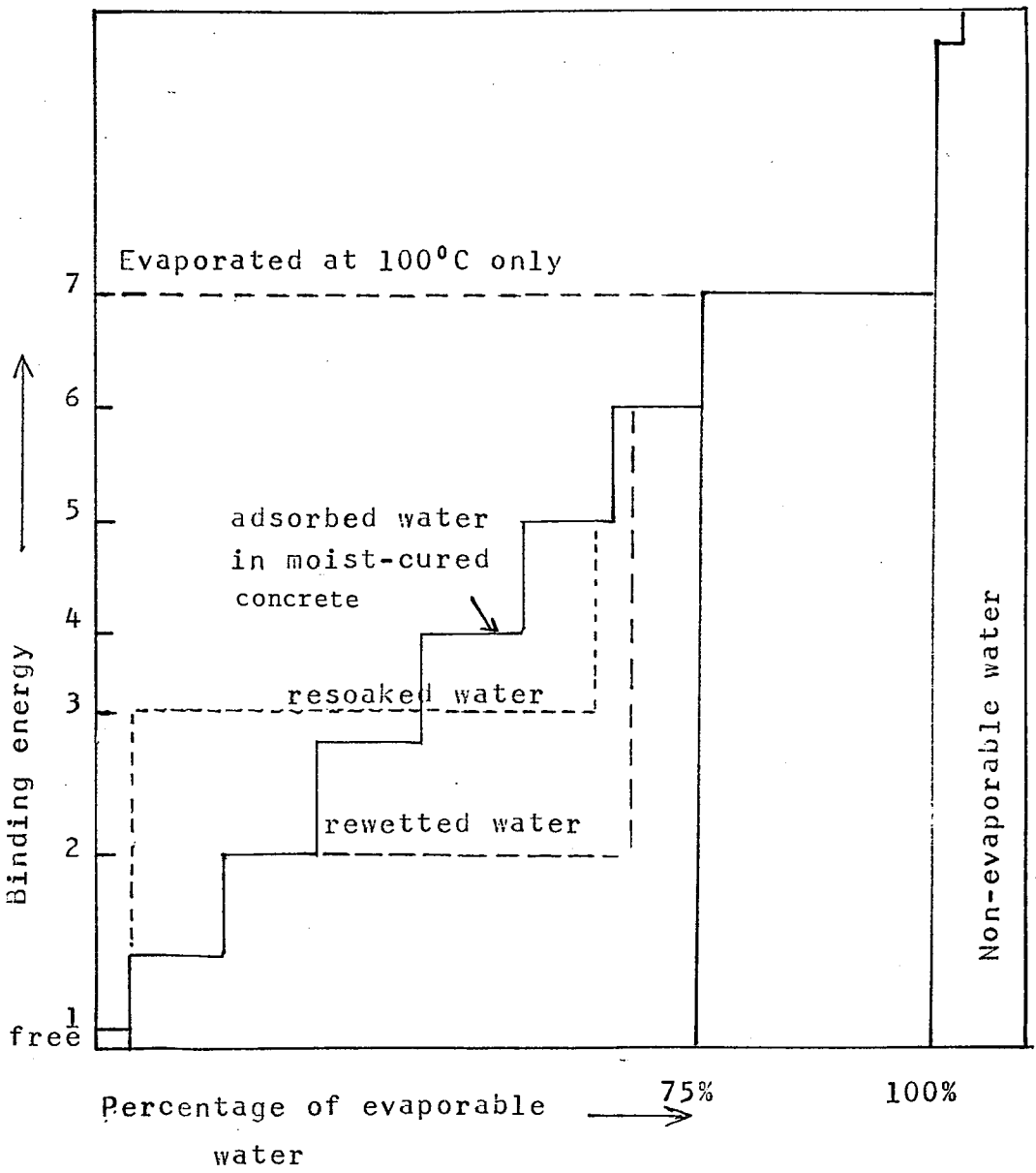

Figure 6.1: Schematic classification of water in concrete.

1 - free water.

2 - absorbed water in rewetted concrete.

3 - absorbed water in resoaked moist-cured concrete.

4, 5, and 6 - adsorbed water.

7 - adsorbed water; similar to interlayer water in clays. Only evaporate at 100°C

7.1 CONCLUSIONS

1. Rewetted water in a dry and rewetted concrete has a different characteristic to the physically adsorbed water in a moist-cured concrete.

2. The rewetted water freezes at higher temperatures, just below 0 ^{0}C.
3. Water in a moist-cured concrete freezes over a temperature range between 0 ^{0}C and -45^{0}C.
4. 75% of the evaporable water in a saturated moist-cured concrete is evaporable in a low humidity condition at 20^{0}C.
5. The evaporable water which evaporates in a low humidity condition is the cause of the large thermal strain suffered by a saturated fully moist-cured concrete.
6. Water in a concrete with 0.30 water- cement ratio is not evaporable in a low humidity condition, unlike higher w/c ratios.
7. Exposing a moist-cured concrete to a cooling cycle may change its internal structure.
8. Water absorbed into a moist-cured concrete sample after the sample has been exposed to a thermal cycle,

causes the permanent expansion that is observed after a further cooling cycle.

9. The original water in a moist-cured concrete has the strongest bound energy among the various levels of binding of physically adsorbed water.

10. Moist-cured concrete samples have a small contraction between 0 ^{0}C and -10^{0}C. It is only below -10^{0}C that expansion effects dependent on the degree of saturation are revealed.

7.2 FINAL REMARKS

These conclusions are based on a limited number of samples, using one type of aggregate, when the reproducibility of experimental results has been a major target in the development of the experimental techniques. They provide further information in gaining an understanding of the use of conventional concrete as a cryogenic material. The conclusions require additional studies to be carried out on different types of concrete before they can be applied for general use.

8 ACKNOWLEDGEMENTS

I wish to express a great gratitude to Dr. R.G. Scurlock, the director of the Institute of Cryogenics, in supervising the present work and the preparation of this thesis.

I am also grateful to all staff of the Institute in giving their assistance during the work.

This investigation was supported by a grant from the Science and Engineering Research council.

9 REFERENCES

1. POWERS, T.C. "The Mechanism of frost action in concrete -stanton walker lecture 1965 part I". Jnl. of cement, Lime and gravel 1966 Vol.41 p143
2. BRUGGELING, A.S.G. "Prestressed concrete for the storage of liquefied gases" A view point publication. Cement and concrete association 1981.
3. HANSEN,W.C. "Twenty-year report on the long time study of cement performance in concrete". Bulletin 175 Portland cement ass. research and development laboratories. 1965
4. JACKSON,F.H. "Long time study of cement performance in concrete." Proceedings American Concrete Institute 1955 vol.52 p159
5. KASAMI,H.,TANAKA,Y.,KISHIMA,Y.,YAMANE,S. "Properties of concrete at very low temperature." Proceedings 1st International Conference of cryogenic concrete. The Concrete Society 1981. p198
6. BROWNE, R.D., BAMFORTH,P.B. "The use of concrete for cryogenic storage: A summary of research past and present." Proceedings 1st International Conference of cryogenic concrete. The Concrete Society. 1981. p135

7. CHEYREZY,M.,STIRNEMANN,G. "Cryogenic concrete design data collection from a testing campaign." Proceedings 2nd International Conference of cryogenic concrete. Amsterdam 1983. The Concrete Society.

8. POWERS, T.C. "Moisture effects in concrete" Proceedings of Building Research Conference 1953, Ottowa. p55

9. POWERS,T.C. "Resistance to weathering -freezing and thawing." ASTM special Technical Publication. No.169 1956. p182

10. POWERS, T.C. "Basic consideration pertaining to freezing and thawing tests." Proceedings ASTM 1955 vol.55 p1132

11. NEVILLE, A.M. "Properties of concrete." Pitman Publishing 1975.

12. TABER,S. "Intensive frost action along Lake Shores." American journal of Science. 1950 vol.248 p784

13. POWER, T.C., COPELAND, L.E.,MANN, H.M. "Capillary continuity or discontinuity in cement paste." Jnl. research and development laboratory Portland cement Ass.. vol.1 no.2 1959 p38

14. POWERS, T.C. "The mechanism of frost action in concrete Part II -Stanton Walker lecture 1965". Jnl

of cement, lime and gravel 1966. Vol.41. p181

15. HELMUTH,R.A. "Capillary size restrictions on ice formation in hardened Portland cement pastes." Proceedings 4th Inter. Symposium on the chemistry of cement 1960. Vol.11 p855

16. VERBECK,G.J., HELMUTH,R.A. "Structures and physical properties of cement paste." Proceed. 5th Inter. Symposium on the chemistry of cement 1968.

17. POWERS,T.C.,BROWNYARD,T.L. "Studies of the physical properties of hardened Portland cement paste." Proceed. Jnl. of American concrete Institute. vol.41 p101

18. POWERS,T.C., HELMUTH,R.A. "Theory of volume changes in hardened Portland cement paste during freezing." Proceeding of Highway research Board. Vol.32 1953 p286

19. COPELAND,L.E. "Specific volume of evaporable water in hardened Portland cement paste." Proceed. Jnl. of American Concrete Institute 1956. Vol.52 p863

20. SELIGMANN, P. "Nuclear magnetic resonance studies of the water in hardened cement paste." Jnl. of research and development Laboratory of Portland cement Ass.. 1968. Vol.10(1) p52

21. VAN BREUGEL,K. "Minimizing of the vulnerability of

storage systems for liquefied energy gases." Proceed. 2nd International Conference of cryogenic concrete 1983. Amsterdams. The Concrete Society.

22. MARSHALL, A.L. "Cryogenic Concrete." Cryogenics. Nov. 1982 p555

23. ROSTASY',F.S., WIEDMANN, G. "Strength, deformation and thermal strains of concrete at cryogenic conditions" Proceedings 1st Inter. Confer. of cryogenic concrete 1981. The Concrete Society. p212

24. FLETCHER, N.H. "The frezzing of water." Science Progress Oxf. 1966 no.54 p227

25. PLANAS, J.,CORESS,H.,CHUECA,R.,ELICES,M. "Influence of load on thermal deformation of concrete during cooling down." Proceed. 2nd Inter. Conf. of cryogenic concrete 1983. Amsterdams. The Concrete Society.

26. HANAOR,A., SULLIVAN, P.J.E. "Experimental evaluation of concrete permeability to cryogenic concrete." Proceed. 2nd Inter. Conf. of cryogenic concrete 1983. Amsterdam. The Concrete Society.

27. SCURLOCK,R.G., MOHD YUSOF,K.B. "Thermal behaviour of concrete between -80 C and 20 C." Proceed. 2nd Intern. Conference of cryogenic concrete 1983. Amsterdams. The Concrete Society.

28. BAMFORTH, P.B., MURRAY, W.T., BROWNE, R.D. "The application of concrete property data at cryogenic temperature to LNG tank design." Proceed. 2nd Inter. Confer. of cryogenic concrete 1983. Amsterdams. The Concrete Society.

29. HOBBS, P.V. "Ice Physics" Oxford University Press 1974.

30. POWELL, R.W. "Thermal conductivity and expansion coefficients of water and ice." Advance Physics. Vol.7 1958 p276

31. DANTL, G. - from reference 29 p350.

32. EISENBERG, D., KAUZMANN, W. "The structure and properties of water." Oxford University Press. London. p296

33. DANTL, G. - from reference 29 page 351.

34. DILLARD, D.S., TIMMERHAUS, K.D. "Low temperature thermal conductivity of solidified H O and D O" Pure Appl. Cryogen. vol.4 1966 p35.

35. ROSINI, et al - from reference 29 page 362.

36. RUMPF and GEIGL - from reference 29 page 468.

37. CWILONG, B.M. "Sublimation in a Wilson chamber." Proceed. of royal soc. A190 1947. p137.

38. MOSSOP, S.E. "The freezing of supercooled water." Proceed. Physics Society. 1955. Vol.68 p193

39. POUND, G.M., MADONNA, L.A., PEAKE, S.L. "Critical supercooling of pure water droplets by new microscope technique." Journal of colloid science. 1953. Vol.8. p187

40. NEMETHY and SCHERAGA, N. "Structure of water and hydrophobic bonding in protiens. I a model for the thermodynamic properties of liquid water." Jnl. of Chemical Physics 1962. Vol.36 p3382

41. TURNBULL,D. and FISHER,J.C. "Rate of nucleation in condensed system." Jnl. of chemical physics. Vol.17. 1949 p71.

42. VALI, G. and STANSBURY, E.J. "Time dependent characteristics of the heterogenous nucleation of ice." Canadian journal of Physics. Vol.44 1966 p477

43. CARTE, A.E. "The freezing of water droplets." Proceedings of Physics Society LXIX 10-B 1956

44. BIGGS,E.K. "The supercooling of water." Proceedings of Physics society. B66 1953 p688

45. KUMAI, M. "Hexagonal and cubic ice at low temperature." Journal of Glaciology . Vol.7 No.49 1968 p95

46. MASON, B.J. and MAYBANK,J. "Ice nucleting properties of some mineral dusts." Quarterly journal of royal meteorogical soc. Vol.84 1958 p235

47. FUKUTA,N. "Experimental investigations on the ice forming ability of various chemical substances" Journal of meteorology Vol.15 1958 p17

48. SELIGMANN, P. "Interpretations and limitations of nuclear magnetic resonance" US Highway research board Bulletin no. 287 special report. 1961 p64

49. AKITT,J.W. "NMR and Chemistry" Chapman Hall, London 1973

50. BLAINE, R.L. "Proton magnetic resonance in clay minerals" US Highway research board. Bulletin 287 special report. 1961 p44

51. ZIMMERMAN,J.R., HOLMES, B.G., LASATER,J.A. "A study of adsorbed water on silica gel by nuclear magnetic resonance techniques." Journal of Physical Chemistry. Vol.60 1956 p1157

52. KAWACHI, K.,MURAKAMI,M.,HIRAHARA,E. "Studies on the hydration and hardening of cement (Experimental studies on nuclear magnetic resonance of water molecules in cement)." from reference no.54

53. FRENCH, C.M. and WARDER, J.F. "Nuclear magnetic resonance investigation of rates of hydration of cement and calcium silicates." Journal of Applied Chemistry. Vol.9 1959 p561

54. SELIGMANN, P. "Possible application of nuclear

magnetic resonance in cement and concrete research." Jnl of the Portland cement assoc. research and development laboratory. Sept. 1960 p20

55. FLETCHER, N.H. "Size effect in heterogenous nucleation." Journal of Chemical physics. Vol.29 1958 p572

56. RABIDEAU,S.W., FINCH,E.D., DENISON,A.B. "Proton and Deutron NMR of ice polymorphs." Journal of Chemical physics. Vol.49 1968 p4660

57. PHILIP, J.R. "Physics of water movement in porous solid." US-Highway research board. Special report 40 1959 p147

58. POWER,T.C., MANN,H.M., COPELAND,L.E. "Flow of water in hardened Portland cement paste." US-Highway research board. Special report 40 1959 p308

59. BROWNSCOMBE, T.L. and HALLET, J. "Experimental and field studies of precipitation particles formed by the freezing of supercooled water." Quarterly journal of royal meteorological society. Vol.93 1967 p455

60. OCHIAI,H., YAMAMURA,H. and FUKUNAGA,K. "A nuclear magnetic resonance study of the water in calcium silicate pastes." Bulletin of the chemical society of Japan. Vol.38 no.6 1965 p945

61. RHOADES,R., MIELENZ, R.Z. "Petrography of concrete aggregate." Journal of the American concrete institute. Vol.17 no.6 1946 p581

62. BRUNAUER,S.,HAYES,J.C. and HASS,W.E. "The heats of hydration of Tricalcium Silicate and -Dicalcium Silicate." Journal of Physical chemistry. Vol.58 1954 p279

63. DIAMOND, S. "Cement paste microstructure- An overview at several levels." Proceed. of a conference at Sheffield University April 1976.

64. BERNAL,J.D. "The structure of cement hydration product." Proceed. 3rd Intern. Symposium on the chemistry of cement. London 1952 p216

65. BRUNAUER,S., MIKHAIL, R.SH., BODOR E.E. "Pore structure analysis without a pore shape model." Journal of colloid and interface science. Vol.24 1967 p451

66. COPELAND,L.E. ,KANTRO,D.L., VERBECK,G. "Chemistry of hydration of Portland cement." Proceedings of 4th Intern. Symp.Chemistry of cement. 1960.

67. ROSTASY',F.S., WEIB,R., WIEDEMANN,G. "Changes of pore structure of cement mortars due to temperature." Cement and concrete research. Vol.10 1980 p157

68. SCHEIDEGGER,A.E. "The physics of flow through porous media." University of Toronto Press. 1963.

69. HAWKSLEY,P.G.W. "The effect of concentration on the settling of suspensions and flow through porous media." Edward Arnolds and Co. London. 1951

70. EYRING,H. "Viscosity, Plasticity and diffusion as examples of absolute reaction rates." Jnl. of chemical Physics Vol.4 1936 p283.

71. GIAUQUE,W.F. and STOUT,J.W. "The entropy of water and the third law of thermodynamics. The heat capacity of ice from 15 C to 273 C." Jnl. of American chemical society. Vol.58 1936 p1144.

72. VUORINEN,J. "On use of dilation factor and degree of saturation in testing concrete for frost resistance." Nordisk Betong Vol.1 1970 p37

73. WHITESIDE,T.M. and SWEET H.S. "Effect of mortar saturation in concrete freezing and thawing tests." Proceedings of highway research board 30 1950 p204

74. WARRIS,B. "The influence of air entrainment on the frost resistance of concrete. Part B: Hypothesis and freezing experiments" Proceed. of Swedish cement and concrete research institute. Stockholm 1964 Nr 36 130p.

75. COPELAND,L.E. and HAYES,J.C. "Porosity of hardened

Portland cement pastes." Jnl. of the American concrete Institute. Vol.27 1955/1956:6 p633

76. KUZMAK,J.M. and SEREDA P.J. "On the mechanism by which water moves through a porous material subjected to a temperature gradient." US Highway research board. Special report No.40 1959 p134

77. HUTCHISON,NIXON and DENBIGH. From reference 8 p60.

78. PARROT,J.E. and STUCKES,A.D. "Thermal conductivity of solids." Pion Ltd. 1975

79. PRATT,A.W. "Heat transmission in low conductivity materials." Thermal Conductivity. Vol.1 Academic Press 1969 p301.

80. ALLEN,D.C. and THORNE,C.P. "The thermal conductivity of concrete." Magazine of concrete research. Vol.15 No.43 1963 p39.

81. SWALIN, A.R. "Thermodynamics of solids" John Wiley & Sons, Inc. 1962.

10 APPENDICES

10.1 APPENDIX A

DERIVATION OF J_{LS} FROM TURNBULL & FISHER(41)

Let μ_L and μ_S be the chemical potentials per molecule in supercooled water and ice respectively. The supercooled water molecules come together in an ice embryo, has volume v and surface area A. Then the free energy G_{LS} of the system is increased by an amount below:

$$\Delta G_{LS} = n_S(\mu_S-\mu_L)v + \sigma_{LS}A \qquad (10.1)$$

where,

n_S is the number of molecules per unit volume of ice.

σ_{LS} is the interfacial free energy between the water and ice.

Since the chemical potentials is given as,

$$\mu = - kT \ln p \qquad (10.2)$$

where p is the saturated vapour pressure. Thus,

$$\mu_S - \mu_L = -kT \ln(p_L/p_S) \qquad (10.3)$$

where, p_L and p_S are the saturated vapour pressures over the surfaces of water and ice at temperature T respectively. K is the Boltzmann's constant. If shape of the ice embryo is taken to be spherical with radius r, the volume and the surface area can be written as, $\frac{4}{3}\pi r^3\alpha$ and $4\pi r^2\beta$,where α and β are numerical factors and have a values of greater than unity because considering that the embryo is not a perfect sphere. Therefore, equation 10.1 becomes,

$$\Delta G_{LS} = -\frac{4}{3}\pi r^3\alpha n_S kT \ln(p_L/p_S) + 4\pi r^2\beta\sigma_{LS} \qquad (10.4)$$

$$\text{or} \quad \frac{\Delta G}{kT}LS = A_o i^{2/3} - B_o i \qquad (10.5)$$

where i is the number of the water molecules in the ice embryo and A_o and B_o are quantities related to the surface free energy of ice-water interface and the bulk free energy difference between supercooled water and ice respectively.

The variation of the total free energy which is given in equation 10.5 is shown in figure 2.2.

From the figure, the radius at the energy barrier ΔG_B is r_B. Thus the critical radius where $\partial G_{LS}/\partial r = 0$ is,

$$r_B = \frac{2\beta\sigma_{LS}}{\alpha n_S kT \ln(p_L/p_S)} \qquad (10.6)$$

and $$\Delta G_B = \frac{16\pi\sigma_{LS}^3\xi}{3\{n_S kT \ln(p_L/p_S)\}^2} \qquad (10.7)$$

where $\xi = \beta^3/\alpha^2$

From statistical mechanics, the number of water molecules forming ice embryos of critical size per unit volume of liquid is given approximately as,

$$n(r_B) = n_L \exp(-\frac{\Delta G_B}{kT}) \qquad (10.8)$$

where n_L is the number of molecules per unit volume of liquid. In order that ice nucleation to take place, the ice embryo has to take further water molecules to achieve the critical size and pass over the hump in figure 2.2. It has been shown that(41), the rate of molecules joining the embryo in order to pass the hump is approximately equal to,

$$\frac{kT}{h} \exp(-\frac{\Delta g}{kT})$$

where h is Plank's constant and Δg is the activation

energy of water molecules to pass through the water-ice boundary. Therefore, the nucleation rate J_{LS} of ice embryo which can grow spontaneously is given as below:

$$J_{LS} = \frac{n_L kT}{h} \exp(-\frac{\Delta g}{kT}) \exp(-\frac{\Delta G_B}{kT}) \qquad (10.9)$$

10.2 APPENDIX B

FREEZING OF WATER DROPLETS MODELS FROM HOBBS(29)

THE STATISTICAL MODEL

The probability of nucleation occuring in volume V within the time interval t to t+dt is $VJ_{LS}(T)dt$, where $J_{LS}(T)$ is the rate of nucleation from equation 10.9 at temperature T. The rate of nucleation can be taken as equal to the rate of freezing $J_F(T)$.

Suppose, we have N of identical drops with volume V and all at the same temperature. If from time t=0 to time t, N_t water drops have frozen, then the probability of nucleation taking place in volume V is,

$$P(V,t) = N_t/N \qquad (10.10)$$

The numbers of drops nucleated within the time from 0 to t+dt is,

$$N_{t+dt} = N_t + (N-N_t)VJ_F(T)dt \qquad (10.11)$$

If we divide equation 10.11 by N,

$$P(V,t+dt) = P(V,t)+\{1-P(V,t)\}VJ_F(T)dt \qquad (10.12)$$

Since,

$$P(V,t+dt) = P(V,t) + \frac{\partial P(V,t)}{\partial t}dt$$

Therefore,

$$\frac{\partial}{\partial t}P(V,t)dt = \{1 - P(V,t)\}VJ_F(T)dt \qquad (10.13)$$

Integrating equation 10.13,

$$\ln\{1 - P(V,t)\} = -\int_0^t VJ_F(T)dt \qquad (10.14)$$

If the probability of nucleation is small (P<<1),

$$P(V,t) = V_o\int_o^t J_F dt \qquad (10.15)$$

If the rate of cooling β_c=dT/dt is constant to time,

$$\text{therefore,}\quad P(V,t) = \frac{V}{\beta_c}\int_o^{T_s} J_F dt \qquad (10.16)$$

where T_s is the supercooled temperature. If we write the integral part of equation 10.16 as below,

$$\int_o^{T_s} J_F dt = D\exp(T_s/\tau_o) \qquad (10.17)$$

$$\text{then,}\quad P(V,t) = \frac{DV}{\beta_c}\exp(T_s/\tau_o) \qquad (10.18)$$

where D and τ_o are constants. The probability of freezing per degree drop in temperature for a cooling rate β_c at a supercooling T_s is,

$$\frac{d}{dT_s}P(V,t) = -\frac{1}{N}\frac{dN}{dT_s} = \frac{EV}{\beta_c}\exp(T_s/\tau_o) \qquad (10.19)$$

where $E = D/\tau_o$

By integrating equation 10.19 and $N=N_o$ at $T_s=0$, then,

$$\ln\left(-\ln\frac{N}{N_o}\right) = \ln\frac{EV\tau_o}{\beta_c} + \frac{T_s}{\tau_o} \qquad (10.20)$$

THE SINGULAR MODEL

This model assumes that every drop nucleates at a temperature determined by the most effective ice nucleus it contains and according to the model, no freezing events would occur at a fixed temperature. If the concentration of ice nuclei which become effective between 0^0 and $-T_s^0C$ is $n(T_s)$, then we assume that $n(T_s)$ is given by,

$$n(T_s) = n_o \exp(T_s/\tau_o) \qquad (10.21)$$

If a drop contains a random distribution of ice nuclei, the probability $P(T_s)$ of water drops freeze while being cooled to $-T_s$ is given by Poisson statistic as,

$$P(T_s) = 1 - \frac{N}{N_o} = 1 - \exp\{-n(T_s)V\} \qquad (10.22)$$

Hence,

$$N = N_o \exp\{- n_o V \exp(T_s/\tau_o)\} \qquad (10.23)$$

$$\text{or,} \quad \ln(- \ln\frac{N}{N_o}) = \ln(n_o V) + T_s/\tau_o \qquad (10.24)$$

CONSTANT a and b

The constants a and b are empirical constants. Where Hobbs(29) has mentioned that,

$$a = 1/\tau_o \qquad (10.25)$$

where τ_o is a parameter which charaterizes the nucleating ability of the ice nuclei and it can be found in equations 10.18, 10.20 or 10.24. While the value b is related to the constant term of equations 10.20 or 10.24.

10.3 APPENDIX C

CALCULATION OF T FROM A LINE-WIDTH FROM SELIGMANN(20)

Theoretically, the shape of an NMR absorption line is given by Lorentz formula,

$$f(\nu) = \frac{2T_2}{1 - 4\pi^2(\nu-\nu_0)^2T_2^2} \qquad (10.26)$$

where $f(\nu)$ is the absorption at frequency ν. ν_0 is the frequency for maximum absorption and T_2 is the transverse relaxation time, is defined as one half the maximum intensity (at $\nu = \nu_0$) for the normalized curve. i.e. for an amplitude adjustment to give unit area under the curve. Then,

$$\int_{-x}^{x} f(\nu)d\nu = 1 \qquad (10.27)$$

a condition that is satisfied by equation 10.26. This formula can be derived from a semiclassical approach; quantum mechanics does not yield a definite line shape.

However, experimental line shapes do not usually conform to this theoretical shape. The shapes of observed lines tend to lie between the Lorentz shape and

the Gaussian shape, which in this context may be written as follows:

$$f(\nu) = 2T_2 \exp\{-4\pi(\nu-\nu_0)^2 T_2^2\} \qquad (10.28)$$

In the following derivation it is shown that both curves lead to the same order of magnitude T_2, within the limits required for the present purpose of comparison with experimental data.

As indicated in chapter 3, NMR instruments measure the absorption as a function of magnetic field strength at a constant frequency, rather than as a function of frequency as in equation 10.28. The relation between the two is given by a simple proportionality,

$$\nu = \frac{\gamma}{2\pi} H \qquad (10.29)$$

where H is the magnetic field strength and γ is a constant known as the gyromagnetic ratio which represents the ratio of the magnetic moment of a spinning particle to its angular momentum.

The broad line instruments do not display the absorption curve directly but only its derivative. The result is shown in figure 10.1. From equation 10.29

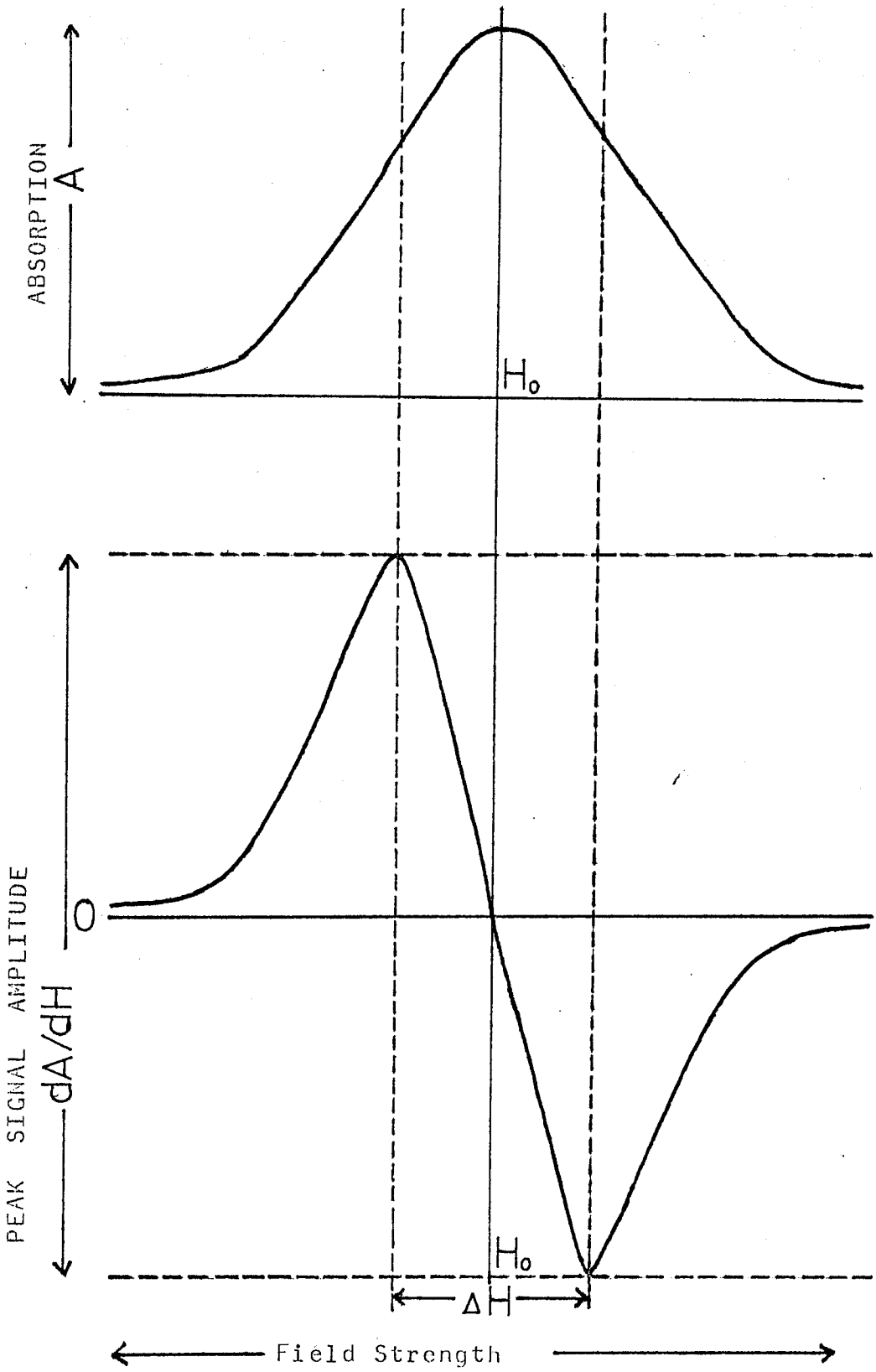

Fig.10.1 :Significance of measurements of Absorption on Broad-line instruments(from ref.20)

and the line-width ΔH, therefore theoretical line width is given as below.

$$\Delta\nu = \frac{\gamma}{2\pi}\Delta H \qquad (10.30)$$

where γ is a constant. Thus the line width are expressible either in magnetic field or frequency units.

The measured quantities must now be related to the theoretical curves. The experimental peaks represent the points at which the derivative is a maximum or minimum. In terms of the parent absorption curve, these points are the inflection points, their location can be determined by setting the second derivative of the parent curve equal to zero. This gives, for the Lorentz shape,

$$\nu_m = \nu_o \pm \frac{1}{2\pi T_2\sqrt{3}} \qquad (10.31)$$

where the ν_m are the frequencies at which the inflections occur. Then the line width, $\Delta\nu$ in frequency unit is,

$$\Delta\nu = 2(\nu_m - \nu_o) = \frac{1}{\pi T_2\sqrt{3}} \qquad (10.32)$$

and the desired relaxation time in terms of the line

width is,

$$T_2 = \frac{1}{\pi \Delta\nu \sqrt{3}} \qquad (10.33)$$

For the Gaussian shape, with a similar method, will give,

$$\nu_m = \nu_o \pm \frac{1}{2T_2\sqrt{2\pi}} \qquad (10.34)$$

The line width is then,

$$\Delta\nu = 2(\nu_m - \nu_o) = \frac{1}{T_2\sqrt{2\pi}} \qquad (10.35)$$

and $$T_2 = \frac{1}{\Delta\nu\sqrt{2\pi}} \qquad (10.36)$$

These results must still be expressed in unit of ΔH, the measured magnetic field width. Substitution of equation 10.30 into equation 10.33 and 10.36 together with the value of 2.67×10^4 gauss^{-1} sec^{-1} for γ, protons yield of the Lorentz shape.

$$T_2 = \frac{2\pi}{\pi\gamma\sqrt{3}\Delta H} = \frac{2}{\gamma\Delta H\sqrt{3}} = \frac{4.33 \times 10^{-5}}{\Delta H} \qquad (10.37)$$

and for the Gaussian shape,

$$T_2 = \frac{2\pi}{\gamma \Delta H \sqrt{2\pi}} = \frac{\sqrt{2\pi}}{\gamma \Delta H} = \frac{9.39X10^{-5}}{\Delta H} \qquad (10.38)$$

The average of equations 10.37 and 10.38 is given below;

$$T_2 = \frac{6.86X10^{-5}}{\Delta H}$$

which is the value used in equation 3.5.

10.4 APPENDIX D

THERMODYNAMIC RELATION BETWEEN c_p and c_v (reference 81)

The specific heat at a constant pressure c_p and the specific heat at a constant volume c_v are equals to $(\partial H/\partial T)_p$ and $(\partial U/\partial T)_v$ respectively. It seems reasonable to start with the definition of enthalpy:

$$H = U + PV \qquad (10.39)$$

and on differentiation,

$$dH = dU + PdV + VdP \qquad (10.40)$$

If we divided the above equation by dT,

$$(dH/dT) = (dU/dT) + P(dV/dT) + V(dP/dT) \qquad (10.41)$$

Placing the restriction of constant pressure we have,

$$(\partial H/\partial T)_p = (\partial U/\partial T)_p + P(\partial V/\partial T)_p \qquad (10.42)$$

We are interested in $(\partial U/\partial T)_V$, so it will be necessary

to eliminate $(\partial U/\partial T)_p$ in favour of $(\partial U/\partial T)_V$. To do this let us express U=f(V,T), thus,

$$dU = (\partial U/\partial T)_T dV + (\partial U/\partial T)_V dT \qquad (10.43)$$

Dividing through by dT and keeping P constant, we find,

$$(\partial U/\partial T)_p = (\partial U/\partial V)_T (\partial V/\partial T)_p + (\partial U/\partial T)_V \qquad (10.44)$$

Substitution of equation 10.44 into 10.42 yields,

$$(\partial H/\partial T)_p = (\partial U/\partial T)_V + ((\partial U/\partial V)_T + P)(\partial V/\partial T)_p \qquad (10.45)$$

$$\text{or} \quad c_p = c_v + ((\partial U/\partial T)_T + P)(\partial V/\partial T)_p \qquad (10.46)$$

Experimentally, one can measure P and $(\partial V/\partial T)_p$ quite easily, but it is generally more difficult to obtain the change of internal energy with volume at constant T, $(\partial U/\partial V)_T$. Therefore, let us attempt to express this quantity in terms of more readily available quantities. By expressing U=f(T,V) we find,

$$dU = (\partial U/\partial T)_V dT + (\partial U/\partial V)_T dV \qquad (10.47)$$

For a reversible process,

$$dU = TdS - PdV \qquad (10.48)$$

and subtracting equation 10.48 from 10.47 we get,

$$dS = \frac{1}{T}\left(\frac{\partial U}{\partial T}\right)_V dT + \frac{1}{T}\left(\left(\frac{\partial U}{\partial V}\right)_T + P\right)dV \qquad (10.49)$$

Equation 10.49 is expressed in terms of dT and dV. Let us now expand S=f(T,V).

$$dS = (\partial S/\partial T)_V dT + (\partial S/\partial V)_T dV \qquad (10.50)$$

By comparison of coefficients in equation 10.49 and 10.50, we see that,

$$(\partial S/\partial T)_V = (1/T)(\partial U/\partial T)_V \qquad (10.51)$$

and $$\left(\frac{\partial S}{\partial V}\right)_T = \frac{1}{T}\left\{\left(\frac{\partial U}{\partial V}\right)_T + P\right\} \qquad (10.52)$$

The second derivative of equation 10.51 with respect to volume at constant temperature and the second derivative of equation 10.52 with respect to temperature at constant volume are equal since

$$\frac{\partial^2 S}{\partial T \partial V} = \frac{\partial^2 S}{\partial V \partial T} \qquad (10.53)$$

and therefore $$\frac{\partial}{\partial V}\left(\frac{\partial S}{\partial T}\right)_V = \frac{1}{T}\frac{\partial}{\partial V}\left(\frac{\partial U}{\partial T}\right)_V$$

and $$\frac{\partial}{\partial T}\left(\frac{\partial S}{\partial V}\right)_T = \frac{\partial}{\partial T}\left\{\frac{1}{T}\left(\left(\frac{\partial U}{\partial V}\right)_T + P\right)\right\}$$

In view of equation 10.53 we get,

$$\frac{1}{T}\frac{\partial}{\partial V}\left(\frac{\partial U}{\partial T}\right)_V = \frac{\partial}{\partial T}\left\{\frac{1}{T}\left(\left(\frac{\partial U}{\partial V}\right)_T + P\right)\right\}$$

and $$\frac{1}{T}\frac{\partial^2 U}{\partial V \partial T} = \frac{1}{T}\left\{\frac{\partial^2 U}{\partial T \partial V} + \left(\frac{\partial P}{\partial T}\right)_V\right\} - \frac{1}{T^2}\left(\frac{\partial U}{\partial V}\right)_T + P$$

Thus $$\left\{\left(\frac{\partial U}{\partial V}\right)_T + P\right\} = T\left(\frac{\partial P}{\partial T}\right)_V \qquad (10.54)$$

In this way, we have eliminated $(\partial U/\partial V)_T$ in favour of $(\partial P/\partial T)_V$, which by experience we know can readily be expressed in terms of easily measurable quantities. Thus $V=f(P,T)$ and,

$$dV = (\partial V/\partial P)_T\, dP + (\partial V/\partial T)_P\, dT$$

Dividing this expression by dT and holding V constant yields,

$$0 = (\partial V/\partial P)_T (\partial P/\partial T)_V + (\partial V/\partial T)_P$$

or $$\left(\frac{\partial P}{\partial T}\right)_V = -\left(\frac{\partial V}{\partial T}\right)_P / \left(\frac{\partial V}{\partial P}\right)_T$$

Since the volume thermal expansion coefficient α, of a substance is defined as,

$$\alpha \equiv \frac{1}{V}\left(\frac{\partial V}{\partial T}\right)_P$$

and the compressibility β is defined as,

$$\beta \equiv -\frac{1}{V}\left(\frac{\partial V}{\partial P}\right)_T$$

we have $$(\partial P/\partial T)_V = \alpha/\beta \qquad (10.55)$$

Substituting equation 10.55 into equation 10.54 and thence into equation 10.46, we have,

$$c_p = c_v + \frac{\alpha^2 VT}{\beta} \qquad (10.56)$$